# PHOTOPHYSICAL AND BIOLOGICAL IMPLICATIONS OF THE FLUOROPHORE POLYMER RATIO

by

Casey A. Dougherty

A dissertation submitted in partial fulfillment
of the requirements for the degree of
Doctor of Philosophy
(Chemistry)
in the University of Michigan
2015

Doctoral Committee:

Professor Mark M. Banaszak Holl, Chair

Professor Anna K. Mapp

Associate Professor Anne J. McNeil

Professor Bradford G. Orr

*For my mom.*

# ACKNOWLEDGEMENTS

I first need to convey my sincere gratitude to my advisor, Dr. Mark Banaszak Holl. I could never truly express my full appreciation for all that you have taught me, and I would have never made it to the end without your guidance. Your encouraging words and constant support have been invaluable during my time in graduate school. What I appreciate most is that you aspire not only push all of us to produce great scientific work, but to also grow to be better scientists and people. Having an advisor as helpful and positive as you has made this lab such a wonderful and welcoming place to work these past few years.

I want to acknowledge my dissertation committee members Dr. Anne McNeil, Dr. Anna Mapp, Dr. Bradford Orr, and Dr. Mohamed El-Sayed for serving on my committee and providing me with excellent feedback. I want to especially thank Dr. Orr, who has been to every group meeting during my time here to see my data week to week and provide helpful comments to further my research.

I also must acknowledge Dr. Cheryl Bradshaw, Dr. Peter Cao, Ankur Desai, Dr. Pascale Leroueil, Dr. Jhindan Mukherjee, and Dr. Doug Mullen from MNIMBS for help and collaboration on a variety of projects throughout my graduate school career. I would also like to thank Dr. Stassi DiMaggio and Janet Manono from Xavier University for not only contributions to the chapters of my thesis, but also for helpful input and thoughts to my project as a whole.

I must acknowledge all of my lab members (past and present) for being a source of constant support, vital feedback, and a great listening ear: Dr. Ahleah Rohr Daniel, Dr. Becky Matz, Dr. Flora Fang, Dr. Rahul Rattan, Dr. Mallory van Dongen Sohmer, Sriram Vaidyanathan, Meagan Cauble, Anisha Shakya, Junjie Chen, and Rachel Merzel. I would not have gotten through these five years without gossiping in the group office with Rachel and Meagan or “Wine & Wii Wednesdays” with Ahleah and Mallory. My dissertation would be incomplete without the

biological expertise from Rahul, Becky, and Sriram. Teaching a chemist cell culture is no easy feat!

This dissertation would not have been written without the following contributions from others to this body of this work: **Chapter I-** I would like to thank Dr. Mallory van Dongen for her contributions to the introduction with her thorough knowledge of theranostic devices and writing contributions to the challenges of conjugation for multivalents polymers in drug delivery. **Chapter II-** I would like to thank Joseph Furgal for his lifetime contributions and Dr. Mallory van Dongen for her HPLC method development. I would also like to thank Dr. Chrys Wesdemiotis and Nadrah Alawani from the University of Akron for mass spectrometry advice. I also want to acknowledge Dr. Janet Manono, Dr. Stassi DiMaggio, and Dr. Theodore Goodson III for their contribution to this work through fruitful discussions. **Chapter III-** I would like to thank Dr. Janet Manono, Kristen Jones, and Dr. Stassi DiMaggio for the synthesis of conjugate materials and to Joshua DeMuth for obtaining dendrimer starting material. **Chapter IV-** I would like thank Sriram Vaidyanathan for this contribution to microscopy and lifetime imaging to this chapter. I would also like to acknowledge Bradford Orr for this contribution to this work through fruitful discussions.

I must also most importantly acknowledge my family and friends. First, I must acknowledge my parents and my brother: Gerry, Yvonne, and Brendan. You have been there for my entire 21 years of school. You have experienced all the triumphs and challenges with me along the way, and this dissertation is a product of all the support all of you have given me through the years. This dissertation is especially dedicated to mom because not only have you always been a constant source for unconditional support and love, but you have been the most amazing role model to me. I wouldn't be standing where I am today without having someone like you to look up to. Laura, Colleen, and Wendi: thank you for your friendship and being here every step of the way in this crazy journey. Lastly, I must thank my amazing boyfriend, Matt. You have been so caring and supportive, and most importantly patient, during this entire graduation process. More than anything else, I am so thankful that graduate school brought me you.

# TABLE OF CONTENTS

# LIST OF FIGURES

# LIST OF SCHEMES

# LIST OF TABLES

## LIST OF APPENDICES

# LIST OF ABBREVIATIONS

Fluorescein = FC

Fluorescence Lifetime Imaging Microscopy = FLIM

Generation 3 poly(amidoamine) = G3 PAMAM

Generation 5 poly(amidoamine) = G5 PAMAM

High Performance Liquid Chromatography = HPLC

Matrix Assisted Laser Desorption Ionization-Time of Flight-Mass Spectrometry = MALDI-TOF-MS

2,5-dioxopyrrolidin-1-yl-6-(1-fluorocycloocty-2-ynecarboxamido)hexanoate = MFCO

Nuclear Magnetic Resonance = NMR

5-carboxytetramethylrhodamine = TAMRA

Ultrahigh Performance Liquid Chromatography = UPLC

# ABSTRACT

Multivalent polymers can be used as gene delivery vectors, diagnostics, and therapeutics when they are conjugated with small molecules such as oligonucleotides, imaging agents, and drugs. The inherent random nature of attaching small molecule ligands to a polymer leads to a large mixture of different ratios of small molecules to polymer that can be approximated by one or more Poisson distributions. The variety of ligand to polymer ratios leads to a large difference in hydrophobic character, which can alter various biological properties. This thesis examines methods for isolating precise ratios of small molecules, specifically fluorophores, to a multivalent polymer. The hydrophobicity ratio has been known to effect the polymer's behavior in solution and in cell. The exact effect of this ratio was determined using precise ratio materials isolated. The precise ratio of fluorophores on a polymer is specifically of interest because of the environmental dependence (pH, concentration, salts, etc.) on fluorophore properties. The precise ratios of a fluorophore on a polymer also provides a model system for understanding how changes in hydrophobicity alter a multivalent polymer's biological behavior.

Precise dye-polymer ratios of fluorescein and TAMRA were obtained on an acetylated generation 5 poly(amidoamine) (G5 PAMAM) dendrimer by using semi-preparative reverse-phase high performance liquid chromatography (semi-prep rp-HPLC). The fluorescein-G5 conjugates were obtained by cycloaddition of an azide functionalized fluorescein molecule with a precise ratio of cyclooctyne ligands on a G5 PAMAM dendrimer. The TAMRA-G5 PAMAM conjugates were obtained by direct conjugation and isolation. Both sets of materials were fully characterized by $^{1}H$ NMR, $^{19}F$ NMR, MALDI-TOF-MS, rp-UPLC, fluorescence spectroscopy, and UV-Vis spectroscopy. Another polymer platform was also chosen in order to determine the polymer effects on the photophysical properties of the fluorophore. Amine-terminated G3 PAMAM dendrimers with precise ratios of TAMRA were obtained and fully characterized in order to determine the photophysical properties of the fluorophore in order to observe the polymer's effects on the fluorophore's properties in a controlled manner. Similar absorption and emission spectra were obtained compared to the neutral TAMRA-G5 materials, with increasing ratio having a decrease in fluorescence intensity.

To determine how precise ratios of fluorophores effect biological behaviors such as biodistribution and cell uptake, precise ratios of TAMRA on amine-terminated G5 PAMAM dendrimers were studied in HEK 293A cells. Dendrimers with 2-4 TAMRA were found to have greater uptake than dendrimers with a single TAMRA. Fluorescence Lifetime Imaging Microscopy (FLIM) showed that the different ratios of TAMRA alone was sufficient to change the fluorescence lifetime of the material observed inside cells. In general, the effects of the ratio of TAMRA to G5 on fluorescence lifetime were consistent with environmentally induced lifetime shifts.

Since a typical multivalent polymer used for biological applications has more than just a fluorophore conjugated to it, such as a targeting agent or drug, multiple distributions of small molecules to the polymer will occur. Using the amine terminated precise ratio TAMRA-G5 material, controlling a second distribution of small molecules on a polymer was investigated. Having the same fluorophore ratio while increasing the ratio of the targeting agent or drug allows for biological studies to determine the effect of multivalency on targeting and therapeutic effects without fluorophore ratio convolution. Multiple strategies are discussed along with the advantages and disadvantages of each strategy.

# Chapter 1.

# Introduction

Portions adapted with permission from:

Dr. Mallory A. van Dongen, Casey A. Dougherty, and Prof. Mark M. Banaszak Holl.

*Biomacromolecules*, **15**, 3215-3234 (2014).



## 1.1. Multivalent Polymers for Biological Applications

Multivalent polymers have been explored in biomedical applications to improve the water solubility, biodistribution, targeting ability, and toxicity of typical small molecule treatments.[1,2] Since multivalent polymers possess a high number of reactive sites, multiple copies of oligonucleotides, antibacterial agents, fluorophores, drugs, or targeting agents can be attached.[1-5,6] The size, structure, and surface functionality of multivalent polymers can also be tuned for a specific desired biological application.[2] Multivalent polymers have especially become of interest in the development of theranostic materials. A theranostic is a material employed that can diagnose and treat a disease. A multivalent polymer is an ideal candidate for theranostic materials since it can easily be functionalized with multiple small molecules, including a therapeutic (drug, oligonucleotide, or antibacterial agent) and imaging agent (fluorophore, quantum dot, fluorescent protein, or MRI contrast agent).[7,8]

The presence of an imaging agent on the polymer to impart diagnostic capabilities is important in all biomedical applications, particularly in the development of theranostic materials.[9-11] Conjugating an imaging agent to the polymer for diagnostics provides the ability to noninvasively observe in cells and tissues where the polymer is going, how much polymer is present, and where the polymer is moving over a period of time.[12-14] Typical imaging agents used for diagnostics include organic fluorophores, paramagnetic metal ions, and radiolabeled small molecules.[15,16] Small molecule imaging agents, however, can suffer from high toxicity, non-specificity, and modification limitations due to a lack of functional groups on a small molecule.[17,18] Multivalent polymers can help increase the stability, biocompatibility, and sensitivity of current small molecule

imaging agents, which in turn can provide a better understanding of molecular pathways involved in diseased processes.[19]

There are many synthetic obstacles to overcome before obtaining useful multivalent polymers for biological studies.[1,20] Control over properties such as the molecular weight distribution and the degree of hydrophobicity is essential to predicting and reproducing a polymer's biological behavior.[21-24] Multivalent polymers inherently have a molecular weight distribution, and modification of the polymer produces a large mixture of varying ratios of small molecules to the polymer. A mixture of different ratios of small molecules on a polymer leads to a range of biological behaviors such as biodistribution and pharmacokinetics differences.[25] The difference in biological behavior arises from the multivalent polymer being typically hydrophilic and the small molecules attached being hydrophobic. The combination of the two opposing properties creates a large difference in how hydrophobic the polymer becomes post conjugation based on the ratio of small molecule to polymer.

This dissertation focuses on providing a better understanding of the hydrophobicity ratio on a hydrophilic multivalent polymer. A more detailed analysis of biological behavior of polymers can be obtained by systematically altering the fluorophore ratio on the polymer on a per particle level, meaning every polymer particle in a given sample has the exact same ratio. The precise ratio of a fluorophore on a polymer provides a model that can also be applied to the biological behavior for different ratios of other hydrophobic small molecules to a polymer, such as for drugs and targeting agents. Altering the fluorophore ratio on the polymer provides the ability to observe both the hydrophobicity effects on the polymer's biological behavior and also the fluorophore's photophysical properties. Complete characterization and application of the materials in solution and in cells will be discussed.

## 1.2. The Synthetic Challenges of Using Multivalent Polymers

Typical conjugations of a small molecule to a multivalent polymer with a large number of reaction sites produces an undesired complicated mixture of products.[22,26] A low

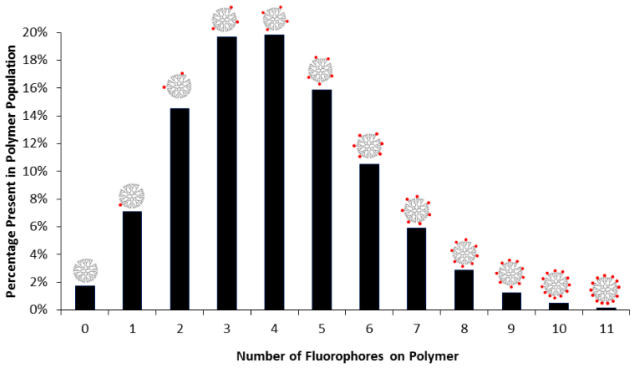


**Figure 1.1.** Example Poisson distribution of a ratio of 4 functional ligands conjugated to a polymer with 128 reaction sites.

average conjugation of a fluorophore, targeting agent, drug, or antibacterial agent to a multivalent polymer with a large number of reaction sites performed under typical reaction conditions leads to a mixture of ratios of small molecule to polymer. The mixture of ratios will resemble a Poisson distribution for the case of a low average conjugation to a multivalent polymer with many reactive sites. For example, when conjugating 4 functional ligands to a polymer with 128 reaction sites, only 20% of the sample actually contains 4 ligands per polymer particle according to a Poisson distribution (Figure 1.1).

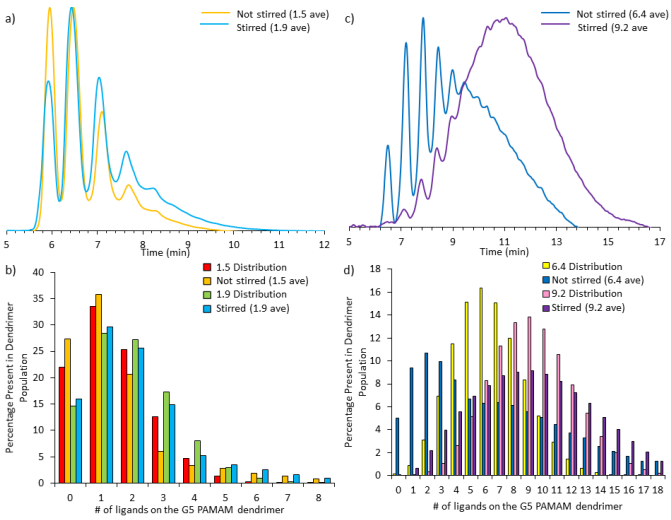


**Figure 1.2.** The variation in ligand-polymer distribution as a function of ligand-polymer ratio and mass transport. a) rp-UPLC traces of 2.5 equiv/dendrimer yielding mean ligand-polymer ratios of 1.5 (yellow) and 1.9 (cyan). b) Distribution obtained from fitting rp-UPLC traces in panel (a) and PD based on mean ligand-polymer ratio. c) rp-UPLC traces of 9 equiv/dendrimer yielding mean ligand-polymer ratios of 6.4 (blue) and 9.2 (purple). d) Distribution obtained from fitting rp-UPLC traces in panel (c) and PD based on mean ligand-polymer ratio.

Poisson statistics describe the ligand distribution in polymer conjugate systems when the materials are synthesized under ideal reaction conditions, such as quick stirring and low concentrations. When ideal conditions are not met, deviations of the Poisson distribution will occur. For instance, when attempting to conjugate an average number of ligands to a polymer under ideal (stirring) and non-ideal (quiescent) conditions, 2 different averages are achieved. As shown in the example of conjugating 2.5 equivalents of 3-(4- (2-azidoethoxy) phenyl) propanoic acid to a generation 5 poly(amidoamine) (G5 PAMAM) dendrimer, averages of 1.9 and 1.5 are achieved for the stirring and quiescent reaction conditions (Figure 1.2a). The distribution of ligand to dendrimer ratios can be resolved using reverse phase ultrahigh performance liquid chromatography (rp-UPLC), and the UPLC trace for each conjugation can be fitted to determine the amount of each ratio in the sample. When the distributions of the stirring and quiescent samples were compared to a Poisson

distribution of the corresponding averages, it can be seen that the quiescent material deviates from the Poisson distribution while the stirred material is in much better agreement with the Poisson distribution (Figure 1.2b). Poisson distribution deviations occur to an even larger degree when conjugating higher averages of ligands to dendrimer, as seen in Figures 1.2c and 1.2d. The effectiveness of mass transport during the reaction is a concern since it can alter, and worsen, the predicted distribution. As is illustrated in Figure 1.2, poor mass transport from non-ideal conditions results in a larger distribution of ligand to dendrimer ratios compared to the Poisson distribution, and the effect becomes more pronounced as the ligand to dendrimer ratio increases.

Multivalent polymers used for a biological application are typically conjugated to more than one hydrophobic small molecule, leading to multiple Poisson distributions.[27-33] For example, when a polymer is reacted with one small molecule and then subsequently reacted with a second small molecule, such as for theranostic materials attaching both a dye and a drug, the resulting distribution is the product of each individual Poisson distribution (Figure 1.3). Figure 1.3 models an average of 4 fluorophores and 5 drugs sequentially conjugated to a polymer with 128 reaction sites. For the ideal Poisson distribution, a total of 196 different species are produced from the double conjugation and only 2.8% of the sample possesses a mean of 4 fluorophores and 5 drugs on the polymer. If the conjugation of the dye and drug to the polymer were performed under non-ideal conditions, as in Figure 1.2, poor mass transport leads to a broader distribution and a larger number of different species.

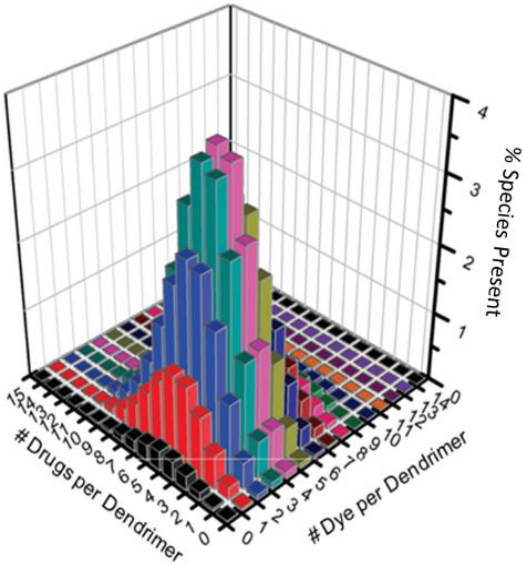


**Figure 1.3.** Example double Poisson distribution of a conjugation of a dye (average of 4) and a drug (average of 5) to a polymer with 128 reaction sites.

Having almost 200 different species with varying ratios of hydrophobicity in a polymer sample is a major issue in biological applications of multivalent polymers because of 1) the inability to reproducibly synthesize a batch of material, 2) the unknown biological behavior from each ratio,

and most notably 3) the large difference in effective concentration of each small molecule, also known as the degree of hydrophobicity, on the polymer.

### 1.3. Hydrophobicity Ratio Effects of Fluorophores on Polymer Behavior

The degree of hydrophobicity has been shown to effect biological observations including cell permeation, biodistribution, and transfection efficiency.[34-37] When the ligand-polymer ratios are present as a mixture, it is difficult to know which ratio is responsible for each biological property observed. A better understanding of how a polymer's hydrophobicity affects its biological behavior is needed in order to most effectively use multivalent polymers to treat and diagnose diseases. To understand how the hydrophobicity ratio affects a polymer's biological behavior, studies have looked at the effects of the local concentration of dye on a polymer and the ratio of dye to polymer as one way to observe hydrophobicity effects.[38-40] Dye-dye interactions have long been understood to impact photophysical properties,[41] so looking at the local concentrations of dye on a polymer can provide information on how small molecules interact with each other and how they can change the polymer's behavior in a cellular environment.

Mier et al. studied the stochastic conjugation of multiple dyes to PAMAM dendrimer including fluorescein, rhodamine, coumarin, and dansyl.[42] With the exception of dansyl, they found that fluorescence intensity decreased with an increasing mean number of dyes due to a combination of a small Stokes shift and the high effective concentration resulting from multiple dyes conjugated to the same polymer core. By way of contrast, dansyl-modified PAMAM gave materials where fluorescence increased the dye-dendrimer ratio, presumably due to the large Stokes shift of 195 nm.

Schroeder et al. examined Cy3 and Cy5 dye optical properties conjugated to G5 PAMAM or G6 PAMAM dendrimer in order to create a new set of materials for biological imaging with enhanced stability and increased accuracy in single molecule imaging.[43] Dendrimer mixtures with an average of 8 Cy5 dyes gave slower photobleaching compared to free dye with a 6 to 10 fold increase in photobleaching lifetime value for G5 PAMAM. The dendrimers with an average of 14 Cy5 dyes on G6 PAMAM showed a ~17x increase in photobleaching lifetime value. Note that the average conjugation numbers used in this case will generate mixtures with <0.5% of the material having zero or one dye, thus helping to ameliorate the most dramatic difference in effective local concentration, and thus photophysical properties, that typically occur as a dye-polymer ratio is varied.

Juliano et al. also studied the effects of the fluorophore to polymer ratio on gene expression using G5 PAMAM dendrimer as the polymer and Oregon Green 488 as the fluorophore.[35] Several ratios of Oregon Green were stochastically conjugated in order to obtain distributions of heterogeneous materials with overall ratios of 0.0, 0.8, 1.75, and 4.0. With an increase in Oregon Green 488 ratio to the dendrimer, an increase in the transfection efficiency of an oligonucleotide expressing a luciferase reporter gene was observed.

Wagner et al. employed stochastically prepared G3 PAMAM dendrimer conjugated to a mean of 1 Alexa Fluor 555 dye to quantify the rate constant of dendrimer uptake in Caplan-1 cells.[44] Following a Poisson distribution, this material should have about 37% of the dendrimer containing no dye, 37% containing one dye, 18% two dyes, and 6% containing three dyes. Interestingly, they did not resolve different species as being present in this case although rp-HPLC is able to achieve this for some ligands.[26,45,46] In this study, both the average uptake rate for the dye conjugate materials and the predicted efflux rate was reported based upon measurements of the mean fluorescence of the mixture. Differences in dye fluorescence as function of conjugation number per dendrimer particle were not addressed as part of the study.

Many studies have been reviewed[41] and shown that the hydrophobicity alters the polymer's cell membrane permeability,[44] transfection efficiency,[35,47-51] colocalization,[43,47] biodistribution,[48] and pharmacokinetics.[53,54] In all the cases discussed, the presence of broad conjugation heterogeneity in the stochastic mixtures of dye polymer conjugates has prevented a detailed understanding of what fraction, or fractions, of the conjugates are providing the observed biological activity.

### 1.4. Controlling Fluorophore Ratio on Polymer: Current Methods in the Field

A number of synthetic strategies to overcome mixtures of ligand-polymer ratios have been employed in order to obtain better defined ratios of fluorophores to polymers. One strategy employed has been a convergent assembly of functionalized dendrons. Convergent synthesis is an

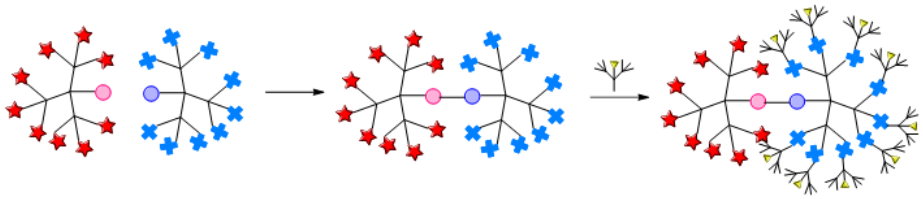

**Figure 1.4.** Example of the use of convergent dendrimers to obtain precise ratios of dyes on a polymer.

interesting strategy to avoid the heterogeneity associated with conjugation to pre-formed polymers, such as divergent dendrimers. An approach making use of three independent dendron units was published by Weck et al. in 2011 (Figure 1.4).[49,50] The functionalizable polymer formed upon linking all three dendrons is designed to have 9 terminal amines and 9 terminal azides on a polymer that contains a theoretical total of 72 terminal groups. The terminal amines and azides can be used to conjugate on a precise ratio of dyes, drugs, or targeting agents. A Poisson distribution would

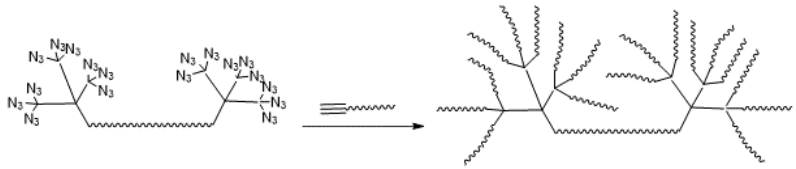

**Figure 1.5.** Schematic of Weck et al. dendron made utilizing Sharpless and Bertozzi click chemistry.

not be observed due to the low number of reaction sites on the polymer and provide precise ratios of the small molecule of choice to the polymer. The final functionalization step employed only 2 equivalents of dye for terminal amine to drive the reaction to completion.

Weck et al. also developed another method to construct generation 2 poly(amide) based dendrons and dendrimer materials using copper catalyzed and copper free click chemistry (Figure 1.5). Click chemistry materials provide the multi-functionality of amine, azide, and alkynes.[51] Applying different click functionalities to dendrons has provided a large step in creating monodisperse dendrimers. The removal of copper from the resulting dendrimers is difficult, and the presence of copper decreases the material's biocompatibility. Because of the metal contamination, cyclooctyne functionalities were added to the dendrons so as to make copper catalysis unnecessary. Dendrimers were formed from dendrons at 100% completion with the cycloocytne and azide functionalities. Completion of reaction for each generation is a major challenge in creating divergent dendrimer materials, including the PAMAM dendrimer commonly used in biological applications.[51] The click-functionalized dendrons were further applied to imaging applications and conjugated with near infrared (IR) cyanine dyes. The fluorescent dendrons clicked together to form monodisperse near IR polymer imaging agents.

Another approach in order to obtain precise ratios of dyes on a polymer is to incorporate the fluorophore in the core of the dendrimer during synthesis.[52] For example, Yin et al. branched off of a fluorophore in order to obtain precisely one dye per polymer particle (Figure 1.6).[53] Using

perylenediimides as the fluorophore of choice and 2-methacryloyloxyethyl acrylate and cystamine as the branches, dendrimers of varying sizes (G1, G2, and G3) were synthesized with one dye in the core having either 8, 16, or 32 cationic charges. It was observed that all peaks from starting materials disappeared in both NMR and MALDI-TOF-MS after excess of 2-methacryloyloxyethyl acrylate was added to the system, indicating 100% completion of the reaction. It was observed that the larger the dendron (with more positive charges), the more enhanced the fluorescence was in aqueous solution. It was also observed that there was higher gene transfection efficiency with increasing dendron generation as well. Zimmerman et al.[54] and Frechet et al.[55] have also looked into using fluorophores at the core of a dendrimer in order to obtain precise dye-polymer ratios. While convergent synthesis and fluorophore at the core prove to be successful at obtaining a specified ratio of dye per polymer, there is a limitation in choice of how many fluorophores can be conjugated to the polymer and there is no opportunity to produce a systematic variation in ratios (n = 1,2,3,…) for one polymer platform.

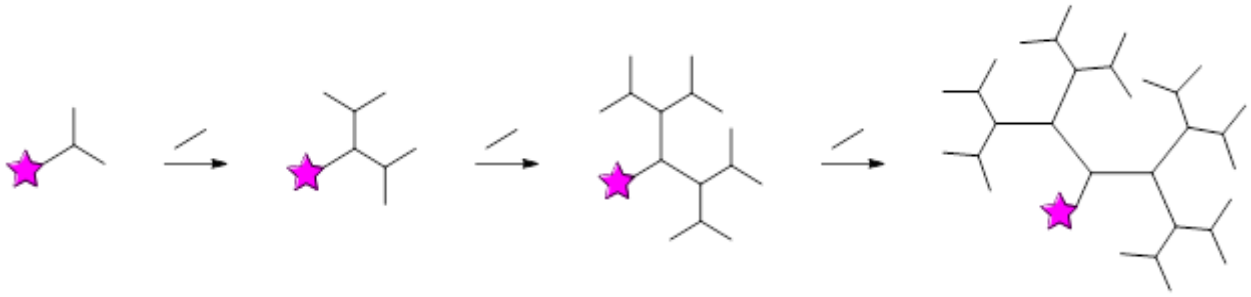

**Figure 1.6.** Synthetic scheme of fluorophore (pink star) as core of dendrimer. Each reaction to add branches leads to a larger generation of dendrimer. Each step has precisely one fluorophore per polymer.

### 1.5. Controlling Fluorophore Ratio on Polymer: Novel Method

In order to obtain systemically varied ratios of dye to polymer, the Banaszak Holl group has developed a unique method to separate out different ratios of ligands to dendrimers using semi-prep rp-HPLC (Figure 1.7). Isolating materials with systematic variation of ratios of click ligands to dendrimer on a G5 PAMAM core has been reported.[26,45] This system is interesting in that dendrimer samples containing precise ratios of ligand to polymer can be isolated even though the divergent G5 dendrimer platform itself retains its normal molecular weight distribution. This suggested two possible paths for obtaining G5 PAMAM dendrimer materials containing precise ratios of dye to polymer: 1) dye conjugation to materials containing precise ratios of click ligand to dendrimer or 2) isolation via direct separation of a stochastic mixture of dye conjugates.

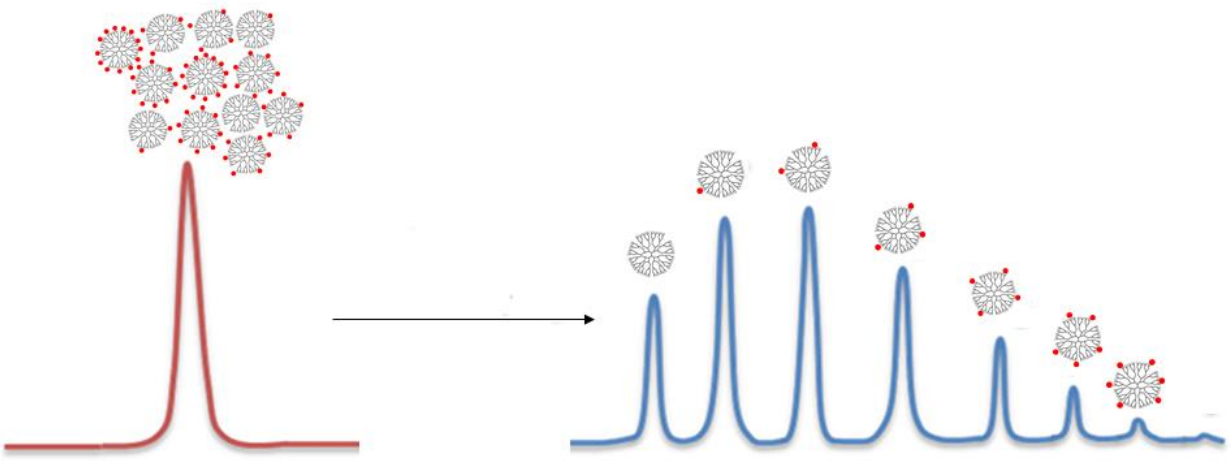

**Figure 1.7.** Isolation of precise ratios of small molecules on a polymer based on small molecule interaction with rp-HPLC column.

### 1.6. Goals of Dissertation

The overall goal of this thesis is to better understand the importance of the dye-polymer ratio in terms of both photophysical and biological properties. This control of the ratio of dye to polymer is important for understanding the biological behavior for polymer-based imaging agents. It also provides a model system for how the ratio of a hydrophobic small molecule (drug, targeting agent, etc.) to a polymer affects the polymer's biological behavior for therapeutic and targeting applications as well. Chapter 2 focuses on the synthesis, isolation, and full characterization of two dye-polymer conjugate platforms using G5 PAMAM dendrimer. Chapter 3 describes the synthesis, isolation, and full characterization a dye-polymer conjugate platform using a G3 PAMAM dendrimer. Chapter 4 uses fully characterized precise ratio dye-polymer G5 PAMAM dendrimers in a biological system to determine how the controlled systematic change in dye ratio alters photophysical properties and biodistribution in cells. Lastly, Chapter 5 looks at the challenges to control not only the one ratio on the polymer, but a second ratio as well on the polymer for potential theranostic and targeted imaging applications.

### 1.7. References

(1) Duncan, R. The dawning era of polymer therapeutics. *Nat Rev Drug Discov* **2003**, *2*, 347-360.

(2) Lee, C. C.; MacKay, J. A.; Frechet, J. M. J.; Szoka, F. C. Designing dendrimers for biological applications. *Nat Biotechnol* **2005**, *23*, 1517-1526.

(3) Roglin, L.; Lempens, E. H. M.; Meijer, E. W. A Synthetic "Tour de Force": Well-Defined Multivalent and Multimodal Dendritic Structures for Biomedical Applications. *Angew Chem Int Edit* **2011**, *50*, 102-112.

(4) Stiriba, S. E.; Frey, H.; Haag, R. Dendritic polymers in biomedical applications: From potential to clinical use in diagnostics and therapy. *Angew Chem Int Edit* **2002**, *41*, 1329-1334.

(5) Sevenson, S.; Tomalia, D. A. Dendrimers in biomedical applications-reflections on the field. *Adv Drug Deliver Rev* **2012**, *64*, 102-115.

(6) Lo, S. T.; Kumar, A.; Hsieh, J. T.; Sun, X. K. Dendrimer Nanoscaffolds for Potential Theranostics of Prostate Cancer with a Focus on Radiochemistry. *Mol Pharmaceut* **2013**, *10*, 793-812.

(7) Wang, Z.; Niu, G.; Chen, X. Y. Polymeric Materials for Theranostic Applications. *Pharm Res-Dordr* **2014**, *31*, 1358-1376.

(8) Krasia-Christoforou, T.; Georgiou, T. K. Polymeric theranostics: using polymer-based systems for simultaneous imaging and therapy. *J Mater Chem B* **2013**, *1*, 3002-3025.

(9) Gao, X. H.; Yang, L. L.; Petros, J. A.; Marshal, F. F.; Simons, J. W.; Nie, S. M. In vivo molecular and cellular imaging with quantum dots. *Curr Opin Biotech* **2005**, *16*, 63-72.

(10) Weissleder, R.; Pittet, M. J. Imaging in the era of molecular oncology. *Nature* **2008**, *452*, 580-589.

(11) Weissleder, R. Scaling down imaging: Molecular mapping of cancer in mice. *Nat Rev Cancer* **2002**, *2*, 11-18.

(12) Li, J. W.; Liu, J.; Wei, C. W.; Liu, B.; O'Donnell, M.; Gao, X. H. Emerging applications of conjugated polymers in molecular imaging. *Phys Chem Chem Phys* **2013**, *15*, 17006-17015.

(13) Weissleder, R.; Ntziachristos, V. Shedding light onto live molecular targets. *Nat Med* **2003**, *9*, 123-128.

(14) Jain, K. K. Nanotechnology in clinical laboratory diagnostics. *Clin Chim Acta* **2005**, *358*, 37-54.

(15) Zhu, Q.; Qiu, F.; Zhu, B.; Zhu, X. Hyperbranched polymers for bioimaging. *RSC Advances* **2013**, *3*, 2071-2083.

(16) Kim, J.-H.; Park, K.; Nam, H. Y.; Lee, S.; Kim, K.; Kwon, I. C. Polymers for bioimaging. *Prog Polym Sci* **2007**, *32*, 1031-1053.

(17) Medintz, I. L.; Uyeda, H. T.; Goldman, E. R.; Mattoussi, H. Quantum dot bioconjugates for imaging, labelling and sensing. *Nat Mater* **2005**, *4*, 435-446.

(18) Resch-Genger, U.; Grabolle, M.; Cavaliere-Jaricot, S.; Nitschke, R.; Nann, T. Quantum dots versus organic dyes as fluorescent labels. *Nat Meth* **2008**, *5*, 763-775.

(19) Moerner, W. E. New directions in single-molecule imaging and analysis. *P Natl Acad Sci USA* **2007**, *104*, 12596-12602.

(20) Characterization of Nanoparticles Intended for Drug Delivery. *Methods Mol Biol* **2011**, *697*, 1-269.

(21) Menjoge, A. R.; Kannan, R. M.; Tomalia, D. A. Dendrimer-based drug and imaging conjugates: design considerations for nanomedical applications. *Drug Discov Today* **2010**, *15*, 171-185.

(22) Mullen, D. G.; Holl, M. M. B. Heterogeneous Ligand-Nanoparticle Distributions: A Major Obstacle to Scientific Understanding and Commercial Translation. *Accounts Chem Res* **2011**, *44*, 1135-1145.

(23) Hakem, I. F.; Leech, A. M.; Johnson, J. D.; Donahue, S. J.; Walker, J. P.; Bockstaller, M. R. Understanding Ligand Distributions in Modified Particle and Particlelike Systems. *J Am Chem Soc* **2010**, *132*, 16593-16598.

(24) Hakem, I. F.; Leech, A. M.; Bohn, J.; Walker, J. P.; Bockstaller, M. R. Analysis of heterogeneity in nonspecific PEGylation reactions of biomolecules. *Biopolymers* **2013**, *99*, 427-435.

(25) Mullen, D. G.; Fang, M.; Desai, A.; Baker, J. R.; Orr, B. G.; Holl, M. M. B. A Quantitative Assessment of Nanoparticle-Ligand Distributions: Implications for Targeted Drug and Imaging Delivery in Dendrimer Conjugates. *Acs Nano* **2010**, *4*, 657-670.

(26) Mullen, D. G.; Borgmeier, E. L.; Desai, A. M.; van Dongen, M. A.; Barash, M.; Cheng, X. M.; Baker, J. R.; Holl, M. M. B. Isolation and Characterization of Dendrimers with Precise Numbers of Functional Groups. *Chem-Eur J* **2010**, *16*, 10675-10678.

(27) Shamay, Y.; Adar, L.; Ashkenasy, G.; David, A. Light induced drug delivery into cancer cells. *Biomaterials* **2011**, *32*, 1377-1386.

(28) Tansey, W.; Ke, S.; Cao, X. Y.; Pasuelo, M. J.; Wallace, S.; Li, C. Synthesis and characterization of branched poly(L-glutamic acid) as a biodegradable drug carrier. *J Control Release* **2004**, *94*, 39-51.

(29) Wang, J. F.; Liu, W. M.; Tu, Q.; Wang, J. C.; Song, N.; Zhang, Y. R.; Nie, N.; Wang, J. Y. Folate-Decorated Hybrid Polymeric Nanoparticles for Chemically and Physically Combined Paclitaxel Loading and Targeted Delivery. *Biomacromolecules* **2011**, *12*, 228-234.

(30) Sharma, A.; Soliman, G. M.; Al-Hajaj, N.; Sharma, R.; Maysinger, D.; Kakkar, A. Design and Evaluation of Multifunctional Nanocarriers for Selective Delivery of Coenzyme Q10 to Mitochondria. *Biomacromolecules* **2012**, *13*, 239-252.

(31) Chandna, P.; Saad, M.; Wang, Y.; Ber, E.; Khandare, J.; Vetcher, A. A.; Soldatenkov, V. A.; Minko, T. Targeted proapoptotic anticancer drug delivery system. *Mol Pharm* **2007**, *4*, 668-678.

(32) Saad, M.; Garbuzenko, O. B.; Ber, E.; Chandna, P.; Khandare, J. J.; Pozharov, V. P.; Minko, T. Receptor targeted polymers, dendrimers, liposomes: Which nanocarrier is the most efficient for tumor-specific treatment and imaging? *J Control Release* **2008**, *130*, 107-114.

(33) Santra, S.; Kaittanis, C.; Perez, J. M. Cytochrome c Encapsulating Theranostic Nanoparticles: A Novel Bifunctional System for Targeted Delivery of Therapeutic Membrane-Impermeable Proteins to Tumors and Imaging of Cancer Therapy. *Mol Pharm* **2010**, *7*, 1209-1222.

(34) Leroueil, P. R.; Hong, S.; Mecke, A.; Baker, J. R.; Orr, B. G.; Banaszak Holl, M. M. Nanoparticle Interaction with Biological Membranes: Does Nanotechnology Present a Janus Face? *Accounts Chem Res* **2007**, *40*, 335-342.

(35) Yoo, H.; Juliano, R. L. Enhanced delivery of antisense oligonucleotides with fluorophore-conjugated PAMAM dendrimers. *Nucleic Acids Res* **2000**, *28*, 4225-4231.

(36) He, C.; Hu, Y.; Yin, L.; Tang, C.; Yin, C. Effects of particle size and surface charge on cellular uptake and biodistribution of polymeric nanoparticles. *Biomaterials* **2010**, *31*, 3657-3666.

(37) Santos, J. L.; Oliveira, H.; Pandita, D.; Rodrigues, J.; Pêgo, A. P.; Granja, P. L.; Tomás, H. Functionalization of poly(amidoamine) dendrimers with hydrophobic chains for improved gene delivery in mesenchymal stem cells. *J Control Release* **2010**, *144*, 55-64.

(38) Selwyn, J. E.; Steinfel.Ji. Aggregation Equilibria of Xanthene Dyes. *J Phys Chem-Us* **1972**, *76*, 762-&.

(39) Lavorel, J. Influence of Concentration on the Absorption Spectrum and the Action Spectrum of Fluorescence of Dye Solutions. *J Phys Chem-Us* **1957**, *61*, 1600-1605.

(40) Valdesaguilera, O.; Neckers, D. C. Aggregation Phenomena in Xanthene Dyes. *Accounts Chem Res* **1989**, *22*, 171-177.

(41) Chen, M. J.; Yin, M. Z. Design and development of fluorescent nanostructures for bioimaging. *Prog Polym Sci* **2014**, *39*, 365-395.

(42) Wangler, C.; Moldenhauer, G.; Saffrich, R.; Knapp, E. M.; Beijer, B.; Schnolzer, M.; Wangler, B.; Eisenhut, M.; Haberkorn, U.; Mier, W. PAMAM Structure-Based Multifunctional Fluorescent Conjugates for Improved Fluorescent Labelling of Biomacromolecules. *Chem-Eur J* **2008**, *14*, 8116-8130.

(43) Kim, Y.; Kim, S. H.; Tanyeri, M.; Katzenellenbogen, J. A.; Schroeder, C. M. Dendrimer Probes for Enhanced Photostability and Localization in Fluorescence Imaging. *Biophys J* **2013**, *104*, 1566-1575.

(44) Opitz, A. W.; Czymmek, K. J.; Wickstrom, E.; Wagner, N. J. Uptake, efflux, and mass transfer coefficient of fluorescent PAMAM dendrimers into pancreatic cancer cells. *Bba-Biomembranes* **2013**, *1828*, 294-301.

(45) Dougherty, C. A.; Furgal, J. C.; van Dongen, M. A.; Goodson, T.; Holl, M. M. B.; Manono, J.; DiMaggio, S. Isolation and Characterization of Precise Dye/Dendrimer Ratios. *Chem-Eur J* **2014**, *20*, 4638-4645.

(46) van Dongen, M. A.; Vaidyanathan, S.; Holl, M. M. B. PAMAM dendrimers as quantized building blocks for novel nanostructures. *Soft Matter* **2013**, *9*, 11188-11196.

(47) Perumal, O. P.; Inapagolla, R.; Kannan, S.; Kannan, R. M. The effect of surface functionality on cellular trafficking of dendrimers. *Biomaterials* **2008**, *29*, 3469-3476.

(48) Seib, F. P.; Jones, A. T.; Duncan, R. Establishment of subcellular fractionation techniques to monitor the intracellular fate of polymer therapeutics I. Differential centrifugation fractionation B16F10 cells and use to study the intracellular fate of HPMA copolymer-doxorubicin. *J Drug Target* **2006**, *14*, 375-390.

(49) Ornelas, C.; Lodescar, R.; Durandin, A.; Canary, J. W.; Pennell, R.; Liebes, L. F.; Weck, M. Combining Aminocyanine Dyes with Polyamide Dendrons: A Promising Strategy for Imaging in the Near-Infrared Region. *Chem-Eur J* **2011**, *17*, 3619-3629.

(50) Ornelas, C.; Pennell, R.; Liebes, L. F.; Weck, M. Construction of a Well-Defined Multifunctional Dendrimer for Theranostics. *Org Lett* **2011**, *13*, 976-979.

(51) Ornelas, C.; Broichhagen, J.; Weck, M. Strain-Promoted Alkyne Azide Cycloaddition for the Functionalization of Poly(amide)-Based Dendrons and Dendrimers. *J Am Chem Soc* **2010**, *132*, 3923-3931.

(52) Zhang, J. D.; Drugeon, G.; L'hermite, N. Synthesis of novel dendrimers incorporating a dye into the core. *Tetrahedron Lett* **2001**, *42*, 3599-3601.

(53) Xu, Z. J.; He, B. C.; Shen, J.; Yang, W. T.; Yin, M. Z. Fluorescent water-soluble perylenediimide-cored cationic dendrimers: synthesis, optical properties, and cell uptake. *Chem Commun* **2013**, *49*, 3646-3648.

(54) Yang, S. K.; Shi, X. H.; Park, S.; Doganay, S.; Ha, T.; Zimmerman, S. C. Monovalent, Clickable, Uncharged, Water-Soluble Perylenediimide-Cored Dendrimers for Target-Specific Fluorescent Biolabeling (vol 131, pg 9964, 2011). *J Am Chem Soc* **2011**, *133*, 13206-13206.

(55) Gilat, S. L.; Adronov, A.; Frechet, J. M. J. Light harvesting and energy transfer in novel convergently constructed dendrimers. *Angew Chem Int Edit* **1999**, *38*, 1422-1427.

# Chapter 2.

# Isolation and Characterization of Precise Dye-Dendrimer Ratios

Reprinted with permission from:

Casey A. Dougherty, Joseph C. Furgal, Dr. Mallory A. van Dongen, Prof. Theodore Goodson III, Prof. Mark M. Banaszak Holl, Dr. Janet Manano, and Prof. Stassi DiMaggio.

*Chemistry- European Journal*, **20**, 4638-4645 (2014).



## 2.1. Introduction

Precise control of dye-polymer ratio has been a major challenge in nanomaterials chemistry.[1-4] For many classes of nanomaterials, there are a large number of functional sites to which a small number of ligands are conjugated. This results in a Poisson distribution of ligand-polymer ratios in the product obtained. For example, a generation 5 poly(amidoamine) (G5 PAMAM) dendrimer with 128 surface sites will generate eight species ranging from 0 to 7 dyes per particle when an average of three dyes is conjugated to the polymer (Figure 2.1). Although deviations from the Poisson distribution can arise from mass transport,[5] as well as site blocking and steric effects,[6] these detailed considerations tend to lead broader, not narrower, distributions. The presence of these distributions complicates

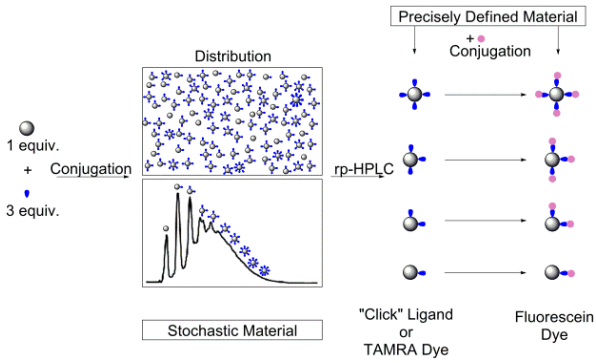


**Figure 2.1.** Outline of procedure for obtaining precise ligand-polymer ratios on a G5 PAMAM dendrimer.

understanding the behavior of these materials and limits their effectiveness for desired applications.

Because nanomaterials containing a Poisson distribution of dye-polymer ratios have a range of photophysical and biodistribution properties, a variety of strategies have been employed to minimize the distribution. A particularly interesting approach for dendrimeric polymers is encapsulation in the internal spaces between the branched arms.[7,8] Dye encapsulation can be tuned depending on concentration, dye structure, and dendrimer structure including generation, length of alkane linker in the core, and end-capping of arms.[7,9-11] Dendrimer structural isomerization can be used to vary the dye hosting capacity.[12] Computer simulations indicate that the dendrimer systems are dynamic and that no static encapsulation volumes exist within the dendrimer arms.[13]

In order to overcome the limitations of encapsulated and stochastically conjugated systems, convergent synthesis methods for dendritic polymers have offered a powerful solution.[14-17] However, convergent synthesis is generally limited to dye-polymer ratios that are multiples of the numbers of dendrimer arms. Convergent strategies are also limited in terms of both dendrimer generation and molecular weight. Alternatively, methods to give a unique conjugation site on the polymer, for example the terminal site of a dendron, have also been employed.[18]

There is a substantial need for advanced fluorescent probes with small dimensions (<10 nm) and well-defined photophysical and biological properties.[19] We desired to develop a general strategy that would allow integer variation of dye-polymer ratios on water soluble, divergent dendrimer platforms. In particular, the goal was to develop materials where the dye-polymer ratio was identical for all particles in the sample (precisely defined), as opposed to an average dye particle ratio made up of a Poisson distribution of materials (stochastic average). Dendrimers synthesized using divergent synthetic methods are generally more defective than convergent materials; however, a greater range of generations, and therefore sizes and molecular weight is available. Acetylated G5 PAMAM dendrimer was selected as a material target because it is large enough to impart aqueous stability to at least ten hydrophobic ligands while it is small enough to escape through vascular pores and disperse through the tissue matrix to reach cells.[20] In addition, it is small enough to be filtered and excreted by the kidney. G5 and G6 PAMAM dendrimers with these properties were recently prepared using stochastic conjugations of Cy3 and Cy5 dyes.[21] The amine-terminated G5 PAMAM dendrimer is of interest because this material, which becomes

positively charged in aqueous solution, is a useful non-viral vector for gene delivery.[22-24] For all of these biological applications, materials with homogenous photophysical and biodistribution properties that also meet the biological criteria discussed above are desired. For this combined set of reasons, we desired to find a solution to obtaining precise ligand-dendrimer ratio materials for divergent, hydrophilic dendrimers.

Recently, we reported isolating materials with systematic variation of 'click ligand'-dendrimer ratio on a G5 PAMAM core.[25] This system is interesting in that dendrimer samples containing precise ligand-particle ratio can be isolated even though the divergent G5 dendrimer platform itself retains its normal molecular weight distribution. This suggested two possible paths for obtaining G5 PAMAM dendrimer materials containing precise dye-particle ratios: 1) dye conjugation to materials containing precise click ligand-dendrimer ratios or 2) isolation via direct separation of a stochastic mixture of dye conjugates. We now report the successful isolation of G5-$(FC)_n$ (n = 1-4) using the click conjugation strategy and G5-$TAMRA_n$ (n = 1-3) using the direct separation of dye conjugates.

## 2.2. Results and Discussion

Conjugation of small numbers of hydrophobic ligands, including click linkers or dyes, to G5 PAMAM dendrimer generates a Poisson distribution of ligand-particle ratios (Schemes 2.1a and 2.2a).[1,2] As highlighted in Schemes 2.1b and 2.2b, the amount of shift induced on a C18 rp-HPLC column by each hydrophobic ligand is substantially greater than the peak width induced by the mass distribution of the dendrimer. The baseline separation achieved for the isolated fractions (Schemes 2.1c and 2.2c) is substantially improved

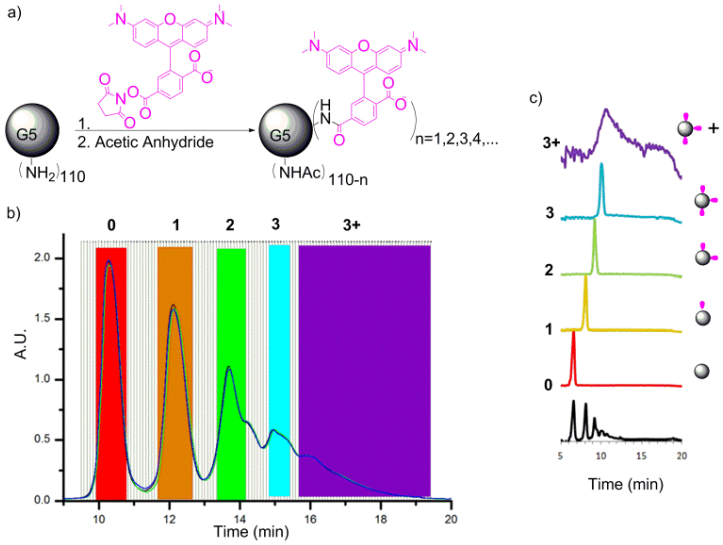


**Scheme 2.1.** Isolation of dendrimer conjugates G5-Ac-$TAMRA_n$ by semi-preparative rp-HPLC. a) Conjugation and full acetylation of G5-Ac-$TAMRA_n$. b) Overlay of semi-preparative rp-HPLC traces for 2 individual runs. Fractions selected for each ligand-dendrimer component are highlighted. c) rp-UPLC traces for the isolated dendrimer conjugates (each trace is baseline corrected and normalized). Both rp-HPLC and rp-UPLC traces detected at 210 nm.

over previous reports[25] because a more highly purified monomer of G5 PAMAM dendrimer was employed from which dimer, trimer, and all trailing generations have been removed by semi-preparative rp-HPLC.[26] The tail end of the G5-Ac-TAMRA stochastic mixture (purple trace in Scheme 2.1c) was combined to generate a mixture of G5-TAMRA conjugates containing ≥ 3 TAMRA dye/dendrimer particle.

rp-UPLC indicates the successful isolation of G5-Ac-TAMRA$_1$, G5-Ac-TAMRA$_2$, and G5-Ac-TAMRA$_3$ as discrete samples containing precise dye-dendrimer ratios within the error of the method (Scheme 2.1c). No shoulders are present on the traces, which would indicate a mixture of ligand-particle ratios, as we have both seen and quantitatively analyzed in previous studies.[1] Each of these samples was also analyzed by $^1$H NMR spectroscopy using methods described previously (Table A.1).[2,25] In order to evaluate relative integral values and estimate the TAMRA-dendrimer ratio, the acetyl methyl peak of the dendrimer at 1.8 ppm was set to a value of 279 protons based on the average number of 93 arms present for monomer-only G5 PAMAM as determined by gel permeation chromatography and titration.[2,26] The 9 aromatic TAMRA protons were used to determine the relative amount of dye. This resulted in an NMR-based estimate of the TAMRA/dendrimer

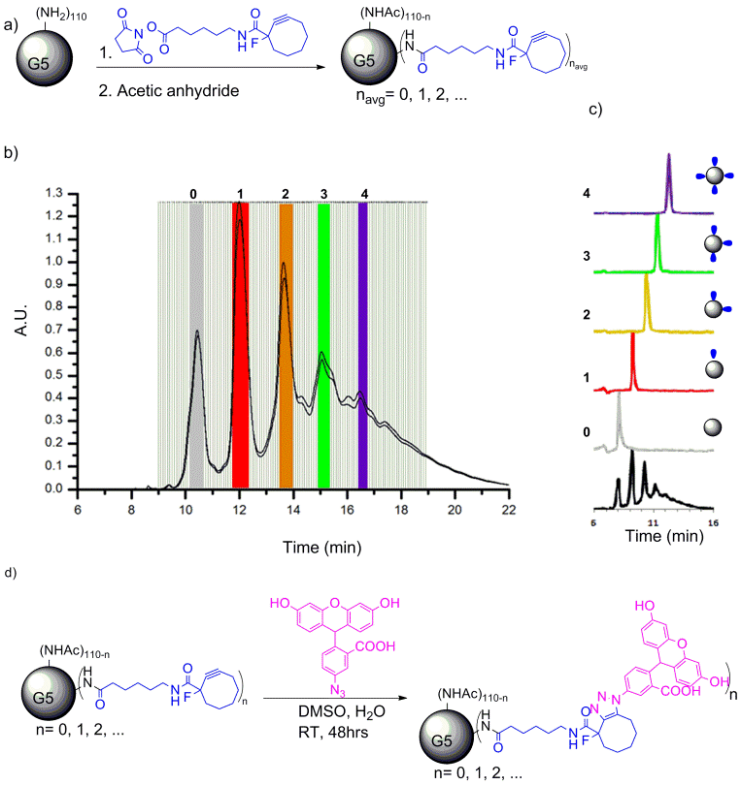


**Scheme 2.2.** Isolation of dendrimer conjugates G5-Ac-MFCO$_n$ by semi-preparative rp-HPLC. a) Conjugation and full acetylation of G5-Ac-MFCO$_n$ . b) Overlay of semi-preparative rp-HPLC traces from 4 individual runs. Fractions selected for each ligand-dendrimer component are highlighted. c) rp-UPLC traces for the isolated dendrimer conjugates (each trace is baseline corrected and normalized). d) Synthesis of precise ratio dendrimer conjugates G5-Ac-Fc$_n$ by 'click' reactions. Both rp-HPLC and rp-UPLC traces detected at 210 nm.

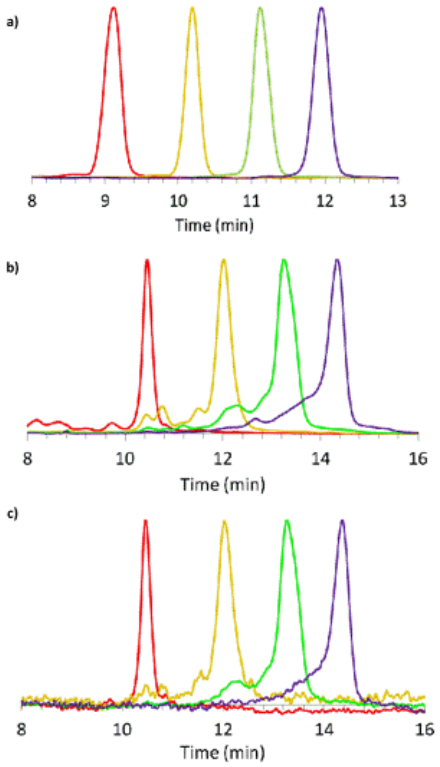


**Figure 2.2.** rp-UPLC traces a) G5-Ac-MFCO$_n$ (n = 1 – 4) at 210 nm b) G5-Ac-FC$_n$ (n = 1 – 4) at 210 nm c) G5-Ac-FC$_n$ (n = 1 – 4) at 491 nm. Sample n= 1 fluorescein (red), 2 (orange), 3 (green), and 4 (purple).

ratios of 0.7, 1.6, 3.1, and 4.4 for the G5-Ac-TAMRA$_1$, G5-Ac-TAMRA$_2$, G5-Ac-TAMRA$_3$, and G5-Ac-TAMRA$_{3+}$ samples, respectively. Unfortunately, the NMR analysis suffers in accuracy from the large difference in the number of dendrimer vs dye protons and the need to use an average value for the number of acetylated protons on the dendrimer.[2,25] In addition, the isolated precise ratio samples derive from only a subset of the full stochastic distribution generated by the synthesis (i.e. the colored bars in Schemes 1b and 2b extend over only part of the peak-width with this fraction decreasing as n increases). This is known error in the use of the GPC and titration data to determine number of dendrimer arms and thus a known error in determination of NMR ratios. This NMR error is also not constant for each sample because the relative size of the collected fraction vs real rp-HPLC peak width varies. For these reasons, we believe the rp-UPLC data provides a better measure of the TAMRA-dendrimer ratio. The full defect structure of the G5 PAMAM dendrimer is subsumed in the rp-UPLC peak width and the peak-to-peak separation is determined by the number of conjugated hydrophobic ligands. Unlike the NMR analysis, this effectively decouples the rp-UPLC assessment of ligand-polymer ratio from the base polymer defect structure. Baseline separation of the click ligand/dendrimer ratios is obtained for the isolated samples (Schemes 2.1c and 2.2c, Figure 2.2a).

In order to generate the G5-Ac-FC$_n$ (n = 1 - 4) samples and drive the click reaction to completion, each G5-Ac-MFCO$_n$ (n = 1 - 4) was allowed to react with a ten-fold excess of azido-flourescein (based on the number of MFCO ligands). rp-UPLC characterization indicated the occurrence of successful click reaction whether the trace was detected at 210 nm (dendrimer backbone absorption) or at 491 nm (FC absorption) (Figure 2.2). For both G5-Ac-FC$_3$ and G5-Ac-FC$_4$ a small amount of n-1 product was detected. Each dye-dendrimer ratio was characterized by $^1$H

NMR spectroscopy (Table A.2). The analysis was directly analogous to that described for the TAMRA case (with the same limitations) and resulted in FC-dendrimer ratios of 1.2, 1.8, 3.3, and 3.0 for the G5-Ac-$FC_1$, G5-Ac-$FC_2$, G5-Ac-$FC_3$, and G5-Ac-$FC_4$ samples, respectively. The MFCO ligand also provides the opportunity to analyze the materials using $^{19}$F NMR spectroscopy.

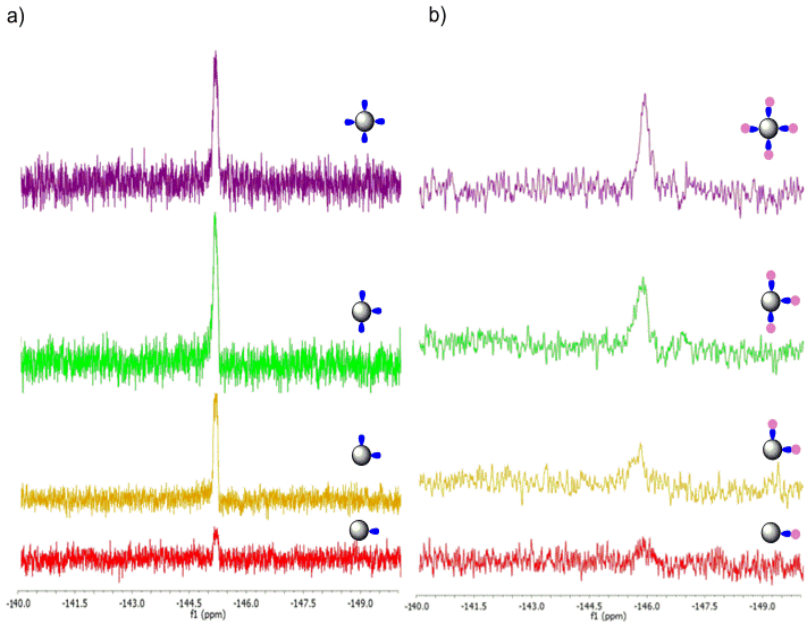


**Figure 2.3.** $^{19}$F NMR of a) pre and b) post click reactions for G5-Ac-$MFCO_n$ and- G5-Ac-$Fc_n$ (n = 1 - 4). Sample n= 1 fluorescein (red), 2 (orange), 3 (green), and 4 (purple).

Spectra for G5-Ac-$MFCO_n$ (n = 1 - 4) ($\delta$ = -145.1 ppm) exhibiting integrated ratios of 1.2, 2.2, 3.2 and 4 are illustrated in Figure 2.3a. After conjugation with azide-FC, the peaks broaden, shift to $\delta$ = -145.8 ppm, and give integrated ratios of 0.8, 1.6, 2.9 and 4. Note that the $^{19}$F NMR analysis does not require the use of average dendrimer arm values but directly measures the number of conjugated arms per dendrimer, independent of structural defects in the polymer scaffold.

The decrease in intensity of the $^{19}$F signal (Figure 2.3b) upon clicking the dye to the cyclooctyne is only observed for dendrimer conjugates. For small molecule click reactions between the MFCO click ligand and fluorescein in the absence of dendrimer, the peak shifts and broadens but does not decrease in intensity (Figure A.1). Since the intensity decrease is unique to the dendrimer conjugates measured in both deuterated DMSO and water, it suggests this change arises from the clicked ligand being internalized into the dendrimer. Hydrophobic dyes can be hosted in the branches of a dendrimer,[7,9,10,13] and it appears the addition of the fluorescein dye favors the fluorinated ligand to be internalized into the dendrimer. Disappearance of the fluorine signal of a small molecule upon encapsulation into a polyglycerol dendrimer has been previously reported.[30] We also observe a decrease in the fluorine signal for clicked small molecules as a stoichiometric amount of the G5 PAMAM dendrimer is added to the solution (Figure A.2) further supporting the

encapsulation hypothesis. MALDI-TOF-MS measurements illustrate an overall increase in molecular weight as function ligand number n for both fluorescein and rhodamine dendrimer samples (Figure A.3). The breadth of the molecular weight distribution for the G5 PAMAM polymer (Figure A.4)[31] limits the value of this approach for accurately determining the number of ligands present on each polymer particle. The defect structure of G5 PAMAM dendrimer results in molecular weight distribution ranging from ~21,000 to 28,000 Da. The click ligand-FC and TAMRA conjugates have a mass of 707 and 527, respectively. As discussed for the NMR analysis, the isolated fractions do not account for the full stochastic distribution of products and will therefore introduce error into attempts using mass spectrometry data to assign ligand-dendrimer ratios. In addition, MALDI-TOF-MS shot noise for these samples is 660 Da, which is similar to the ligand mass. For these reasons, MALDI-TOF-MS is of limited use in assigning numbers of ligand per polymer. MALDI-TOF-MS was of greater use in characterizing precise ratios clusters of G5 PAMAM dendrimers where the mass shifts were ~30,000 Da.[31] The precise ratio G5(G5)n dendrimer clusters were generated using the same precise ratio linker samples illustrated in Scheme 2.2.

Both sets of precise dye-dendrimer ratio samples, G5-Ac-$FC_n$ (n = 1 – 4) and G5-Ac-$TAMRA_n$ (n = 1 – 3, 3+), were characterized in terms of absorption and fluorescent emission. Absorption spectra of G5-Ac-$FC_n$ show the anticipated increase in intensity at 491 nm associated with the fluorescein dye (Figure 2.4), although the extinction coefficient does not vary linearly with concentration (Table A.3). This non-linearity is expected as these samples, although dilute in terms of polymer concentration, hold the conjugated dyes in close proximity to each other and therefore do not meet the criteria for Beer's Law in terms of local dye concentration. These samples of 0.1 mg/mL concentration of polymer

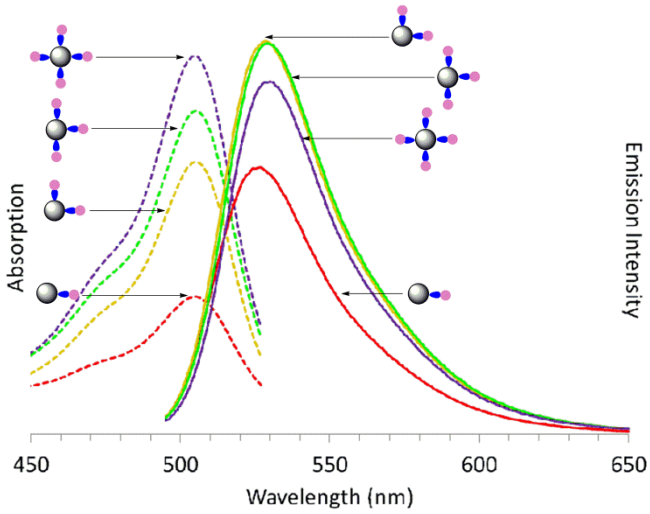


**Figure 2.4.** Absorption (dotted line) and emission (solid line) spectra of precisely defined G5-Ac-$FC_n$ (n = 1 – 4) conjugates (0.1 mg/mL). Sample n= 1 fluorescein (red), 2 (orange), 3 (green), and 4 (purple).

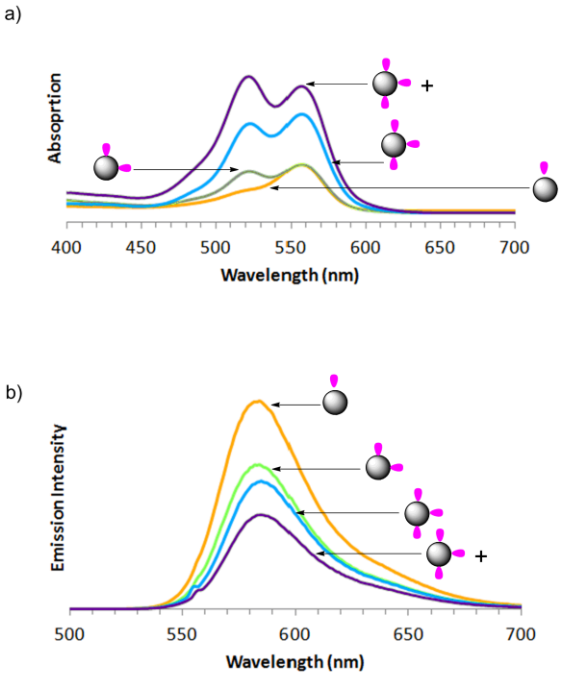


**Figure 2.5.** a) Absorption and b) emission spectra of precisely defined G5-Ac-TAMRA$_n$ (n = 1 – 3, 3+) conjugates (0.1 mg/mL). Samples n= 1 TAMRA (orange), 2 (green), 3 (blue), and 3+ TAMRA (purple).

correspond to approximately 1 x $10^{-6}$ M polymer and dye for G5-Ac-FC$_n$ where n = 1; however for n = 2, 3, and 4 the local concentration of dye is roughly 9, 13.5 and 18 M respectively. The emission spectra, centered at 526 nm, deviate even more strongly from a linear response as a function of n. The emission intensity of G5-Ac-FC$_3$ and G5-Ac-FC$_2$ are identical and the emission for G5-Ac-FC$_4$ is less intense than that observed for n = 2 or 3. These observations belie the general strategy that placing more dye on a dendrimer will result in greater emission intensity. Absorption spectra of the G5-Ac-TAMRA$_n$ samples also deviate from a linear Beer's law response and exhibit a transition from monomer to dimer-like spectral bands that is consistent with the rhodamine small molecule absorption behavior reported as a function of concentration in solution (Figure 2.5a).[32] The spectrum for G5-Ac-TAMRA$_1$ is identical to that observed for unconjugated TAMRA at a dye concentration of 3.0 x $10^{-6}$ M, known to give a monomer absorption spectra. The spectrum for G5-Ac-TAMRA$_2$ exhibits the increase in intensity at 520 nm associated the formation of TAMRA dimers and provides additional evidence that this sample contains a precise ratio of TAMRA-dendrimer particles as opposed to a stochastic distribution. Note the G5-Ac-TAMRA$_2$ sample has a local dye concentration of about 9 M. This overall peak shape is also observed for G5-Ac-TAMRA$_3$ and the 520 nm peak supersedes the 555 nm peak in intensity for the G5-Ac-TAMRA$_{3+}$ sample. The fluorescence emission intensity shows an inverse relationship with the TAMRA-dendrimer ratio (Figure 2.5b).

The absorption spectra of the G5-Ac-TAMRA$_n$ (n = 1 – 3, 3+) samples provide an opportunity to better understand the spectra obtained for fluorescent dye encapsulated in G5 dendrimer. By applying the absorption spectra obtained from the precisely defined samples, we can better

determine how precise encapsulation of small molecules in dendrimers is. A series of spectra are presented in Figure 2.6 at a constant dye concentration of 3.0 x $10^{-6}$ M in water, which would normally result in a monomer absorption signature,[32] and the impact of dye encapsulation into the both G5-$NH_2$ and G5-Ac dendrimer is illustrated. At a 16:1 TAMRA:G5-$NH_2$ ratio, the 520 nm peak is more intense than the 550 nm peak, consistent with the conjugate containing 3+ TAMRA dye per dendrimer and an effective local dye concentration of > 14 M. The 8:1 and 4:1 TAMRA:G5-$NH_2$ ratios have absorption peak shapes similar to the G5-Ac-$TAMRA_3$ conjugate. Interestingly, for all three ratios ranging from 16:1 to 4:1 TAMRA:G5-$NH_2$, the 550/520 nm peak ratio suggests little if any monomer TAMRA is present in solution. The 550/520 nm peak ratio for both the 1:1 and 1:2 TAMRA:G5-$NH_2$ ratios indicate that species containing both 1 and 2 encapsulated dye-dendrimer exist in solution. The intensity of the 550 nm peak definitively indicates that neither the stoichiometric 1:1 ratio, nor even the case where there are two dendrimers for every dye, succeeds in generating a defined sample containing 1 dye encapsulated per dendrimer. Since the absorption behavior of the encapsulated one equivalent of TAMRA dye is different than the conjugated precisely defined material, this also agrees with the claim that precisely one dye is conjugated to the denrimer material previously discussed. It is not until a four-fold excess of dendrimer is employed that the dye absorption

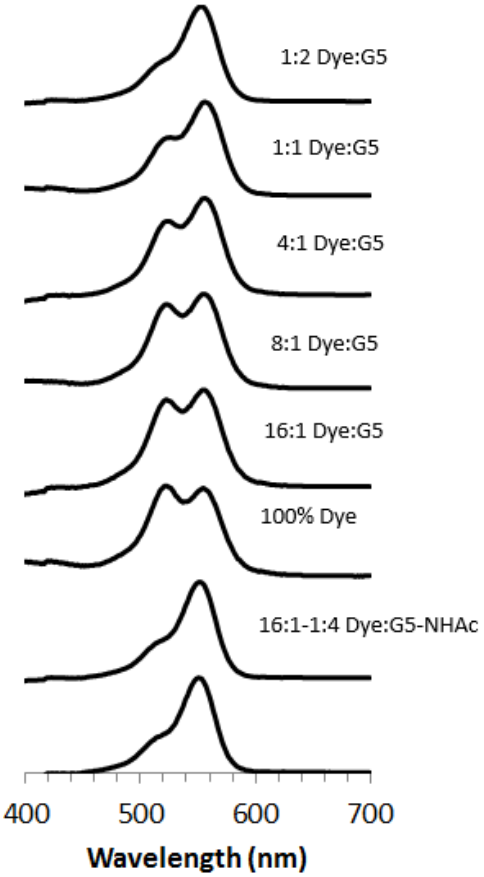


**Figure 2.6.** Absorption spectra of 3.0 x $10^{-6}$ M TAMRA dye in water with varying amounts of G5-$NH_2$ or G5-Ac added to solution. The TAMRA only absorbance is at a concentration where only monomer behavior is present. Once G5-$NH_2$ dendrimer is added the TAMRA becomes encapsulated and shows dimer absorption behavior. The monomer absorption behavior is not seen until a large excess of dendrimer has been added. The addition of G5-Ac does not cause any change in the absorption over the range of 16:1 to 1:4 dye:G5-Ac ratios.

spectrum is consistent with that of monomer dye. The absorption data indicate that attempts to form stoichiometric TAMRA:G5-$NH_2$ ratios using encapsulation actually results in a distribution of ratios, similar to conjugation of small molecules to dendrimers. Similar aggregation phenomena have been reported previously for the interaction of methylene blue with generations 1.5 to 7.5 PAMAM dendrimer terminated with carboxylic acid groups.[11] For this case involving a positively charged dye and negatively charged dendrimer, monomer, dimer, and higher aggregates were observed. For the interaction of neutral G5-Ac with TAMRA, the absorption data for all ratios of TAMRA:G5-Ac, 16:1 to 1:4, only the monomer absorption was observed (Figure 2.6). This suggests that although it is favorable for TAMRA to intercalate into the G5-$NH_2$ dendrimer for a water solution, intercalation into the G5-Ac dendrimer does not occur or is limited to a single dye. This difference is consistent with previous observations that amine-terminated PAMAM dendrimer in water is extended with available volume between the arms if solvent is displaced whereas acetylated PAMAM is a compact, condensed structure with little available volume.[33]

| **# Fluoresceins per G5** | **QY %** | **Short (ps)** | **Long (ps)** | **$R^2$** |
|---|---|---|---|---|
| **1** | 21±2 | 13±2 | 199±40 | 0.94 |
| **2** | 20±1 | 14±1 | 188±19 | 0.98 |
| **3** | 13±1 | 15±1 | 166±21 | 0.99 |
| **4** | 14±1 | 11±1 | 155±9 | 0.99 |
| **Fluorescein** | 79 | 8.5±1.3 | 223±36 | 0.93 |

**Table 2.1.** Fluorescence lifetime kinetic data for G5-Ac-MFCO-$FC_n$ (n = 1 – 4) samples. Data obtained by Joseph C. Furgal.

In order to better understand the trends in the absorption and emission spectra of the fluorescein samples, we also carried out fluorescence lifetime as well as quantum yield measurements. The fluorescence lifetime measurements were carried out with femtosecond fluorescence upconversion spectroscopy, which is very sensitive to small changes in the decay rates. The lifetime data suggests a two component decay with an initial short relaxation time on the order of ~15 ps and a longer decay of approximately ~200 ps (Table 2.1). In addition to this overall decay profile, the G5-Ac-$FC_1$ and G5-Ac-$FC_2$ samples have long decay components close to ~200 ps, while those for G5-Ac-$FC_3$ and G5-Ac-$FC_4$ appeared to have shorter decay components (~165 ps), albeit within the error the measurement. This possible difference between the G5-Ac- $FC_1$/G5-Ac-$FC_2$ and G5-Ac-$FC_3$/G5-Ac-$FC_4$ samples is also supported by a similar trend in the quantum yield.

Combining these two results suggests that the decrease in the quantum yield observed for the G5-Ac-$FC_3$ and G5-Ac-$FC_4$ is related to the increased decay rate of these samples. Physically, the average distance between chromophores is becoming smaller in these samples and the possibility of chromophore-chromophore interactions and promotion of non-radiative pathways in the system is increased. This type of trend has been observed previously for chromophores stochastically attached to dendrimers where the increased loading of the chromophores on the surface of the dendrimer was not linear in terms of the quantum yield or fluorescence lifetime with number of chromophores.[34-36] Attempts to obtain lifetime data for these TAMRA sample were unsuccessful due to poor overlap of the laser emission with the TAMRA absorption. Quantum yield data showed the expected decrease as the number of TAMRA dyes per particle increased (Table A.4).

**2.3. Conclusions**

In summary, two approaches to the formation of G5 PAMAM samples containing precise dye-dendrimer ratios have been presented. The first approach, using direct separation based on dye hydrophobicity, generated a set of TAMRA containing dendrimer, G5-Ac-$TAMRA_n$ (n = 1 – 3, 3+). The second approach, using click chemistry strategy, generated a set of fluorescein containing dendrimer, G5-Ac-$FC_n$ (n = 1 – 4), using a method that could be readily extended to any azide-containing dye or other desired functional group. Both absorption and emission spectra show a strong dependence on the dye/dendrimer ratio.

**2.4. Experimental Methods**

Biomedical grade G5 PAMAM dendrimer was purchased from Dendritech Inc. and purified using rp-HPLC method to obtain G5 dendrimer without trailing generations (G1-G4), dimers, and trimers.[26] Aminofluorescein, trifluoroacetic acid, triethylamine, and acetic anhydride were purchased from Sigma-Aldrich (St. Louis, MO) and used as received. HPLC grade water,acetonitrile, and methanol, as well as dimethyl sulfoxide, hydrochloric acid, sodium azide, and sodium nitrite, were purchased from Fisher-Scientific and used as received. Click-Easy™ MFCO-N-hydroxysuccinimide was purchased from Berry & Associates Synthetic Medicinal Chemistry (Dexter, MI) and used as received. 5-carboxytetramethylrhodamine (TAMRA) succinimidyl ester was purchased from Life Technologies and used as received. Azido-fluorescein was synthesized using a literature protocol.[27] A 500 MHz Varian NMR instrument was used for all $^{1}H$ and $^{19}F$ NMR measurements. $^{19}F$ spectra were referenced to the $^{19}F$ signal of internal

trichlorofluoromethane using a Ξ of 94.0940110. All MALDI-TOF-MS measurements were performed on a Bruker Ultraflex III.

**2.4.1. Synthesis of G5-Ac-MFCO Conjugates (stochastic average).** MFCO-N-hydroxysuccinimide (0.0062g, 0.0240mmol, 4.4 equiv) was dissolved in dimethyl sulfoxide (1.6 mL) and added dropwise to a solution of G5 PAMAM dendrimer (0.1554 g, 0.0055 mmol, 1.0 equiv) in water (34.4 mL). The mixture was stirred at 21 °C overnight and purified by centrifuge washing twice with 1X PBS and 5 times with deionized water. Upon lyophilization a white solid was obtained (61% yield). The white solid (0.0936 g, 0.0033 mmol, 1.0 equiv) was dissolved in anhydrous methanol (17.3 mL), 0.11 mL of triethylamine was added (0.07 mol, 224 equiv) was added, and the mixture stirred for 15 minutes. Acetic anhydride (0.06 mL, 0.60 mmol, 179 equiv) was added slowly until the solution turned clear and the mixture was stirred at room temperature for 4 hours. The solvent was removed, dissolved in 2.5 mL 1X PBS, and purified using centrifuge washing twice with 1X PBS and 5 times with deionized water. Upon lyophilization a white solid was obtained (73% yield).

**2.4.2. Synthesis of G5-Ac-TAMRA Conjugates (stochastic average).** TAMRA succinimidyl ester (0.0102 g, 0.0194 mmol, 3.5 equiv) was dissolved in dimethyl sulfoxide (2.5mL), added dropwise to G5 PAMAM dendrimer (0.1520 g, 0.0054 mmol, 1.0 equiv) dissolved in water (33.7mL), and stirred at 21 °C overnight. The reaction mixture was passed through a sephadex column (GE Healthcare protocol) to remove unreacted TAMRA and lyophilized resulting in a purple solid (78% yield). The purple solid (0.1178 g, 0.0042 mmol, 1.0 equiv) was dissolved in anhydrous methanol (22.4mL), 0.15 mL triethylamine (0.09mol, 224 equiv) was added, and the mixture stirred for 15 minutes. Acetic anhydride (0.08mL, 0.8mmol, 179 equiv) was added slowly until the solution becomes transparent. The mixture was stirred at 21 °C for 4 hours and then solvent was removed The sample was re-dissolved in 2.5 mL 1X PBS and purified using centrifuge washing twice with 1X PBS and 5 times with deionized water. Upon lyophilization, a purple solid was obtained (72% yield).

**2.4.3. Isolation of Precise Ratio G5-Ac-MFCO$_n$ (n = 1 – 4).** rp-HPLC separation was carried out using a Waters Delta 600 HPLC with a C18 silica-based rp-HPLC column (250 x 21.20 mm, 5 μm particles) connected to a C18 guard column (50 x 21.20 mm). The mobile phase consisted of a linear gradient beginning with 95:5 (v/v) water/acetonitrile mixture and ending with 55:45 (v/v) water/acetonitrile over 30 minutes at a flow rate of 16.37 mL/min. The water/acetonitrile mixture

contained 0.10 wt % trifluoroacetic acid (TFA). Elution traces of the dendrimer-ligand conjugate were obtained at 210 nm. A concentration of 30 mg/mL per injection was used. The auto sampler fractions were 5 seconds long and 120 fractions were collected starting at 9 minutes and 1 second. The fractions were then combined to obtain each G5-Ac-$MFCO_n$ sample based upon analysis of the chromatogram in Origin-Pro.

**2.4.4. General procedure for copper-free click reactions.** A 54 mM stock solution of azido-fluorescein in dimethyl sulfoxide was prepared. Each G5-Ac-$MFCO_n$ was dissolved in methanol at a concentration of 2 mM based on MFCO. 10 equivalents of azido-fluorescein per each MFCO were added and the mixture stirred at 21 °C for 48 hours. Following lyophilization the solid was re-dissolved in 2.5 mL 10x PBS, eluted through a sephadex column (GE Healthcare protocol) to remove excess azido-fluorescein. The 3.5 mL total solution was transferred to a 10,000 molecular cutoff dialysis bag (10 mL) and dialyzed versus 2 rounds of 1 L nanopure water. Lyophilization resulted in an orange solid.

**2.4.5. Isolation of Precise Ratio G5-Ac-$TAMRA_n$ (n = 1 – 3, 4+).** General rp-HPLC protocols and solvents were identical to those described for above. A concentration of 25 mg/mL per injection was used. The auto sampler fractions were 5 seconds long and 120 fractions are collected starting at 10 minutes and 1 second. The fractions were then combined to obtain each G5-Ac-$TAMRA_n$ sample based upon analysis of the chromatogram in Origin-Pro.

**2.4.6. Analytical reverse-phase Ultra-high Performance Liquid Chromatography (rp-UPLC).** A Water Acuity system with a C18 silica-based UPLC column (Agilent) was employed with a linear gradient mobile phase beginning with 95:5 (v/v) water/acetonitrile and ending with 55:45 (v/v) water/acetonitrile over 22 minutes at a flow rate of 2.0mL/min. The water/acetonitrile mixture contained 0.10 wt % trifluoroacetic acid (TFA). Elution traces were measured at 210 nm (dendrimer) and 491nm (dye). The instrument was also controlled by Empower 2 software.

**2.4.7. Absorption and Emission Measurements.** Fluorescence and UV-Vis measurements were taken at a concentration of 0.1 mg/mL using a Fluoromax-4 (slit width 2 nm) and a Shimadzu UV-1601 UV/vis spectrometer, respectively. For fluorescein conjugates an excitation of 491 nm and emission of 521 nm was employed. For TAMRA conjugates an excitation of 560 nm and emission of 580 nm was employed.

**2.4.8. MALDI-TOF-MS Measurements.** Three solutions were prepared: 1) 10 mg/mL dendrimer in water 2) 20 mg/mL sinnipinic acid in 1:1 acetonitrile: water and 3) 20 mg/mL sodium

trifluoroacetate in water. These were then combined in a ratio of 10:2:1 of matrix:dendrimer:salt solution. The plate was spotted with 1 uL volumes of solution and allowed to dry. At least 100 scans were averaged per measurement and a smoothing factor of 12 channels was employed.

**2.4.9. Photoluminescence quantum yields ($\Phi_{PL}$)[28]**. $\Phi_{PL}$ were recorded on a Fluoromax-4 (slit width 2.5 nm) and determined by a comparison method between a standard and sample of equal concentration and an excitation wavelength. Fluorescein samples were compared for $\Phi_{PL}$ with a standard solution of fluorescein in water at pH 11 (excitation 490 nm, $\Phi_{PL}$ = 0.70). TAMRA samples were compared for $\Phi_{PL}$ with a standard solution of Rhodamine-B in ethanol (excitation 560 nm, $\Phi_{PL}$ = 0.70). The solutions were diluted to three sets of concentrations each with absorption ranging from 0.02-0.08, to reduce fluorimeter saturation and excimer formation. The total area of emission for each sample and standard was calculated by subtracting out the background signal and calculating the area in Origin. To obtain the best accuracy, the slope of a plot of emission versus absorption was determined and calculated according to equation (1);

$$\Phi_{PL}(x) = \left(\frac{A_s}{A_x}\right)\left(\frac{F_x}{F_s}\right)\left(\frac{n_x}{n_s}\right)^2 \Phi_{PL}(s) \quad (1)$$

where $\Phi_{PL}$ is the quantum yield, A is the absorption at the excitation wavelength, F is the total integrated emission, and n is the refractive index of the solution, which due to low concentration, can be approximated as the refractive index of the solvent. Subscripts x and s refer to the sample and reference, respectively.

**2.4.10. Fluorescence Upconversion Kinetics**.[29] The sample solution was excited with frequency-doubled light from a mode-locked Ti-sapphire laser (Tsunami, Spectra Physics). This produces pulses of approximately 100 fs duration at a wavelength of 400 nm. Our upconversion apparatus also consists of the basic unit of the FOG-100 system (CDP). The polarization of the excitation beam for the anisotropy measurements was controlled with a Berek compensator. The sample cuvette was of 1 mm thick and was held in a rotating holder to avoid possible photo-degradation and other accumulative effects. The horizontally polarized fluorescence emitted from the sample was upconverted in a nonlinear crystal of β-barium borate using a pump beam at 800 nm that was first passed through a variable delay line. The instrument response function (IRF) was determined from the Raman signal of water for 400 nm excitation. Lifetimes were obtained by convoluting the decay profile with the instrument response function. Spectral resolution was achieved by dispersing the upconverted light in a monochromator and detecting it by using a photo-multiplier

tube (Hamamatsu R1527P). The average excitation power was kept at a level below 3 mW to reduce excitation beam response. G5-MFCO-Fluorescein-NHAc and fluorescein samples were set to an absorption of ~0.4 at 400 nm in a 1 mm rotating sample cell. Fluorescence was collected at 515 nm, and compared at the 10 and 250 ps time scales. The fluorescence decay curves were then analyzed using a bi-exponential fitting procedure in Origin 7.0 (Origin Lab). TAMRA samples were not analyzed by fluorescence upconversion techniques due to limitations in the excitation wavelength.

### 2.5. References


(1) Mullen, D. G.; Banaszak Holl, M. M.: Heterogeneous ligand-nanoparticle distributions: a major obstacle to scientific understanding and commercial translation. *Acc. Chem. Res.* **2011**, *44*, 1135-1145.

(2) Mullen, D. G.; Fang, M.; Desai, A.; Baker, J. R.; Orr, B. G.; Banaszak Holl, M. M.: A Quantitative Assessment of Nanoparticle Ligand Distributions: Implications for Targeted Drug and Imaging Delivery in Dendrimer Conjugates. *ACS Nano* **2010**, *4*, 657-670.

(3) Mullen, D. G.; Desai, A. M.; Waddell, J. N.; Cheng, X. M.; Kelly, C. V.; McNerny, D. Q.; Majoros, I. J.; Baker, J. R.; Sander, L. M.; Orr, B. G.; Holl, M. M. B.: The implications of stochastic synthesis for the conjugation of functional groups to nanoparticles. *Bioconjugate Chem.* **2008**, *19*, 1748-1752.

(4) Roglin, L.; Lempens, E. H. M.; Meijer, E. W.: A Synthetic "Tour de Force": Well-Defined Multivalent and Multimodal Dendritic Structures for Biomedical Applications. *Angew. Chem., Int. Ed.* **2011**, *50*, 102-112.

(5) Mullen, D. G.; Borgmeier, E. L.; Fang, M.; McNerny, D. Q.; Desai, A.; Baker, J. R.; Orr, B. G.; Holl, M. M. B.: Effect of Mass Transport in the Synthesis of Partially Acetylated Dendrimer: Implications for Functional Ligand-Nanoparticle Distributions. *Macromolecules* **2010**, *43*, 6577-6587.

(6) Hakem, I. F.; Leech, A. M.; Johnson, J. D.; Donahue, S. J.; Walker, J. P.; Bockstaller, M. R.: Understanding Ligand Distributions in Modified Particle and Particlelike Systems. *Journal of the American Chemical Society* **2010**, *132*, 16593-16598.

(7) Jansen, J. F. G. A.; de Brabander-van der Berg, E. M. M.; Meijer, E. W.: Encapsulation of guest molecules into a dendritic box. *Science* **1994**, *266*, 1226-1229.

(8) Bosman, A. W.; Janssen, H. M.; Meijer, E. W.: About Dendrimers: Structure, Physical Properties, and Applications. *Chem. Rev.* **1999**, *99*, 1665-1688.

(9) Schenning, A.; Peeters, E.; Meijer, E. W.: Energy transfer in supramolecular assemblies of oligo(p-phenylene vinylene)s terminated poly(propylene imine) dendrimers. *Journal of the American Chemical Society* **2000**, *122*, 4489-4495.

(10) Balzani, V.; Ceroni, P.; Gestermann, S.; Gorka, M.; Kauffmann, C.; Vogtle, F.: Fluorescent guests hosted in fluorescent dendrimers. *Tetrahedron* **2002**, *58*, 629-637.

(11) Jockusch, S.; Turro, N. J.; Tomalia, D. A.: Aggregation of Methylene Blue Adsorbed on Starburst Dendrimers. *Macromolecules* **1995**, *28*, 7416-7418.

(12) Puntoriero, F.; Ceroni, P.; Balzani, V.; Bergamini, G.; Vogtle, F.: Photoswitchable dendritic hosts: A dendrimer with peripheral azobenzene groups. *Journal of the American Chemical Society* **2007**, *129*, 10714-10719.

(13) Teobaldi, G.; Zerbetto, F.: Molecular dynamics of a dendrimer-dye guest-host system. *Journal of the American Chemical Society* **2003**, *125*, 7388-7393.

(14) Ornelas, C.; Lodescar, R.; Durandin, A.; Canary, J. W.; Pennell, R.; Liebes, L. F.; Weck, M.: Combining Aminocyanine Dyes with Polyamide Dendrons: A Promising Strategy for Imaging in the Near-Infrared Region. *Chemistry-a European Journal* **2011**, *17*, 3619-3629.

(15) Ornelas, C.; Pennell, R.; Liebes, L. F.; Weck, M.: Construction of a Well-Defined Multifunctional Dendrimer for Theranostics. *Organic Letters* **2011**, *13*, 976-979.

(16) Wangler, C.; Moldenhauer, G.; Saffrich, R.; Knapp, E. M.; Beijer, B.; Schnolzer, M.; Wangler, B.; Eisenhut, M.; Haberkorn, U.; Mier, W.: PAMAM Structure-Based Multifunctional Fluorescent Conjugates for Improved Fluorescent Labelling of Biomacromolecules. *Chemistry-a European Journal* **2008**, *14*, 8116-8130.

(17) Zill, A. T.; Licha, K.; Haag, R.; Zimmerman, S. C.: Synthesis and properties of fluorescent dyes conjugated to hyperbranched polyglycerols. *New Journal of Chemistry* **2012**, *36*, 419-427.

(18) McNerny, D. Q.; Kukowska-Latallo, J. F.; Mullen, D. G.; Wallace, J. M.; Desai, A. M.; Shukla, R.; Huang, B. H.; Holl, M. M. B.; Baker, J. R.: RGD Dendron Bodies; Synthetic Avidity Agents with Defined and Potentially Interchangeable Effector Sites That Can Substitute for Antibodies. *Bioconjugate Chem.* **2009**, *20*, 1853-1859.

(19) Wang, F.; Tan, W. B.; Zhang, Y.; Fan, X. P.; Wang, M. Q.: Luminescent nanomaterials for biological labelling. *Nanotechnology* **2006**, *17*, R1-R13.

(20) Baker, J. R.: Why I believe nanoparticles are crucial as a carrier for targeted drug delivery. *Wiley Interdisciplinary Reviews-Nanomedicine and Nanobiotechnology* **2013**, *5*, 423-429.

(21) Kim, Y.; Kim, S. H.; Tanyeri, M.; Katzenellenbogen, J. A.; Schroeder, C. M.: Dendrimer Probes for Enhanced Photostability and Localization in Fluorescence Imaging. *Biophys. J.* **2013**, *104*, 1566-1575.

(22) Kukowska-Latallo, J. F.; Bielinska, A. U.; Johnson, J.; Spindler, R.; Tomalia, D. A.; Baker, J. R.: Efficient transfer of genetic material into mammalian cells using Starburst polyamidoamine dendrimers. *Proc. Natl. Acad. Sci. U. S. A.* **1996**, *93*, 4897-4902.

(23) Haensler, J.; Szoka, F. C.: Polyamidoamine Cascade Polymers Mediate Efficient Transfection of Cells in Culture. *Bioconjugate Chem.* **1993**, *4*, 372-379.

(24) Tang, Y.; Li, Y. B.; Wang, B.; Lin, R. Y.; van Dongen, M.; Zurcher, D. M.; Gu, X. Y.; Holl, M. M. B.; Liu, G.; Qi, R.: Efficient in Vitro siRNA Delivery and Intramuscular Gene Silencing Using PEG-Modified PAMAM Dendrimers. *Molecular Pharmaceutics* **2012**, *9*, 1812-1821.

(25) Mullen, D. G.; Borgmeier, E. L.; Desai, A.; van Dongen, M. A.; Barash, M.; Cheng, X. M.; Baker, J. R.; Banaszak Holl, M. M.: Isolation and Characterization of Dendrimer with Precise Numbers of Functional Groups. *Chem. Eur. J.* **2010**, *16*, 10675-10678.

(26) van Dongen, M. A.; Desai, A.; Orr, B. G.; Baker, J. R.; Banaszak Holl, M. M.: Quantitative Analysis of Generation and Branch Defects in G5 Poly(amidoamine) Dendrimer. *Polymer* **2013**, *54*, 4126-4133.

(27) Salic, A.; Mitchison, T. J.: A chemical method for fast and sensitive detection of DNA synthesis in vivo. *Proc. Natl. Acad. Sci. U. S. A.* **2008**, *105*, 2415-2420.

(28) Maciejewski, A. S., R., 1986; Vol. 35; pp 59-69.

(29) Varnavski, O. G. I., T. ; Chem. Phys. Lett. , 2000; Vol. 320; pp 688-696.

(30) Lee, H.; Ooya, T.: F-19-NMR, H-1-NMR, and Fluorescence Studies of Interaction between 5-Fluorouracil and Polyglycerol Dendrimers. *J. Phys. Chem B* **2012**, *116*, 12263-12267.

(31) van Dongen, M. A.; Vaidyanathan, S.; Banaszak Holl, M. M.: PAMAM Dendrimers as Quantized Building Blocks for Novel Nanostructures. *Soft Matter* **2013**, *9*, 11188-11196.

(32) Selwyn, J. E.; Steinfeld, J. I.: Aggregation Equilibria of Xanthene Dyes. *J. Phys. Chem.* **1972**, *76*, 762-774.

(33) Kelly, C. V.; Leroueil, P. R.; Nett, E. K.; Wereszczynski, J. M.; Baker, J. R.; Orr, B. G.; Holl, M. M. B.; Andricioaei, I.: Poly(amidoamine) dendrimers on lipid bilayers I: Free energy and conformation of binding. *J. Phys. Chem B* **2008**, *112*, 9337-9345.

(34) Wang, Y.; Xie, X. B.; Goodson, T.: Enhanced third-order nonlinear optical properties in dendrimer-metal nanocomposites. *Nano Lett.* **2005**, *5*, 2379-2384.

(35) Goodson, T. G.: Optical excitations in organic dendrimers investigated by time-resolved and nonlinear optical spectroscopy. *Acc. Chem. Res.* **2005**, *38*, 99-107.

(36) Cho, M. J.; Choi, D. H.; Sullivan, P. A.; Akelaitis, A. J. P.; Dalton, L. R.: Recent progress in second-order nonlinear optical polymers and dendrimers. *Progress in Polymer Science* **2008**, *33*, 1013-1058.

# Chapter 3.

# Generation 3 PAMAM Dendrimer TAMRA Conjugates Containing Precise Dye-Dendrimer Ratios

In collaboration with Prof. Stassi DiMaggio, Dr. Janet Manono, Kristen Davis, Joshua Demuth and Prof. Mark M. Banaszak Holl. This Chapter has been submitted to *Materials Today* (2015).

## 3.1. Introduction

Cationic dendrimers have been extensively explored both as vectors for nonviral gene delivery and carriers in targeted drug delivery.[1-3] In order to image the location of the material in biological environments, a fluorescent dye is often conjugated to the dendrimer scaffold; however, the Poisson distribution of dye-dendrimer ratios resulting from typical stochastic synthesis conditions[4-6] gives rise to a range of photophysical and biodistribution properties that limit interpretation of these experiments.[7]

The experimental problems arising from the distribution of fluorophore to scaffold ratio is widely appreciated for polymers. Many groups have explored strategies to improve the control over fluorophore-dendrimer ratios since the relatively lower polydispersity index (PDI) of dendrimers and/or synthetic methodologies make this class of scaffold attractive for addressing the challenges.[7-14] Approaches include dye encapsulation,[12-14] employing the core of the dendrimer as the dye,[11] and convergent synthesis starting with the dye.[8,9] All of these approaches have particular advantages and limitations.

In our approach, we have stochastically dye-modified the divergently synthesized, commercially available, generation 3 poly(amidoamine) (G3 PAMAM) dendrimer system and employed reverse-phase high performance liquid chromatography (rp-HPLC) to separate the resulting population into the desired precise ratio dye-dendrimer fractions.[4,7,15] Obtaining the precise ratio of dye-G3 dendrimer (i.e. 1, 2, or 3 dyes per particle) using this strategy generates all ratios present in the typical stochastic mixture, allowing us to get better insight into the properties and biological behavior of each ratio. In a recent review article by Sokolova and Epple on synthetic pathways to make nanoparticles fluorescent, conjugating fluorescent dyes to polymer surfaces was touted as

being one of the most efficient ways to achieve fluorescence in a nanoparticle due to the ease of the synthetic process and high fluorescent yield.[16] However, the major disadvantage was the need to ensure excess dye is removed as well as the formation of a polydisperse particle population. [7,16] The desire for a divergent synthesis of a covalently attached fluorescent dye to a polymer platform can also be noted in the need for quality cellular delivery materials such as gene delivery agents. Recently it has been reported that even slight differences in nanoparticle size and surface charge can affect the efficiency and pathway of cellular uptake.[17,18] In addition, the transfection efficiencies of dendrimers have been shown to correlate inversely with hydrophobicity of their surface groups[19] while other studies have shown that the conjugation of a hydrophobic fluorophore to a dendrimer increased the ability to deliver oligonucleotides to the nucleus of a cell.[20] The mechanisms for the molecular size fractionation and dye-hydrophobicity effects remain unknown, however the ability to further analyze the cellular uptake and biodistribution of the nanoparticle would benefit immensely by the introduction of better probes, specifically ones that are precisely controlled with respect to size, molecular weight, and numbers of fluorescent markers.

The isolation and characterization of precise dye-dendrimer ratios (fluorescein and TAMRA) for G5 PAMAM dendrimer has already been reported.[7] Lower generation dendrimers are also of great interest for biological applications because of their reduced cost and, for some applications, preferred size.[21,22] For controlled photophysical and biodistribution properties, it is important to control MW as well dye-dendrimer ratio.[23] Defects expected in G3 PAMAM dendrimers include trailing generations (G1 and G2) as well as G3-G3 dimer, which give a molecular weight range from ~1400 to 14000 Da for the nominally 6909 Da material.[24] We now report the semi-preparative scale purification of commercially available G3-PAMAM dendrimer. The G3 monomer (G3m) material was isolated and employed in the synthesis, separation, and characterization of G3m containing precise ratios of 5-carboxytetramethylrhodamine dye to dendrimer (G3-$NH_2$-$TAMRA_n$ where n = 1, 2, 3, and 4+). The isolated fractions were characterized by $^1$H nuclear magnetic resonance (NMR) spectroscopy, reverse-phase ultrahigh performance liquid chromatography (rp-UPLC), matrix-assisted laser desorption-ionization time-of-flight mass spectrometry (MALDI-TOF-MS), and emission and absorption spectroscopy.

**3.2. Results and Discussion**

In order to prepare materials with uniform photophysical and hydrophobicity properties, one must control both dye-polymer ratio and polymer MW distribution. For the strategy using the divergently synthesized PAMAM polymer described here, the approach must start with purification and characterization of the commercial G3 PAMAM scaffold. Semi-preparative rp-HPLC reveals 3 major components in the as-received commercial sample: trailing generation G2 (2 %), G3m (86 %), and G3-G3 dimer (12 %) (Scheme 3.1a). G2 dimer is also likely present in small amounts and is expected to elute along with the G3m fraction (estimated to be < 0.3% of G3m peak based on the G3m to G3-G3 dimer ratio). Purification via dialysis using a membrane with a 3,500 kDa cutoff successfully removed the lower MW trailing generations; however, similar to the results previously obtained for G5 PAMAM,[25] it does not change the G3m to G3-G3 dimer ratio. We therefore employed semi-preparative rp-HPLC to isolate each major component. Fractions indicated by the colored bars (trailing generation G2 (purple), G3m (red), G3-G3 dimer (blue) were collected and analyzed by rp-UPLC and MALDI-TOF-MS (Scheme 3.1b and Figure 3.1). MALDI-TOF-MS of the isolated fractions shows a change in m/z ratio with MW values of 3550, 6850, and 13100 Da for trailing G2, G3m, and G3-G3 dimer, respectively (Table B.1). We confirmed using MALDI-TOF-MS that the tail on the right side (high MW) of the dimer peak consisted only of dimer and contained no detectable G3-G3-G3 trimer. Thus, the MW distribution is ~3,500-13,000 for the as-received commercial sample. For the materials used in this report, G3 PAMAM purified by

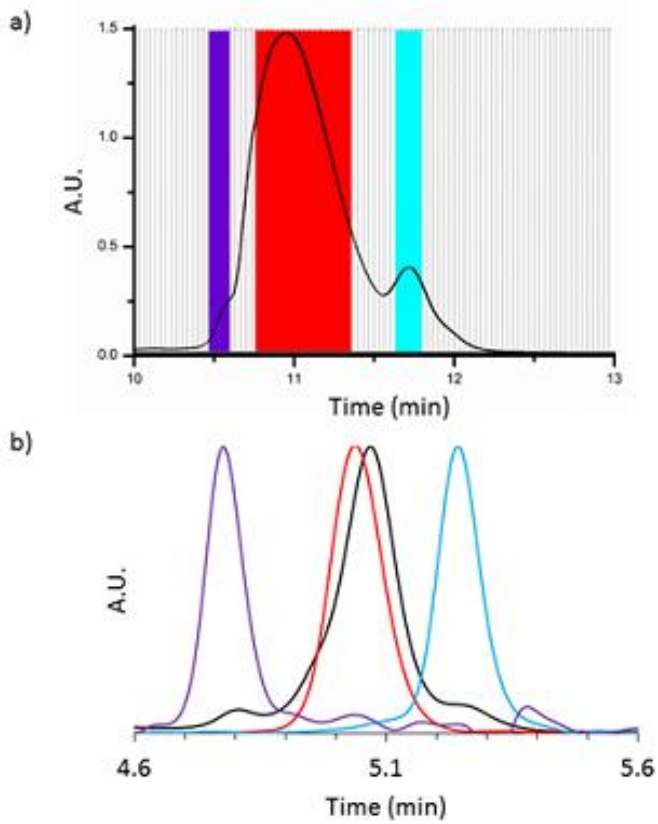


**Scheme 3.1.** Isolation of as-received commercial G3-$NH_2$ PAMAM dendrimer by semi-preparative rp-HPLC. a) Semi-preparative rp-HPLC trace with isolated fractions indicated by colored bars. Data obtained by Joshua Demuth. b) Analytical rp-UPLC traces for each isolated dendrimer fraction: as-received (black), trailing generation G2 (purple), G3 monomer (red), and G3-G3 dimer (blue). Each trace is baseline corrected and normalized.

dialysis (G3d) has a MW distribution of ~6000 to 14000 Da and the G3m material has a MW distribution of approximately 6,000-7,300 Da.

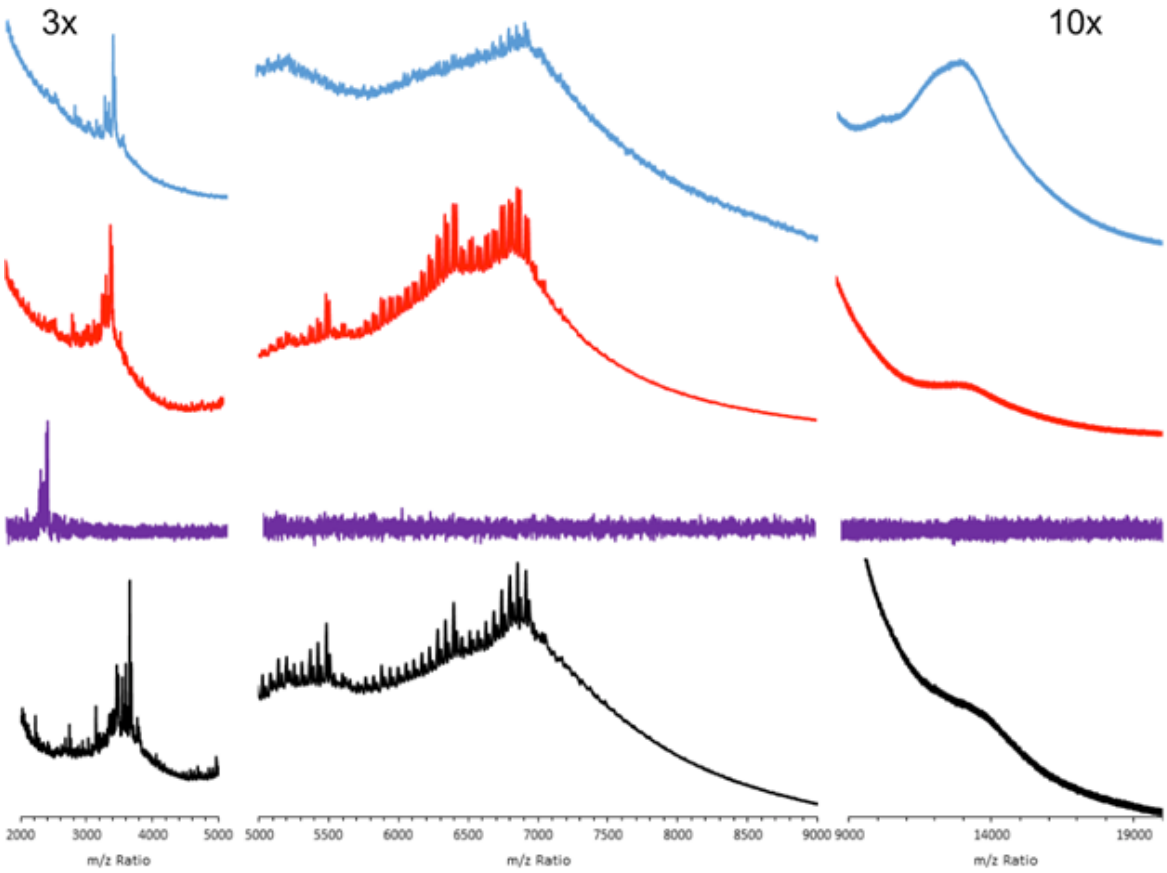


**Figure 3.1.** A stacked plot of MALDI-TOF-MS spectra for G3 PAMAM material fractions: as-received (black), trailing generation G2 (purple), G3m (red), and G3-G3 dimer (blue).

G3-$NH_2$-$TAMRA_n$ samples were prepared using both G3d and G3m materials as the starting scaffold (Scheme 3.2). In both cases, G3-$NH_2$-$TAMRA_n$ (n = 1, 2a, 2b, 3, 4+) was prepared by first performing a stochastic conjugation in which the succinimidyl ester of the TAMRA was allowed to react with an amine group on the dendrimer surface to yield an amide bond. The resulting mixtures (G3d-$NH_2$-$TAMRA_{2.2(avg)}$ and G3m-$NH_2$-$TAMRA_{3.8(avg)}$) were separated using semi-preparative rp-HPLC to isolate fractions containing well-defined dye-dendrimer ratios. The composition and purity of the isolated fractions were determined by $^1H$ NMR spectroscopy, reinjection onto an analytical rp-UPLC column (Schemes 3.2c & 3.2e), and MALDI-TOF MS (Figures 3.2 and Figure B.1).

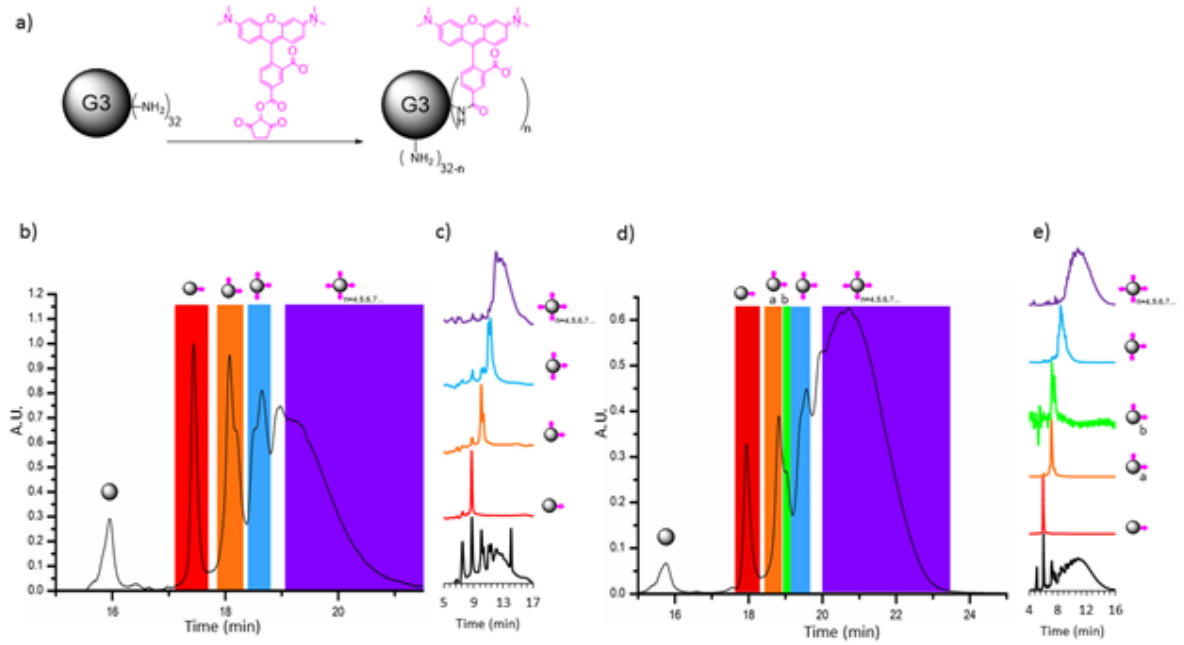


**Scheme 3.2.** Isolation of dendrimer conjugates G3-TAMRA$_n$-NH$_2$ (n = 1, 2a, 2b, 3, 4+) by semi-preparative rp-HPLC. a) Stochastic conjugation to form G3-TAMRA$_n$-NH$_2$. b) Semi-preparative rp-HPLC trace for G3d-TAMRA$_{2.2(avg)}$ material with isolated bands identified. c) Analytical rp-UPLC traces for G3d isolated fractions. d) Semi-preparative rp-HPLC trace for G3m-TAMRA$_{3.8(avg)}$ material with isolated bands identified. e) Analytical rp-UPLC traces for G3m isolated fractions. Analytical rp-UPLC traces are baseline corrected and normalized. All rp-HPLC data obtained by Dr. Janet Manono and Kristen Davis.

In both the semi-preparative (Schemes 3.2b & 3.2d) and analytical rp-HPLC data (Schemes 3.2c and 3.2e) double peaks are observed for orange/green and blue fractions assigned as G3-TAMRA$_2$ and G3-TAMRA$_3$ ratios, respectively. Interestingly, double peaks were not observed for either scaffold for the material assigned as G3-TAMRA$_1$. For the material formed using the G3d scaffold, we hypothesize that the multiple peaks arise from the presence of regioisomers resulting from TAMRA conjugation to different arms on the G3 scaffold (different elution times may occur for two TAMRA conjugated to the same major branch as opposed two TAMRA being conjugated to different branches) or from the presence of dye conjugated to both G3 monomer and G3-G3 dimer (different elution times result from the difference in MW between the G3m and G3-G3 dimer scaffolds). We have not previously observed such effects when separating G5-Ac-TAMRA$_n$ or G5-NH$_2$-TAMRA$_n$;[4,7,15] however, the peak width of G3-NH$_2$ is about 1.4 times narrower than G5-NH$_2$ due to the approximately four-fold difference in MW between the generations. The

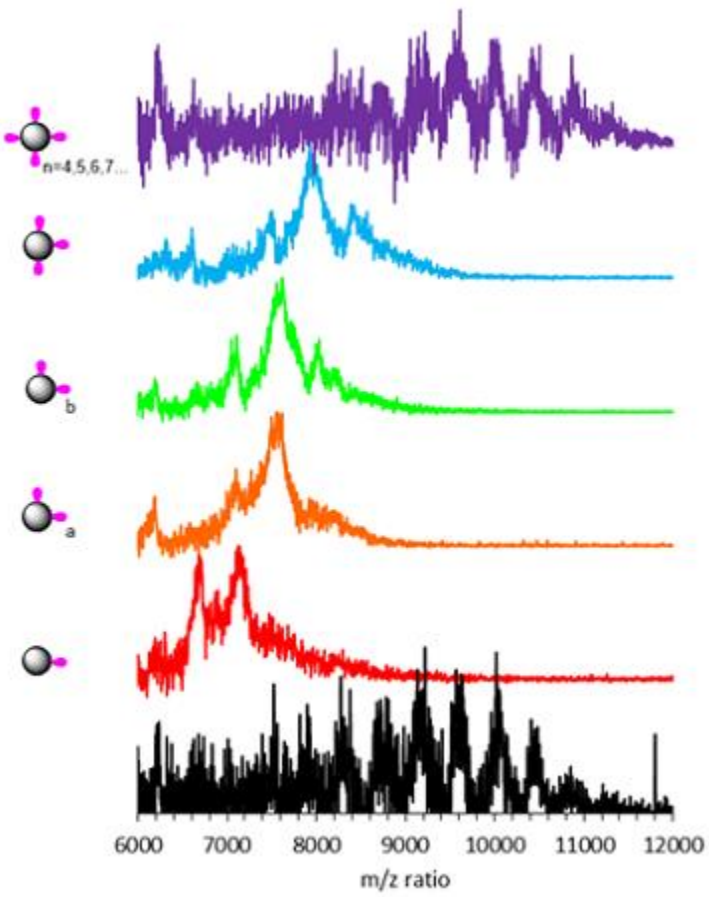


**Figure 3.2.** A stacked plot of MALDI-TOF-MS spectra for G3m-$NH_2$-$TAMRA_{3.8(avg)}$ (black) and G3m-$NH_2$-$TAMRA_n$ (n = 1, 2a, 2b, 3, 4+) conjugates.

observations that i) the double peaks were still observed for the G3m scaffold and ii) no peak splitting was observed for either scaffold for G3-$TAMRA_1$ supports the hypothesis that the peaking splitting arises from the presence of regioisomers. In order to further test the physical origin of the peak splitting, we isolated fractions n = 2a and n = 2b for the G3m scaffold (Scheme 3.2d) and characterized them using rp-UPLC, MALDI-TOF-MS, and $^1$H NMR, absorption, and fluorescence spectroscopies. Although there was a difference in retention time in the UPLC (Scheme 3.2e), the average number of TAMRA as determined by $^1$H NMR spectroscopy (2a = 2.0; 2b = 2.1) and similar MW as measured by MALDI-TOF-MS (2a = 7620; 2b = 7650) support the assignment of both peaks as resulting from G3m-$TAMRA_2$ material. As expected for regioisomers, the emission (Figure 3.3a) and absorption spectra (Figure 3.3b) for 2a and 2b are somewhat different; however, they are more similar to each other than they are to the spectra for G3m-$TAMRA_1$ or G3m-$TAMRA_3$. The ability to resolve dye regioisomers for G3d and G3m because of narrower scaffold MW distribution is consistent with ability to resolve the different TAMRA/dendrimer ratios for the G3-$NH_2$-$TAMRA_{n(avg)}$ and G3-$NH_2$-$TAMRA_{4+}$ materials by MALDI-TOF-MS (Figures 3.2 and Figure B.1). By way of contrast, the different ratios of G5m-$TAMRA_n$ were not resolvable by mass spectroscopy and the regioisomers present were not resolved.[7] The resolution of the various dye-dendrimer ratios by MALDI-TOF-MS provides important new proof that the isolation protocols presented here, and

previously published,[7] is successful in providing materials with a single dye-dendrimer starting from commercially available, divergently synthesized dendrimer material.

$^1$H NMR spectroscopy measures mean dye-dendrimer ratios and is routinely used to confirm stochastic averages for conjugation reactions[4,5,7,15,26] as well as to confirm the mean number of ligand-dendrimer present for sample fractions isolated using rp-HPLC.[4,7,15] The accuracy of this approach is limited by the dispersion of dendrimer MW, which generates a variation in number of protons present on the dendrimer scaffold. In order to provide the NMR estimate of the number of TAMRA-dendrimer, the number of terminal protons had to be determined for G3d and G3m by titration of each scaffold. Titration indicated a mean of 30 and 25 $-NH_2$ end groups for G3d and G3m, respectively out of the 32 theoretically possible for G3 PAMAM. Using approaches previously developed to quantify the number of non-exchangeable internal protons present for G5 PAMAM,[5] it was determined that the G3d and G3m material contained means of 466 and 382 of such protons, respectively. These values were employed to determine the mean TAMRA-G3d and TAMRA-G3m ratios from $^1$H NMR spectra. Integration of the TAMRA peaks present in the $\delta = 6.5 - 8.5$ ppm region (9 protons) and the G3 PAMAM peaks from $\delta = 2.0–3.7$ ppm (466 or 382 protons) was used to determine the mean values of G3d-TAMRA$_{2.2(avg)}$ and G3m-TAMRA$_{3.8(avg)}$ for the as-prepared stochastic mixtures.

Assuming the 25 $-NH_2$ end groups for G3m arise from the presence of missing arm defects,[23] and using the measured MW of 6850 Da for G3m from MALDI-TOF-MS and NMR integration value, a MW of 8423 Da is predicted for G3m-$NH_2$-TAMRA$_{3.8(avg)}$. The measured MALDI-TOF-MS value is 9184 Da, which is within 8% error of the calculated estimate. A similar analysis for G3d-$NH_2$-TAMRA$_{2.2(avg)}$ gives a predicted MW of 7780 Da, which is within 9% of the measured mass of 8520 Da. Analysis of NMR integrations also provided the mean number of TAMRA for each isolated fraction and gave ratios of 0.8, 1.9, 2.0, 2.9, and 6.0 for G3m-$NH_2$-TAMRA$_n$ (n = 1, 2a, 2b, 3, and 4+), respectively. (Table B.2). A similar analysis of the $^1$H NMR integrations for G3d-$NH_2$-TAMRA$_n$ (n = 1, 2, 3, and 4+) gave ratios of 0.8, 2.4, 3.3, 4.6, respectively (Table B.3). The accuracy of this analysis is limited because each fraction does not contain the full MW distribution of the G3m (Scheme 3.1b) or G3d material. Instead, a subset of the full distribution was obtained for each fraction as illustrated in Schemes 3.2b & 3.2d, and thus the assignment of a mean of 466 (G3d) or 382 (G3m) internal protons for the calculation of the ratio is approximate in each case.

The increased number of TAMRA per dendrimer will result in an increase of molecular weight of 414 Da per dye conjugated. The molecular weight of each G3m-$NH_2$-$TAMRA_n$ isolated fraction (Scheme 3.2d) (n = 1, 2a, 2b, 3, and 4+) was measured using MALDI-TOF-MS. The average masses were 7190, 7620, 7650, and 7980 Da for n = 1, 2a, 2b, and 3, respectively (Figure 3.2). The observed peak-to-peak mass shifts observed for n = 4+ and for G3m-$NH_2$-$TAMRA_{3.8(avg)}$ are roughly 420 and 450 Da, respectively in reasonable agreement with varying amount of TAMRA present for these two materials. Similar good agreement of 434 and 420 Da was observed for the peak to peak-to-peak mass shifts for n = 4+ and for G3d-$NH_2$-$TAMRA_{2.2(avg)}$ (Figure B.1). Using the MALDI-TOF-MS molecular weight difference between the G3m-$TAMRA_n$ (n = 1-3) samples and the G3m-PAMAM, it can be estimated that the TAMRA/dendrimer ratios corresponding to the n = 1, 2a, 2b, and 3 samples are 0.8, 1.9, 1.9, and 2.7, respectively. A similar analysis for the G3d-$TAMRA_n$ (n = 1-3) samples gives TAMRA-dendrimer ratios corresponding to 0.7, 1.8, and 2.8, respectively. The use of MALDI-TOF-MS to assign these ratios suffers from the same fundamental problem as the NMR analysis. Assigning the difference of the G3m-$TAMRA_n$ and G3m mass as resulting from a mass change due to TAMRA conjugation is approximate because only a fraction of the G3m molecular weight distribution is obtained during isolation of G3m-$TAMRA_n$. This means that an indeterminate convolution of the change in G3m mass distribution is present in the MALDI-TOF-MS determined ratios. UPLC does not have the weakness of sampling only a fraction of the peak width distribution when assigning the TAMRA-dendrimer ratio. In this case, the full MW distribution, albeit a different one than the G3m starting material, is included in the analysis. For these reasons, we believe UPLC is the most accurate method for determining the TAMRA-dendrimer ratio for these materials.

Studies were also carried out to examine the impact of the dye to polymer ratio on the absorption and emission spectra. The absorption spectra of G3m-$NH_2$-$TAMRA_n$ (n = 1, 2a, 2b, 3, 4+) show an increase in intensity at 520 nm and 560 nm (Figure 3.3b). Although these samples are dilute in terms of polymer concentration (~$10^{-5}$ M), the extinction coefficient does not show a linear relationship between absorption value and concentration as the conjugated dyes are held in close proximity to each other and do not follow Beer's Law.[7,27,28] The absorption spectrum for G3-$TAMRA_{2-4+}$ shows the classic pattern intensity observed for J-aggregate TAMRA dimers,[27,28] despite being at a total concentration of dye in solution that is expected to give a monomer absorption profile (1.4x$10^{-5}$ M). The effective "local dye concentration" for the TAMRA dye held

in close proximity on the dendrimer is about 0.3 M for G3-TAMRA$_2$. The observation of the J-aggregate absorption pattern provides independent confirmation that two or more dye molecules are present on the dendrimer. We also note that the absorption patterns observed for G3m- NH$_2$-TAMRA$_3$ and G3- NH$_2$-TAMRA$_{4+}$ samples are not simple additions of monomer and dimer spectra and that more complicated absorption processes result when three or more TAMRA are held in close proximity (Figure 3.3c and 3.3d). A similar set of data was obtained for of G3d-NH$_2$-TAMRA$_n$ (n = 1, 2a, 2b, 3, 4+) and is illustrated in Figure B.2.

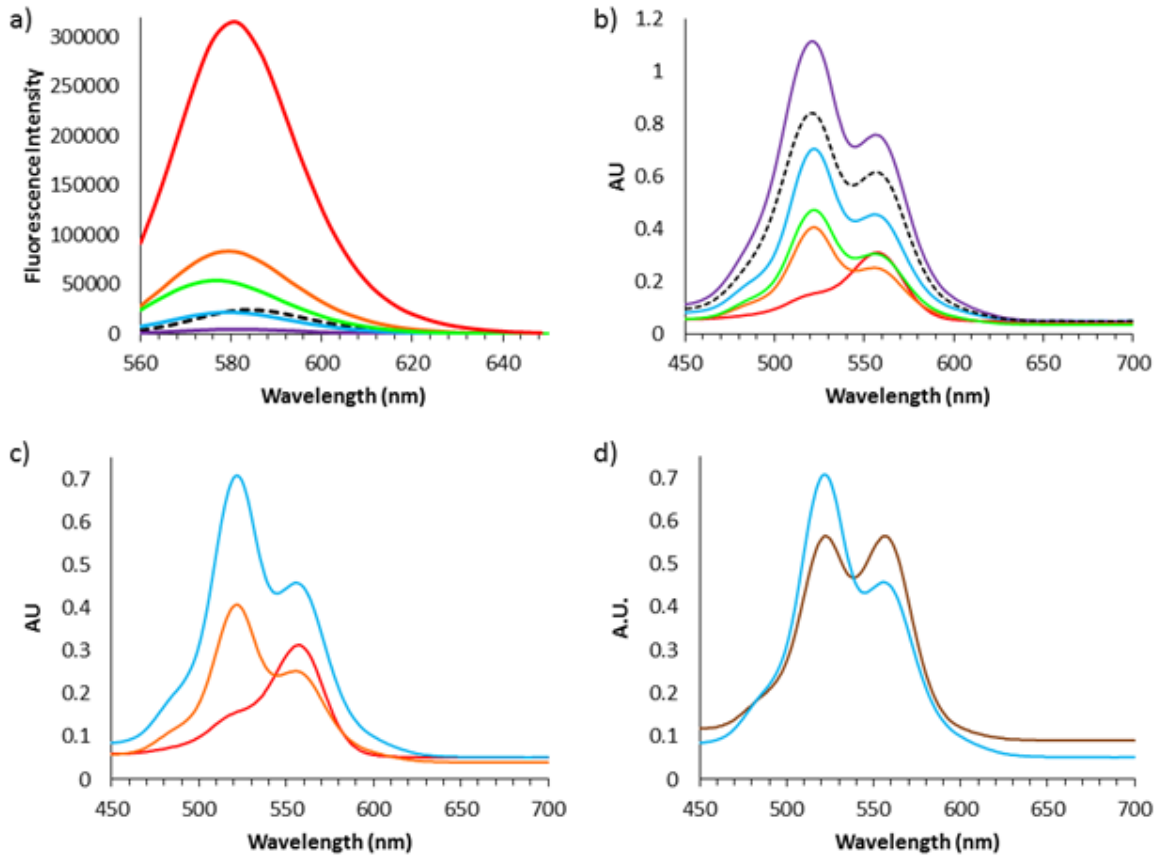


**Figure 3.3.** a) Emission and b) absorption spectra of G3m-TAMRA$_n$-NH$_2$ (n = 1, 2a, 2b, 3, 4+) conjugates at 1 x $10^{-5}$ M; 1 TAMRA (red), 2a (orange), 2b (green), 3 (blue), 4+ (purple), and average (black). c) Absorbance of TAMRA n = 1, 2, and 3 at a concentration of 3 x $10^{-5}$ M. d) Absorbance of n=3 (blue) and an equimolar mixture of n = 1 and n = 2 (brown).

The emission spectra centered at 580 nm decrease in intensity with concentration, exhibiting the largest degree of quenching as the ratio of dye-polymer increases from 1 to 2 (Figure 3.3a). These data indicate that for a stochastic sample the optimal mean value of n for TAMRA dye on G3 PAMAM to obtain highest degree of average fluorescence is about 1.2 (Figure B.3). This value is

obtained by considering the weighted average of emission for all G3 components of a stochastic distribution including n = 0.

### 3.3. Conclusions

In summary, commercially available G3 PAMAM dendrimer was purified by dialysis to remove trailing generations (G3d) and by semi-preparative rp-HPLC to remove trailing generations and oligomers (G3m). The direct conjugation of TAMRA to G3d and G3m resulted in a stochastic mixture that was separated into precise ratios of dye to dendrimer yielding G3-$NH_2$-$TAMRA_n$ conjugates (n = 1 to 3). With these materials, we were able to measure the relative absorption and emission properties and directly relate these properties to the number of dye per polymer particle. Absorption increased with increasing n and emission decreased with increasing n. The absorption spectra also showed distinctive TAMRA dimer behavior for dye/dendrimer ratios greater than one. $^1$H NMR spectroscopy and MALDI-TOF-MS provided valuable information for characterization of TAMRA to dendrimer ratios but were noted to suffer from the need to approximate key values employed in the ratio determination. Therefore, rp-UPLC was determined to be the most reliable for determining dye/dendrimer ratio.

### 3.4. Experimental Methods

Biomedical grade Generation 3 PAMAM dendrimer was purchased from Dendritech Inc. and purified by dialysis. 5-carboxytetramethylrhodiamine (5-TAMRA) was purchased from Life Technologies and used as received. HPLC grade water, HPLC grade acetonitrile, and deuterium oxide were purchased from Fisher-Scientific and used as received. A 500 MHz Varian NMR instrument and deuterium oxide solvent were used for all $^1$H NMR measurements. All MALDI-TOF-MS measurements were performed using a sinapinic acid/sodium trifluoroacetate matrix on a Bruker Autoflex Speed MALDI MS.

**3.4.1. Isolation of G3 PAMAM monomer (G3m).** Semi-Preparative rp-HPLC was performed on Waters Delta 600 HPLC system equipped with a Waters 2998 photodiode array detector, a Waters 2707 autosampler, and Waters Fraction collector III. The instrument was controlled by Empower 2 software. For analysis of the conjugates, a C18 silica-based RP HPLC column (250 × 10.0 mm, 300 Å) connected to a C18 guard (10×10 mm) was used. The mobile phase for elution of the conjugates was a linear gradient beginning with 95:5 (v/v) water/acetonitrile (ACN) and ending

with 55:65 (v/v) water /ACN over 18 min at a flow rate of 12.00 mL/min. Trifluoroacetic acid (TFA) at 0.10 wt % concentration in water or ACN was used as a counter ion to make the dendrimer surfaces hydrophobic. The conjugates were dissolved in the mobile phase (water with 0.1% TFA). The injection volume was 910 µL with a sample concentration of approximately 15 mg/mL. Detection of eluted samples was performed at 210 nm.

**3.4.2. Conjugation of 5-TAMRA to G3 PAMAM dendrimer.** 6.35 mL of 5-TAMRA (1 mg/mL DMSO) was added dropwise to a solution of G3 PAMAM dendrimer monomer (20.40 mg, $3.0 \times 10^{-6}$ mol) in 0.1 M $NaHCO_3$ (8.0 mL) over a period of 2 hrs by a syringe pump. The reaction mixture was left stirring at 20 ºC for 24 hrs. The product was purified by Sephadex G-25 column eluted with MilliQ water. The first band collected was dialysed with a 3,500 MWCO membrane cassette against MilliQ water for three days, exchanging washes every two hours. The purified dendrimer conjugate was lyophilized for three days to yield a red powder material (20.3 mg, 80%).

**3.4.3 Isolation of Precise Dye-Dendrimer Ratios.** The rp-HPLC was identical to that described above. For isolation of the conjugates, a C5 silica-based rp-HPLC column (250 × 10.0 mm, 300 Å) connected to a C5 guard (10×10 mm) was used. The mobile phase for elution of the conjugates was a linear gradient beginning with 100:0 (v/v) water/acetonitrile (ACN) and ending with 20:80 (v/v) water/ACN over 30 min at a flow rate of 2.75 mL/min. Trifluoroacetic acid (TFA) at 0.14 wt % concentration in water as well as in ACN was used as a counter ion to make the dendrimer surfaces hydrophobic. The conjugates were dissolved in the mobile phase (90:10 water/ACN). The injection volume was 500 µL with a sample concentration of approximately 5 mg/mL, and the detection of eluted samples was performed at 210 and 547 nm.

**3.4.4 Analytical rp-UPLC.** An analytical Waters Acquity UPLC (C18 silica-based column) controlled by Empower 2 software was employed to analyze G3-TAMRA conjugates for purity. A linear gradient mobile phase was employed beginning with 95:5 (v/v) water/acetonitrile and ending with 55:45 (v/v) water/acetonitrile over 22 minutes at a flow rate of 2.0 mL/min. Trifluoroacetic acid (TFA) at 0.14 wt % concentration in water as well as in ACN was used as a counter ion to make the dendrimer surfaces hydrophobic. The injection volume was 3 µL with a sample concentration of approximately 1 mg/mL, and the detection of eluted samples was performed at 210 nm.

**3.4.5. Emission Measurements.** Fluorescence measurements were taken at a concentration of 1.0 x $10^{-5}$ M using a Fluoromax-4 spectrometer. Excitation of 520 nm and emission of 580 nm was used with a slit width of 2 nm for all measurements taken.

**3.4.6. Absorption Measurements.** A Shimadzu UV-1601 UV/vis spectrometer was used for all absorption measurements. Studies used a concentration of 1.0 x $10^{-5}$ M solution and slit width of 2.0 nm.

**3.5. References**


(1) Sevenson, S.; Tomalia, D. A. Dendrimers in biomedical applications-reflections on the field. *Adv Drug Deliver Rev* **2012**, *64*, 102-115.

(2) Mintzer, M. A.; Simanek, E. E. Nonviral Vectors for Gene Delivery. *Chem Rev* **2009**, *109*, 259-302.

(3) Pack, D. W.; Hoffman, A. S.; Pun, S.; Stayton, P. S. Design and development of polymers for gene delivery. *Nat Rev Drug Discov* **2005**, *4*, 581-593.

(4) Mullen, D. G.; Borgmeier, E. L.; Desai, A. M.; van Dongen, M. A.; Barash, M.; Cheng, X. M.; Baker, J. R.; Holl, M. M. B. Isolation and Characterization of Dendrimers with Precise Numbers of Functional Groups. *Chem-Eur J* **2010**, *16*, 10675-10678.

(5) Mullen, D. G.; Fang, M.; Desai, A.; Baker, J. R.; Orr, B. G.; Holl, M. M. B. A Quantitative Assessment of Nanoparticle-Ligand Distributions: Implications for Targeted Drug and Imaging Delivery in Dendrimer Conjugates. *Acs Nano* **2010**, *4*, 657-670.

(6) Mullen, D. G.; Banaszak Holl, M. M. Heterogeneous Ligand–Nanoparticle Distributions: A Major Obstacle to Scientific Understanding and Commercial Translation. *Accounts of Chemical Research* **2011**, *44*, 1135-1145.

(7) Dougherty, C. A.; Furgal, J. C.; van Dongen, M. A.; Goodson, T.; Holl, M. M. B.; Manono, J.; DiMaggio, S. Isolation and Characterization of Precise Dye/Dendrimer Ratios. *Chem-Eur J* **2014**, *20*, 4638-4645.

(8) Ornelas, C.; Lodescar, R.; Durandin, A.; Canary, J. W.; Pennell, R.; Liebes, L. F.; Weck, M. Combining Aminocyanine Dyes with Polyamide Dendrons: A Promising Strategy for Imaging in the Near-Infrared Region. *Chem-Eur J* **2011**, *17*, 3619-3629.

(9) Ornelas, C.; Pennell, R.; Liebes, L. F.; Weck, M. Construction of a Well-Defined Multifunctional Dendrimer for Theranostics. *Org Lett* **2011**, *13*, 976-979.

(10) Wangler, C.; Moldenhauer, G.; Saffrich, R.; Knapp, E. M.; Beijer, B.; Schnolzer, M.; Wangler, B.; Eisenhut, M.; Haberkorn, U.; Mier, W. PAMAM Structure-Based Multifunctional Fluorescent Conjugates for Improved Fluorescent Labelling of Biomacromolecules. *Chem-Eur J* **2008**, *14*, 8116-8130.

(11) Zill, A. T.; Licha, K.; Haag, R.; Zimmerman, S. C. Synthesis and properties of fluorescent dyes conjugated to hyperbranched polyglycerols. *New J Chem* **2012**, *36*, 419-427.

(12) Balzani, V.; Ceroni, P.; Gestermann, S.; Gorka, M.; Kauffmann, C.; Vogtle, F. Fluorescent guests hosted in fluorescent dendrimers. *Tetrahedron* **2002**, *58*, 629-637.

(13) Puntoriero, F.; Ceroni, P.; Balzani, V.; Bergamini, G.; Vogtle, F. Photoswitchable dendritic hosts: A dendrimer with peripheral azobenzene groups. *J Am Chem Soc* **2007**, *129*, 10714-10719.

(14) Jockusch, S.; Turro, N. J.; Tomalia, D. A. Aggregation of Methylene-Blue Adsorbed on Starburst Dendrimers. *Macromolecules* **1995**, *28*, 7416-7418.

(15) van Dongen, M. A.; Vaidyanathan, S.; Holl, M. M. B. PAMAM dendrimers as quantized building blocks for novel nanostructures. *Soft Matter* **2013**, *9*, 11188-11196.

(16) Sokolova, V.; Epple, M. Synthetic pathways to make nanoparticles fluorescent. *Nanoscale* **2011**, *3*, 1957-1962.

(17) He, C. B.; Hu, Y. P.; Yin, L. C.; Tang, C.; Yin, C. H. Effects of particle size and surface charge on cellular uptake and biodistribution of polymeric nanoparticles. *Biomaterials* **2010**, *31*, 3657-3666.

(18) Duan, X. P.; Li, Y. P. Physicochemical Characteristics of Nanoparticles Affect Circulation, Biodistribution, Cellular Internalization, and Trafficking. *Small* **2013**, *9*, 1521-1532.

(19) Shakhbazau, A.; Isayenka, I.; Kartel, N.; Goncharova, N.; Seviaryn, I.; Kosmacheva, S.; Potapnev, M.; Shcharbin, D.; Bryszewska, M. Transfection efficiencies of PAMAM dendrimers correlate inversely with their hydrophobicity. *Int J Pharmaceut* **2010**, *383*, 228-235.

(20) Yoo, H.; Juliano, R. L. Enhanced delivery of antisense oligonucleotides with fluorophore-conjugated PAMAM dendrimers. *Nucleic Acids Res* **2000**, *28*, 4225-4231.

(21) Beg, S.; Samad, A.; Alam, M. I.; Nazish, I. Dendrimers as Novel Systems for Delivery of Neuropharmaceuticals to the Brain. *Cns Neurol Disord-Dr* **2011**, *10*, 576-588.

(22) Kulczynska, A.; Frost, T.; Margerum, L. D. Effect of PAMAM dendrimer size and pH on the electrostatic binding of metal complexes using cyclic voltammetry. *Macromolecules* **2006**, *39*, 7372-7377.

(23) van Dongen, M. A.; Desai, A.; Orr, B. G.; Baker, J. R.; Holl, M. M. B. Quantitative analysis of generation and branch defects in G5 poly(amidoamine) dendrimer. *Polymer* **2013**, *54*, 4126-4133.

(24) Peterson, J.; Allikmaa, V.; Subbi, J.; Pehk, T.; Lopp, M. Structural deviations in poly(amidoamine) dendrimers: a MALDI-TOF MS analysis. *Eur Polym J* **2003**, *39*, 33-42.

(25) Mullen, D. G.; Desai, A.; van Dongen, M. A.; Barash, M.; Baker, J. R., Jr.; Banaszak Holl, M. M. Best practices for purification and characterization of PAMAM dendrimer. *Macromolecules* **2012**, *45*, 5316-5320.

(26) Kim, Y.; Kim, S. H.; Tanyeri, M.; Katzenellenbogen, J. A.; Schroeder, C. M. Dendrimer Probes for Enhanced Photostability and Localization in Fluorescence Imaging. *Biophys J* **2013**, *104*, 1566-1575.

(27) Rohatgi, K. K.; Singhal, G. S. Nature of Bonding in Dye Aggregates. *J Phys Chem-Us* **1966**, *70*, 1695-&.

(28) Selwyn, J. E.; Steinfel.Ji. Aggregation Equilibria of Xanthene Dyes. *J Phys Chem-Us* **1972**, *76*, 762-&.

# Chapter 4.

# Fluorophore-Dendrimer Ratio Impacts Cellular Uptake and Intracellular Fluorescence Lifetime

Reprinted with permission from: Casey A. Dougherty, Sriram Vaidyanathan,
Prof. Bradford G. Orr, and Prof. Mark M. Banaszak Holl.
*Bioconjugate Chemistry*, **26**, 301-315 (2015).


## 4.1. Introduction

Cationic polymers are employed for a variety of biological applications involving transport of the polymer into cells including transfection agents for oligonucleotides, antibacterial agents, and drug delivery agents.[1-5] In order to probe the uptake and cellular localization properties, the polymer is often modified with fluorescent dye.[6] In this case, it is important to understand how the presence of dye modifies the behavior of the polymer. Such dye-modified polymers are also of interest as models for the biodistribution behavior of the polymer when it is modified with multiple hydrophobic moieties, such as targeting agents or drugs. Dye-polymer conjugates are often complex mixtures. Dye conjugated to a large excess of reactive sites on the polymer will result in a Poisson distribution of dye-polymer particle ratios that is superimposed on the molecular weight (MW) distribution of the base polymer.[7, 8] Materials containing a large degree of dispersion in both MW and hydrophobicity per particle are expected to exhibit a range of biological uptake and distribution behavior.[9-12] An additional complication is the impact of dye conjugation, specifically the impact that the localization of multiple dyes on a given polymer particle has on the photophysical properties of the dye. This high effective concentration of dye can result in substantial differences in both fluorescence intensity and lifetime per polymer particle.[6, 13, 14] Given the importance of dye-conjugates to probing the mechanisms of cationic polymers as antibacterial agents and as vectors for gene and drug delivery, we have explored the ways in which employing distributions of dye-conjugates impacts interpretations of cell uptake and localization for polycationic polymers.

The generation of systematically varied dye-polymer ratios for a cationic polymer is a challenging problem. Most commonly, a mean variation in dye-polymer ratio is achieved under stochastic reaction conditions that generates a statistical distribution of ratios and a mixture of hydrophobic and photophysical properties. The distribution of ratios is quite broad with substantial overlap of materials for different means, making comparisons between different conjugate averages difficult to interpret. Table 4.1 provides an illustrative example for the case of stochastic conjugates containing an average of 1-4 dyes for generation 5 poly(amidoamine) (G5 PAMAM) dendrimer. For these cases, the population of the mean percentage varies between about $1/5^{th}$ and $1/3^{rd}$ of the total material.

| | Percentage of each dye:dendrimer ratio | | | | | | | | | | |
|---|---|---|---|---|---|---|---|---|---|---|---|
| Avg n | 0 | 1 | 2 | 3 | 4 | 5 | 6 | 7 | 8 | 9 | 10 |
| 1 | 36.6 | **37.0** | 18.5 | 6.1 | 1.5 | 0.3 | 0.1 | - | - | - | - |
| 2 | 13.2 | 27.1 | **27.4** | 18.2 | 9.0 | 3.5 | 1.1 | 0.3 | 0.1 | - | - |
| 3 | 4.7 | 14.7 | 22.5 | **22.8** | 17.1 | 10.1 | 5.0 | 2.0 | 0.7 | 0.2 | 0.1 |
| 4 | 1.7 | 7.0 | 14.5 | 19.8 | **20.0** | 16.0 | 10.5 | 5.9 | 2.8 | 1.2 | 0.5 |

**Table 4.1.** Statistical conjugation heterogeneity for a G5 PAMAM (G5-dye$_n$) containing 93 arms and 1-4 conjugated dyes. For each value of n, the percentage for the mean value is highlighted in bold.

In order to prepare a set of cationic polymer samples containing a uniform dye-polymer ratio across all particles in the sample, it is necessary to decouple the number of dyes per particle from the particle MW. This is synthetically challenging since a large polymer particle will generally have more functional attachment sites, and therefore have a statistically greater chance of multiple dye conjugation. We achieved the decoupling of conjugation number from MW by separating a stochastic mixture of TAMRA dye conjugates based on the differential hydrophobicity imparted to each dendrimer particle by the presence of dye. In this study, we report the semi-preparative reverse-phase high performance liquid chromatography (rp-HPLC) fractionation of the stochastic mixture of dye:dendrimer ratios in G5-$NH_2$-$TAMRA_{1.5(avg)}$ into samples containing a single dye-dendrimer ratio (n = 1-4) as well as a sample containing n >5: G5-$NH_2$-$TAMRA_n$ (n = 1 - 4, 5+). Characterization of the precise dye-dendrimer ratio fractions was carried out by analytical reverse-

phase ultrahigh performance liquid chromatography (rp-UPLC), $^{1}$H NMR spectroscopy, and MALDI-TOF mass spectrometry.

With this new set of precise ratio dye conjugates available, the following implicit and explicit hypotheses were tested that underlie previous literature studies employing mixtures containing stochastic distributions of dye-polymer ratios:

H1) Uptake of cationic polymers can be quantified by measuring the change in mean fluorescence of cells using flow cytometry.

H2) The components of a stochastic distribution of dye-polymer ratios have a similar collective trend in terms of environmental lifetime response, so the mixture can be used to probe internal cellular environments.

H3) The changes in environment-based lifetime response are large as compared to difference in lifetime response associated with differences in dye-polymer ratio.

The three hypotheses were tested by measuring the uptake, fluorescence emission, and fluorescence lifetime of G5-$NH_2$-$TAMRA_n$ (n = 1 - 4, 5+, $1.5_{avg}$) in HEK293A cells using flow cytometry, fluorimetry, and fluorescence lifetime imaging microscopy (FLIM). In addition, fluorescence emission and lifetime control experiments were performed in aqueous solutions with controlled pH, ionic strength, and biomolecule concentration to test the impacts of these conditions on the fluorescence properties. We show that contrary to the expectations of H1, mean fluorescence is a poor measure for comparing the relative cellular uptake of differing dye-polymer ratios. FLIM studies of the dye-conjugates taken up into the HEK293A cells suggest the fluorescence lifetime response to the cellular environment is very sensitive to the dye-polymer ratio, raising concerns about H2 and H3. These studies indicate caution should be exercised when interpreting FLIM data for stochastic dye mixtures in biological systems. Biological systems have the capacity for fractionating a sample,[9-12, 15] much like an HPLC column, prior to the fluorescence measurement. For such a system, this study indicates that it is critical to know the dye-polymer ratio dependent properties of the material being measured in order to accurately compare fluorescence intensities or to make use of differences in fluorescence lifetime.

**4.2. Results and Discussion**

The importance of cationic polymers for biological applications has led to a number of recent studies addressing the use of dye conjugates. Mier et al. studied the stochastic conjugation of multiple dyes including fluorescein, rhodamine, coumarin, and dansyl to PAMAM dendrimers.[16]

With the exception of dansyl, they found that fluorescence intensity decreased as the mean number of dyes per dendrimer increased. The intensity decrease was attributed to a combination of a small Stokes shift leading to quenching and the high effective concentration that results from multiple dyes conjugated to the same polymer core. By way of contrast, in dansyl-modified PAMAM materials, fluorescence increased with increasing dye-dendrimer ratio, presumably due to the large Stokes shift of 195 nm. Schroeder et al. examined Cy3 and Cy5 dye optical properties conjugated to generation 5 (G5) PAMAM or G6 PAMAM dendrimer in order to create a new set of materials for biological imaging with enhanced stability and increased accuracy in single molecule imaging.[17] Dendrimer mixtures with an average of 8 Cy5 dyes gave slower photobleaching compared to free dye with a 6 to 10 fold increase in photobleaching lifetime value for the G5 PAMAM conjugates. The dendrimer conjugates with an average of 14 Cy5 dyes on G6 PAMAM showed a ~17 fold increase in photobleaching lifetime value. The mean conjugation numbers employed in this case generate mixtures with <0.5% of the material having zero or one dye. This eliminates the most dramatic difference in effective local concentration and the related variation in photophysical properties that occurs when the dye-polymer ratio changes from 1 to 2. Wagner et al. employed stochastically prepared G3 PAMAM dendrimer conjugated to a mean of 1 Alexa Fluor 555 dye to quantify the rate constant of dendrimer uptake in Caplan-1 cells.[18] Interestingly, reverse-phase high performance liquid chromatography (rp-HPLC) did not resolve different species as being present in this case, although separation has been achieved for other dye ligands.[14] In this study, an effective mass transfer coefficient was determined for the mixture of dye-dendrimer ratios present in the sample. Many additional studies addressing the uptake of polycationic polymer-dye conjugates have been discussed in a series of comprehensive reviews.[6] These studies are of broad interest because the level of hydrophobicity is known to alter a polymer's ability to permeate cell membranes,[19] as well as impact transfection efficiency,[20-24] biodistribution,[15] and pharmacokinetics.[25, 26] Colocalization of polymer-fluorophore conjugates based on surface functionality[17, 27] has also been shown. In all cases, the presence of broad conjugation heterogeneity in the stochastic mixtures of polymer-dye conjugates has prevented a detailed understanding of what fraction or fractions of the conjugates are providing the desired biological activity.

In order to focus this study on the impact of dye conjugation heterogeneity, it was necessary to employ a cationic polymer that contained a minimal MW distribution while remaining convenient

for generating a systematic change in the dye-polymer ratio. In addition, the polymer MW must be large enough to accommodate a number of dyes and still maintain good water solubility for all dye-polymer ratios. We selected G5 PAMAM dendrimer as this material is readily available commercially, has excellent water solubility, and has a sufficiently large MW (theoretically 28,826 Da) to maintain solubility upon conjugation with multiple dyes. In addition, we have developed rp-HPLC protocols that remove all of the trailing generations (G1-G4; 1,430 to 14,215 Da MW) as well as the dimer, trimer, and tetramer oligomers (~50,000 to 120,000 Da range) typically present in G5 PAMAM dendrimer.[28] The purified G5 PAMAM material obtained from the rp-HPLC purification has an average of 93 primary amine terminal arms per particle (as compared to the theoretical 128 arms), a $M_n$ of 25,130 Da, and a $M_w$ of 27,140 Da ($M_n/M_w$ = 1.08). The full mass range of the isolated monomer G5 PAMAM material was 21,000 to 30,000 Da.

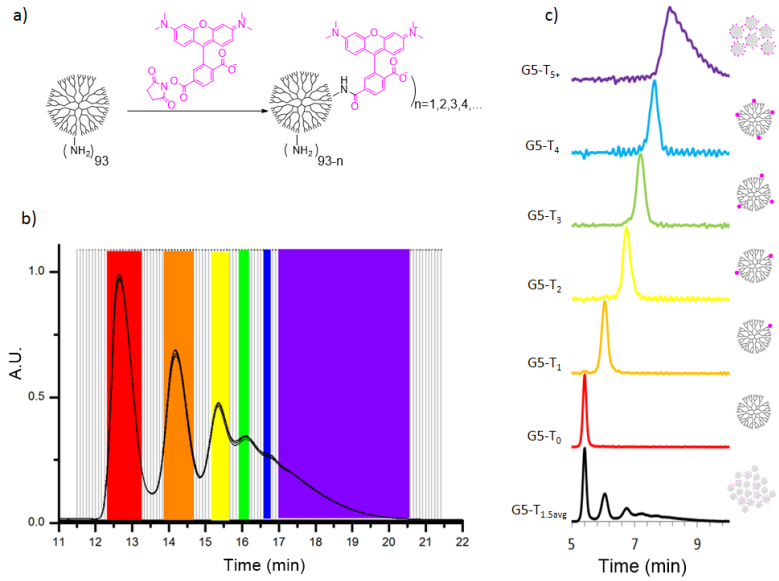


**Scheme 4.1.** Synthesis, isolation, and characterization of G5-$NH_2$-$TAMRA_n$ ( n = 0, 1, 2, 3 , 4, 5+, $1.5_{avg}$) samples. a) Stochastic conjugation of TAMRA to G5 PAMAM dendrimer b) Isolation of G5-$NH_2$-$TAMRA_n$ employing semi-preparative rp-HPLC c) Reinjection of combined fractions on analytical rp-UPLC to determine purity. n = $1.5_{avg}$ (black), 0 (red), 1 (orange), 2 (yellow), 3 (green), 4 (blue), and 5+ (purple).

Direct conjugation of TAMRA to G5 PAMAM dendrimer results in a Poisson distribution of dye:dendrimer ratios (Scheme 4.1a). The material was separated using semi-preparative rp-HPLC (Scheme 4.1b) into fractions containing precise dye:dendrimer ratios (n = 1-4) as well as a sample where $n \geq 5$. The isolated fractions were reinjected into an analytical UPLC to determine purity (Scheme 4.1c) and further characterized using $^1$H NMR spectroscopy, emission and absorption measurements, MALDI-TOF-MS, and fluorescence lifetime imaging microscopy (FLIM).

Analytical UPLC provides the most sensitive measure of the number of dyes present per dendrimer particle.[14] The shift resulting from the addition of each dye to the dendrimer scaffold for the first two dyes is substantially larger than the breadth of the peak resulting from the MW distribution of the G5 PAMAM dendrimer (Scheme 4.1c). As the number of dyes increases, the incremental value of the hydrophobicity induced shift decreases. The UPLC method detects the dye-dendrimer particle ratio induced shifts in the context of the full defect structure of the polymer, which generates the observed peak width.[14] The number of dyes measured for each fraction G5-$NH_2$-$TAMRA_n$ are n = 0.0, 1.0, 2.0, 3.0, 4.0, and an average of 6.8 dye-dendrimer for the $n \geq 5$ fraction (Table C.1). The average number of TAMRA dyes per dendrimer was also assessed using $^1$H NMR spectroscopy by comparing the integration of the TAMRA protons to the integration of the internal protons in the G5 PAMAM dendrimer (1,210 protons).[7, 29] The averages of n = 0.0, 0.9, 1.8, 3.3, 4.5, and 6.9 are in reasonable agreement with the UPLC data. The NMR values are less reliable than the UPLC values because a) the isolated fraction does not fully represent the material used to determine the internal proton count of 1,210, thus introducing error into the comparison of the integrated ratios and b) we are determining the ratio by comparing a small number of TAMRA protons to a large number of dendrimer protons. MALDI-TOF-MS was also used to characterize each isolated fraction (Table C.1, Figure C.1). A trend towards higher mass was observed as n increased from 1 to 4 as well as for 5+; however, obtaining dye-dendrimer ratios from such data is inaccurate because we are sampling a different subfraction of the entire MW distribution for each G5-$NH_2$-$TAMRA_n$ (see the HPLC separation in Scheme 4.1b). The impact of the differential subfractionation is highlighted by the 300 Da decrease observed when comparing G5-$NH_2$-$TAMRA_0$ to G5-$NH_2$-$TAMRA_1$. In our previous work discussing the synthesis of related dye-dendrimer conjugates, we compared the relative ability of UPLC, $^1$H NMR spectroscopy, and MALDI-TOF-MS data to assign dye-dendrimer ratios in detail.[14]

The impact of the dye:dendrimer ratio on photophysical properties was assessed using a combination of FLIM and absorption and emission spectroscopies (Figure 4.1). The absorption and emission spectra were obtained for 0.1 mg/mL G5-$NH_2$-$TAMRA_n$ solutions in water, which corresponds to roughly 3-4 μM solutions. As expected for this concentration of dye, the absorption spectrum for G5-$NH_2$-$TAMRA_1$ exhibited a single maximum at 560 nm.[14, 30] Although the total solution concentration for dye in G5-$NH_2$-$TAMRA_2$ was still micromolar, the absorption now showed the classic two peak pattern, at 525 and 560 nm, typically associated with formation of

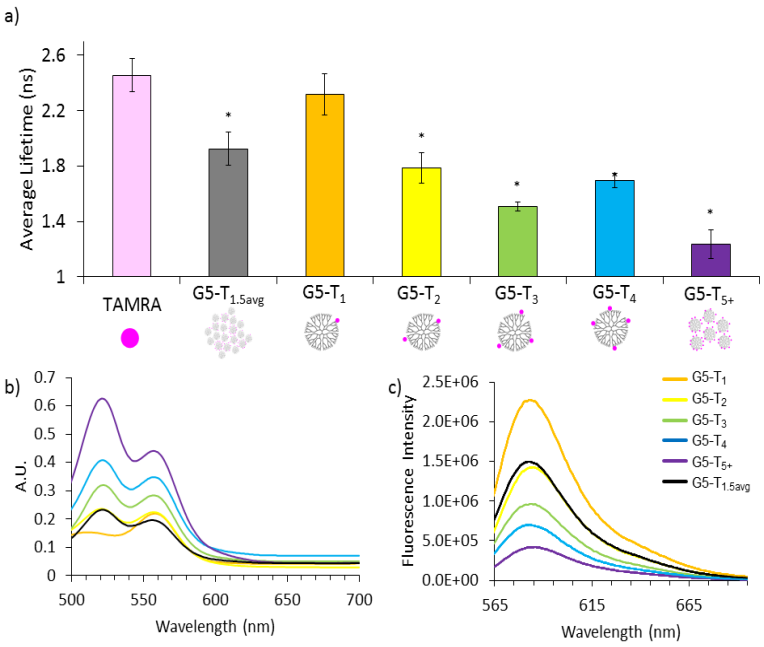


**Figure 4.1.** a) Fluorescence lifetime values (data obtained with Sriram Vaidyanathan), b) absorption spectra, and c) emission spectra of 0.1 mg/mL G5-$NH_2$-$TAMRA_n$ ( n = 0, 1, 2, 3, 4, 5+, $1.5_{avg}$) in aqueous solution. A significant decrease in lifetime value (denoted by *) was observed for samples with n > 1 as compared to free TAMRA dye (pink) and G5-$NH_2$-$TAMRA_1$. The absorption increases while the emission decreases with increasing n.

TAMRA dimers in highly concentrated solutions.[30] This pattern provided additional evidence for the absence of n ≥ 2 materials in the sample assigned as G5-$NH_2$-$TAMRA_1$. In addition, the relative intensity ratio of the 525 and 560 nm peaks indicated little if any n = 1 material was present in the G5-$NH_2$-$TAMRA_2$ sample. The two peaks remained present, and the 525 nm peak grew in relative intensity as n increased. For all these samples, the local concentration of dye, which is restricted on each dendrimer particle to a hydrodynamic sphere of 3.1 nm radius,[31] was on the order of 10 M. The impact of the dye:dendrimer ratio was also observed in the fluorescence spectra taken in water. The most fluorescent material, as a function of dendrimer concentration, is G5-$NH_2$-$TAMRA_1$. It had roughly twice the fluorescence emission of G5-$NH_2$-$TAMRA_2$, which had twice as much dye, and three times the fluorescence emission of G5-$NH_2$-$TAMRA_4$, which had four times as much dye. G5-$NH_2$-$TAMRA_1$ also had roughly twice the fluorescence emission of stochastically prepared G5-$NH_2$-$TAMRA_{1.5(avg)}$, which consisted of n = 0, 1, 2, 3, 4 ,5 in percentages of 22, 34, 25, 13, 5, and 1%, respectively. The impact of n is further demonstrated in the FLIM analysis. The fluorescence lifetime for free TAMRA in water (0.2 μM) was measured to be 2.5 ± 0.1 ns and a similar lifetime value for G5-$NH_2$-$TAMRA_1$ (0.2 μM) was obtained of 2.3 ± 0.2 ns. In all cases, increased dye-dendrimer ratios resulted in a decreased lifetime value as compared to G5-$NH_2$-$TAMRA_1$. The change was not linear, and G5-$NH_2$-$TAMRA_3$ had a lower lifetime value (1.5 ± 0.1 ns) than the G5-$NH_2$-$TAMRA_4$ (1.7 ± 0.1 ns)

(Figure 4.1). Additional unexpected trends in lifetime values occurred when using the samples for cellular uptake and in biological environment modeling studies (*vida infra*). Fluorescence lifetime values for all samples in water, as well as for aqueous solutions with controlled ionic strength and biomolecule concentration, are provided in Table C.2.

Fluorophore-polymer ratio has been reported to influence biological behavior;[22, 24] however, the mechanism of these effects has been obscured by stochastic distributions of dye-dendrimer ratios. In this study, we focus on the real and apparent impacts of dye-dendrimer ratio on cellular uptake. As a model system, we employed mean fluorescence as measured by flow cytometry to quantify uptake in HEK293A cells. Cells were exposed to 0.5 μM G5-$NH_2$-$TAMRA_n$ (n = 1 - 4, 5+, $1.5_{avg}$) for 3 hours at 37 °C and mean fluorescence was determined by measurement of 10,000 cells (Figure 4.2). The raw mean fluorescence data exhibited the largest mean value for G5-$NH_2$-$TAMRA_1$ and the magnitude continued to decrease with increasing dye-dendrimer ratio; however, our independent measures of the fluorescence intensity of the conjugates (Figure 4.1) indicated that an accurate assessment of dendrimer uptake required a correction for the relative degree of fluorescence intensity for each conjugate.

In order to determine the correction factors, we measured the absorbance, emission, and lifetime characteristics of 0.1 mg/mL (3.5 μM) G5-$NH_2$-$TAMRA_n$ (n = 1, 2, 3, 4, 5+, $1.5_{avg}$) solutions in a variety of aqueous solutions to model potential interactions from both salt and biomolecules. The measurements were performed in aqueous solution (Figure 4.1), NaCl, PBS, and undiluted fetal bovine serum (FBS). We also included controls containing bovine serum albumin (BSA) and glucose in water (at concentrations present in our FBS control) to independently evaluate the impact of these two components. Ficoll was used as a control for biomolecule crowding effects. The impact of interaction with negatively charged macromolecules was modeled using 1:1 and 1:10 N:P ratios of both plasmid DNA (pDNA)

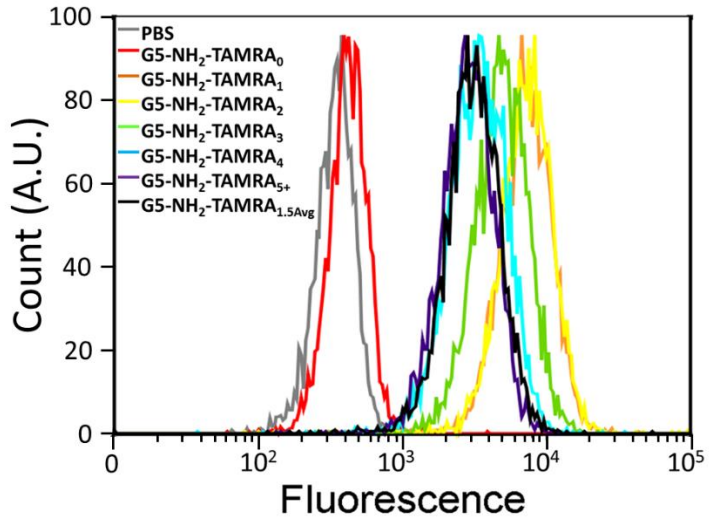


**Figure 4.2.** Flow cytometry of one repeat for the G5-$NH_2$-$TAMRA_n$ (n = 0, 1, 2, 3, 4, 5+, $1.5_{avg}$) samples showing cell count versus fluorescence intensity.

and antisense DNA (asDNA) (N is the number of dendrimer primary amines and P is the number of DNA phosphates). Lastly, we employed HEK293A cell lysate at 100,000 cells per mL as a final, comprehensive control solution (Figures C.2 and C.3). The cell lysate was prepared by osmotically lysing cells followed by sonication. This lysate contains all of the cell lipids and protein and is detergent free, and thus differs from conventional lysates. For all conditions studied, G5-$NH_2$-$TAMRA_1$ exhibited the most intense fluorescence emission. In order to compare the emission intensities for the various conjugates under a given model condition, we defined the brightest emission of G5-$NH_2$-$TAMRA_1$ as 1 and determined the relative fraction of emission for the remaining conjugates (Table 4.2). The overall trend was a decrease in emission with increasing dye-dendrimer ratio. The overall magnitude of the non-quenched fluorescence varied greatly with the addition of the second dye (G5-$NH_2$-$TAMRA_2$), ranging from 93% for ficoll to 42% for PBS. When considering just the G5-$NH_2$-$TAMRA_n$ (n = 1, 2, 3, 4) fluorescence, the change in intensity as a function of n was monotonic; however, when the more complex n = $1.5_{avg}$ and n = 5+ samples were considered, multiple deviations in the monotonic trend were associated with both samples. The origins of this complex fluorescence emission behavior are not clear. The data show the difficulty in extrapolating behavior for such heterogeneous mixtures of conjugated fluorophores. Fluorescence lifetime measurements for G5-$NH_2$-$TAMRA_1$ (2.3 ± 0.2 ns) and TAMRA (2.5 ± 0.1

| | Fluorescence Ratios for Control Solutions of 200 µM G5-$NH_2$-$TAMRA_n$ | | | | | | | |
|---|---|---|---|---|---|---|---|---|
| | water | PBS | NaCl | BSA | ficoll | pDNA | FBS | asDNA |
| G5-$(TAMRA)_{1.5avg}$-$NH_2$ | 0.54 | 0.53 | 0.7 | 0.69 | 0.93 | 0.59 | 0.54 | 0.77 |
| G5-$(TAMRA)_0$-$NH_2$ | - | - | - | - | - | - | - | - |
| G5-$(TAMRA)_1$-$NH_2$ | 1 | 1 | 1 | 1 | 1 | 1 | 1 | 1 |
| G5-$(TAMRA)_2$-$NH_2$ | 0.53 | 0.42 | 0.45 | 0.83 | 0.93 | 0.81 | 0.72 | 0.77 |
| G5-$(TAMRA)_3$-$NH_2$ | 0.43 | 0.24 | 0.27 | 0.57 | 0.59 | 0.44 | 0.43 | 0.47 |
| G5-$(TAMRA)_4$-$NH_2$ | 0.34 | 0.17 | 0.17 | 0.42 | 0.33 | 0.25 | 0.29 | 0.44 |
| G5-$(TAMRA)_{5+}$-$NH_2$ | 0.22 | 0.18 | 0.21 | 0.42 | 0.51 | 0.2 | 0.26 | 0.31 |

**Table 4.2.** Fluorescence emission intensity characterization summary for G5-$NH_2$-$TAMRA_n$ material. For each condition the intensity for G5-$NH_2$-$TAMRA_1$ is defined as 1 and the fractional intensity observed for each n = 2, 3, 4, 5+ and $1.5_{avg}$ is indicated.

ns) in water were essentially identical, and lifetimes decreased, as expected for the decrease in emission intensity, as a function of n. Based on these studies, we employed the fluorescence correction factors determined from aqueous solution, FBS solution (which also matched trends observed for the cell-based lifetime studies, *vida infra*), and cell lysate in order to correct the mean fluorescence values obtained from flow cytometry.

Application of the fluorescence emission correction factors (Table 4.2) to the mean fluorescence data obtained from flow cytometry (Figure 4.2) resulted in the trends in mean fluorescence illustrated in Figure 4.3. For each correction factor, the data for G5-$NH_2$-$TAMRA_1$ (G5-$T_1$) was normalized to the intensity observed for raw emission data. All three corrections trend in the same

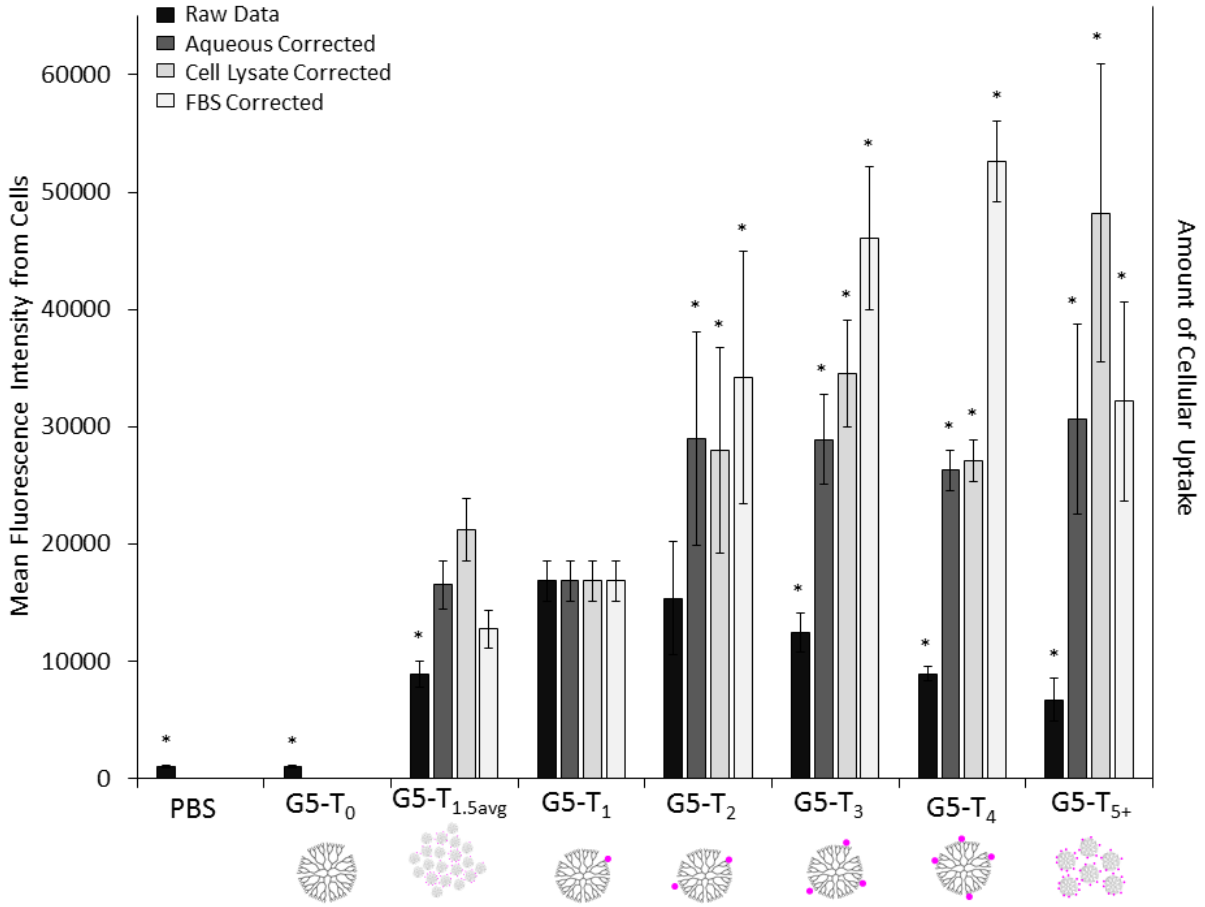


**Figure 4.3.** Uptake and binding of G5-$NH_2$-$TAMRA_n$ as measured by flow cytometry after 3 hours of incubation with HEK293A cells. The bar graphs illustrate the uptake trend as measured by raw mean fluorescence data and the trends after correction using relative fluorescence emission in aqueous solution, FBS solution, and cell lysate. All correction factors are summarized in Table 4.2 from the data shown in Figures 4.1c, C.2, and C.3. Significance for differences in G5-$NH_2$-$TAMRA_n$ fluorescence intensity (denoted by *) as compared to G5-$NH_2$ –$TAMRA_1$ intensity was assessed using a Games-Howell analysis.

direction and indicate that the uptake of the $n \geq 2$ conjugates is significantly underestimated when only raw mean fluorescence data is considered. Indeed, the data indicate that *uptake does not decrease as a function of n* as implied by comparison of the raw mean fluorescence intensities. Rather, $n \geq 2$ conjugates give greater uptake than does the n = 1 conjugate. These data also suggest that studies with dye conjugates overestimate the uptake rates of dye-free G5 PAMAM dendrimer into cells, although the rates may be a reasonable estimate for dendrimer containing other moieties of similar hydrophobicity, such as drugs. Lastly, these data indicate that the use of raw mean fluorescence data to quantify dye uptake *in vivo* using stochastic dye-dendrimer, or more generally dye-polymer, conjugates can lead to errors of at least a factor of 3-5 if the biological fractionation effects on the materials are unknown.

The G5-$NH_2$-$TAMRA_n$ (n = 1, 2, 3, 4, 5+, and $1.5_{avg}$) conjugates varied in terms of fluorescence intensity as a function of n (Figures 4.1-4.3). The variation of intensity with n indicates that interpreting the uptake of materials into the cell using relative brightness in the confocal fluorescence images will not give reliable results (Figure 4.4). In this case, HEK293A cells were treated with 1 μM G5-$NH_2$-$TAMRA_n$ (n = 1, 2, 3, 4, 5+, and $1.5_{avg}$) conjugates for 3 hours. All

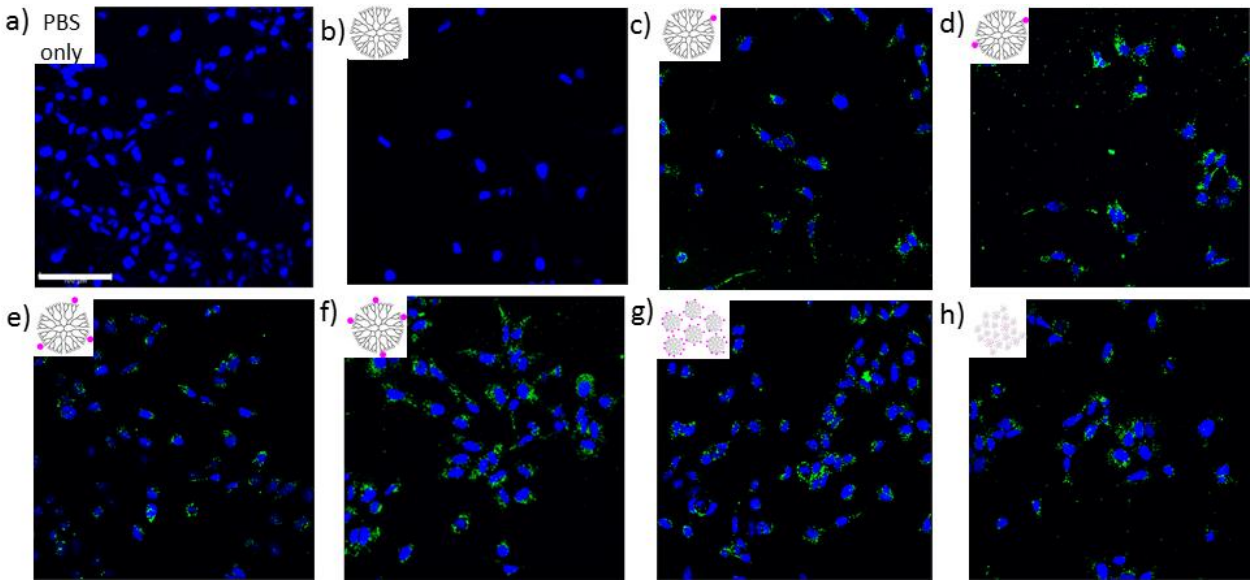


**Figure 4.4.** Confocal Microscopy Images of HEK293A cells incubated for three hours with a) PBS only b) G5-$NH_2$ c) G5-$NH_2$-$TAMRA_1$ d) G5-$NH_2$-$TAMRA_2$ e) G5-$NH_2$-$TAMRA_3$ f) G5-$NH_2$-$TAMRA_4$ g) G5-$NH_2$-$TAMRA_{5+}$ h) G5-$NH_2$-$TAMRA_{1.5avg}$. TAMRA fluorescence is shown in green. The fluorescence deriving from DAPI-stained cell nuclei is shown in blue. Images were obtained with a 40x oil immersion objective. The same set of image locations is presented in Figure 4.5 using FLIM. Scale bar is 100 μm. Data obtained by Sriram Vaidyanathan.

treated cells exhibited a punctate distribution of fluorophore uptake (TAMRA = green), which was in general agreement with the flow cytometry data (Figures 4.2 & 4.3). The mixtures G5-$NH_2$-$TAMRA_{5+}$ (Figure 4.4g) and G5-$NH_2$-$TAMRA_{1.5avg}$ (Figure 4.4h) were expected to contain fluorescent particles with intensity levels varying by up to a factor of 5. Therefore, even within a given cell or field of cells, relative intensity variation may not be correlated with extent of uptake. FLIM offers an alternative method of fluorescence image contrast that is generally insensitive to intensity-based artifacts. In addition, the fluorescence lifetimes measured are sensitive to the microenvironment including pH, ion concentration, and molecular association.[32] FLIM images were obtained for the same locations as the confocal microscopy data presented in Figure 4.4. The

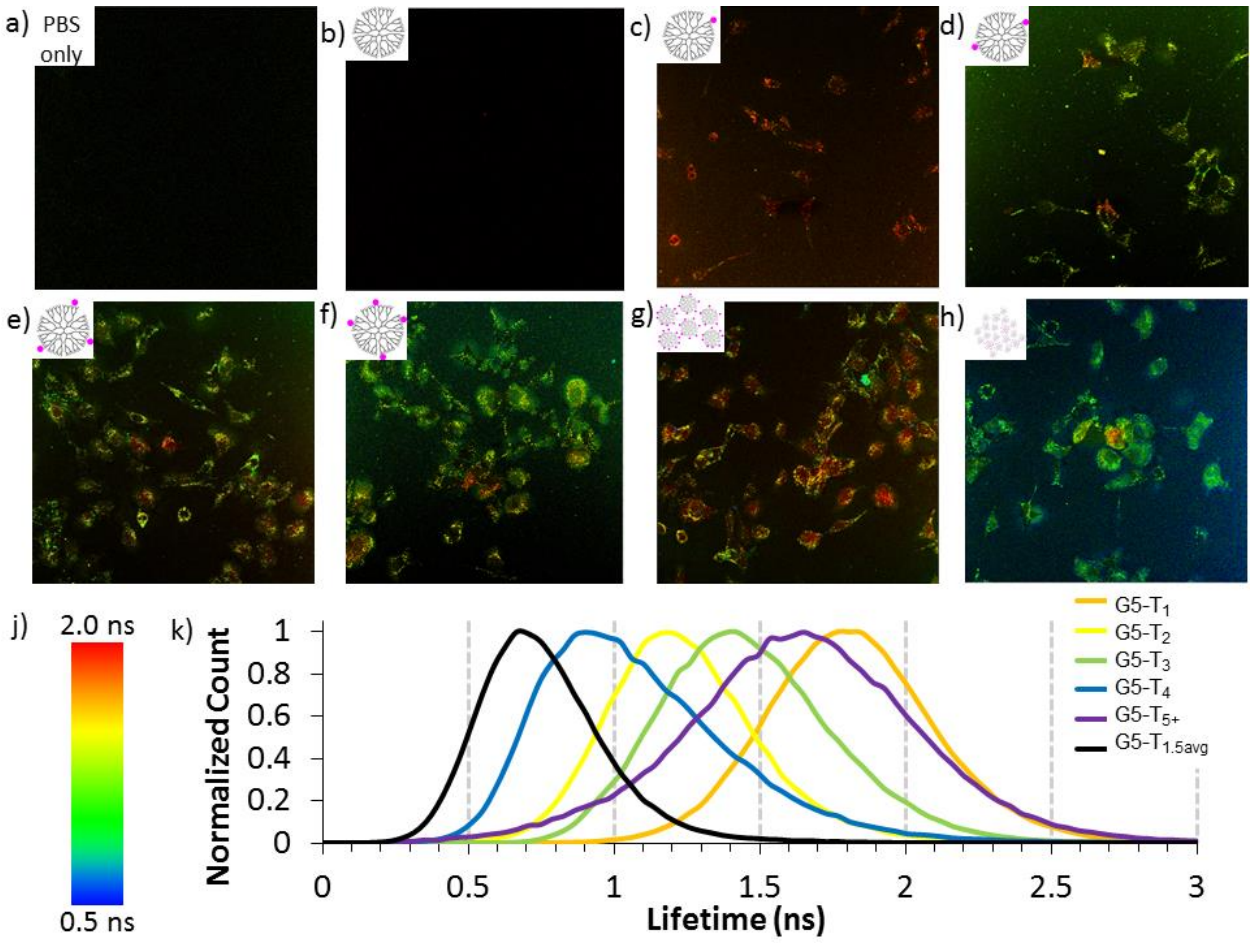


**Figure 4.5.** FLIM images of HEK293A cells incubated for three hours with a) PBS only b) G5-$NH_2$ c) G5-$NH_2$-$TAMRA_1$ d) G5-$NH_2$-$TAMRA_2$ e) G5-$NH_2$-$TAMRA_3$ f) G5-$NH_2$-$TAMRA_4$ g) G5-$NH_2$-$TAMRA_{5+}$ h) G5-$NH_2$-$TAMRA_{1.5avg}$. j) Color code for FLIM images. k) Histograms of fluorescence lifetimes for FLIM images. Images were obtained with a 40x oil immersion objective. The same set of image locations is presented in Figure 4.4 using confocal fluorescence microscopy. Data obtained by Sriram Vaidyanathan.

G5-$NH_2$-$TAMRA_{1.5avg}$ treated sample (Figure 4.5h) gave an average lifetime of 0.7 ± 0.2 ns which is significantly lower than the 1.9 ± 0.1 ns obtained for aqueous solution. This value is also substantially lower than observed for all other samples with the exception of G5-$NH_2$-$TAMRA_4$. The G5-$NH_2$-$TAMRA_1$ treated cells exhibited uniformly higher lifetimes of 1.8 ± 0.5 ns (Figure 4.5c), which itself was substantially lower than the 2.3 ± 0.2 ns observed in aqueous solution. Despite the fact that the G5-$NH_2$-$TAMRA_{1.5avg}$ sample contained 34% G5-$NH_2$-$TAMRA_1$, the 1.8 ns lifetimes associated with $T_1$ material did not appear in the cell images (Figure 4.5h). The G5-$NH_2$-$TAMRA_{5+}$ treated cells also exhibited amongst the highest lifetime value with an average of 1.6 ± 0.6 ns. Surprisingly, this value was greater than the average values observed for G5-$NH_2$-$TAMRA_n$ (n = 2, 3, 4), as well as for the G5-$NH_2$-$TAMRA_{5+}$ aqueous value of 1.2 ± 0.1 ns. Images of individual cells measured using a 40x oil objective with an additional optical zoom of 6.25x are provided in Figure C.4. The lifetimes in the zoomed images show a similar trend as the non-zoomed images. The zoomed-in images highlight the punctate distribution of the G5-TAMRA within cells. Further experiments with markers for cellular organelles are needed to determine if samples with different dye-dendrimer ratios are transported to different organelles. The observation that most of the samples exhibited dynamic quenching in the cell, resulting from possible environmental differences such as pH, ionic strength, or biomolecule interactions, was expected. It was surprising that the G5-$NH_2$-$TAMRA_{1.5avg}$ treated cells did not show the full range of lifetimes represented by the dye-dendrimer ratios present and that the lifetime of G5-$NH_2$-$TAMRA_{5+}$ increased in cells, indicating a reduction in dynamic quenching.

In order to gain a greater understanding of how these changes in lifetime varied as a function of n, a series of control experiments were carried out. Fluorescence lifetimes were measured for solutions of G5-$NH_2$-$TAMRA_n$ (n = 1, 2, 3, 4, 5+, and $1.5_{avg}$) in cell lysate, 1X PBS, 137 mM NaCl, 0.3 mM BSA, 7.0 mM glucose, 0.001 mM ficoll, and undiluted fetal bovine serum (FBS) (Figure 4.6). Additional lifetime measurements were made for aqueous solutions using pH 3 and 5 buffers and for aggregates of G5-$NH_2$-$TAMRA_n$ (n = 1, 2, 3, 4, 5+, and $1.5_{avg}$) generated by mixing with anionic oligonucleotides (both plasmid and antisense DNA) (Figures C.5 and C.6). The undiluted FBS was used to generate a high concentration of biomolecules comparable to that found in the cellular environment. The concentrations of NaCl, BSA, and glucose were set to the levels of the FBS control. Ficoll was set at 5 equiv per dendrimer. 1x PBS is a standard buffer

system with an overall salt concentration similar to blood and the same NaCl concentration as the FBS.

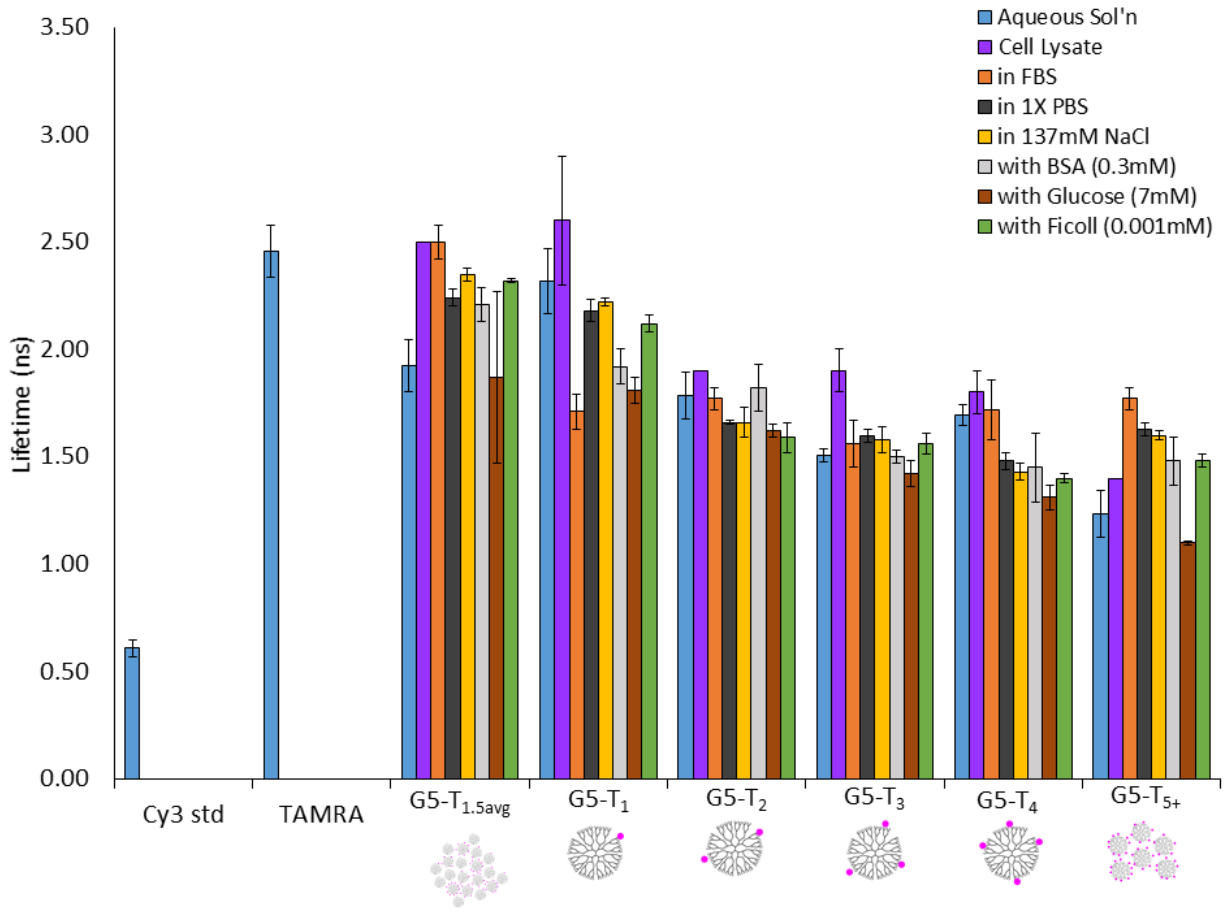


**Figure 4.6.** Fluorescence lifetime measurements of G5-$NH_2$-$TAMRA_n$ (n = 0, 1, 2, 3, 4, 5+, $1.5_{avg}$) in aqueous solution under various conditions. Cy3 and TAMRA dyes in water were used as calibration standards. See Table C.2 for summary of numerical values. Data obtained with Sriram Vaidyanathan.

The FBS control best matched the cell FLIM data as it gave both the increase in dynamic quenching (lower lifetime) of the G5-$NH_2$-$TAMRA_1$ material and the decrease in dynamic quenching (higher lifetime) observed for G5-$NH_2$-$TAMRA_{5+}$ (Figure 4.6). In order to understand how the components of FBS might lead to these lifetime changes, solutions were tested containing salt (PBS, NaCl) and biomolecule components (BSA, glucose) as well as a ficoll. The results point to a complex mixture of static and dynamic quenching mechanisms present in the G5-$NH_2$-$TAMRA_n$ conjugates. For G5-$NH_2$-$TAMRA_1$, NaCl and PBS alone or the presence of ficoll did not generate a significant change in fluorescence lifetime; however, both BSA and glucose did

cause a change. For G5-$NH_2$-$TAMRA_{5+}$, NaCl, PBS, BSA, and ficoll all caused a significant increase in fluorescence lifetime, although glucose did not. For both G5-$NH_2$-$TAMRA_n$ (n = 2, 3), little change in fluorescence lifetime was observed for any simple controls, although cell lysate caused a significant increase in lifetime for n =3. For G5-$NH_2$-$TAMRA_4$, all conditions but FBS and cell lysate were observed to decrease lifetime. Since fluorescence lifetime is also known to change for a fluorophore based on pH,[33] the conjugates were also measured in pH =3, 5, and 7 aqueous buffers. Treatment of G5-$NH_2$-$TAMRA_1$ with pH 3 and 5 buffers caused no change in lifetime, whereas both buffers resulted in an increase in lifetime for G5-$NH_2$-$TAMRA_{5+}$ (Figure C.5). No clear lifetime trends were observed for the impact of aggregate formation induced by plasmid and antisense DNA, although a decrease in lifetime for G5-$NH_2$-$TAMRA_1$ and an increase in lifetime for G5-$NH_2$-$TAMRA_{5+}$ were again observed (Figure C.6). These observations can be compared to the measurements of TAMRA fluorescence lifetime of 2.28 ± 0.01 ns in buffer and 2.48 ± 0.01 ns on a DNA aptamer.[34]

The cell FLIM data can be rationalized in part based upon the control experiments. The most surprising result, the increase of fluorescence lifetime for G5-$NH_2$-$TAMRA_{5+}$ in HEK293A cells, was reproduced under a variety of control conditions. This behavior may result from a dye-dye static quenching interaction present in a fraction of the G5-$NH_2$-$TAMRA_{5+}$ sample. Upon addition of salt and biomolecules, the dye-dye interactions may be broken up leading to a lifting of the static quenching and the observation of a new, longer lifetime value. In addition, the salt and biomolecule interaction with the dye may change the nature of the dynamic quenching that leads to the 1.2 ± 0.1 ns lifetime in aqueous solution, which could also lead to an increase in observed lifetime. This balancing of effects only appears operative for n ≥ 5 dyes per G5 PAMAM dendrimer.

Many previous studies have demonstrated that the punctate G5 PAMAM dendrimer distribution in cells arise from localization into endosomes and lysomes;[35] however, the control data for pH effects (Figure C.5) does not explain the decrease in lifetimes observed in the FLIM images (Figures 4.5 and C.4.). Based on our series of control experiments, it appears that changes in ionic strength or interactions with other biomolecules present in the endosomes or lysomes are more likely causes of the decreased fluorescence lifetimes for these dye-dendrimer conjugates in the HEK293A cells.

**4.3. Conclusions**

G5-$NH_2$-$TAMRA_n$ (n=1-4, 5+, $1.5_{avg}$) samples have been synthesized and characterized by UPLC, $^1$H NMR, and MALDI-TOF-MS. The absorbance, fluorescence emission, and fluorescence lifetime properties have been measured in aqueous solution as well as in a variety of biologically relevant control conditions. By preparing this set of dye-dendrimer conjugates with well-defined dye-dendrimer ratios, we hope to elucidate the behaviors of the stochastic mixtures of dye-dendrimer ratios typically employed to understand cationic polymer uptake and localization.

During the course of this study we showed that dendrimer uptake varied as a function of n. In addition, knowledge of how fluorescence intensity for G5-$NH_2$-$TAMRA_n$ varies as a function of n is required for properly understanding the relative degree of uptake. These observations raise the greatest concerns for studies in which a stochastic mixture can be "separated" by the interaction with the biological systems, i.e. exhibit a hydrophobic dependency on biodistribution,[15, 19, 25, 26] and when biological tissues are evaluated for uptake by fluorescence without knowledge of the fraction of the dye-polymer conjugate present. Thus, for materials containing stochastic dye-polymer distributions, hypothesis (H1) that the uptake of cationic polymer can be quantified by the change in mean fluorescence of cells should be used with caution. For low Stokes shift dyes similar to TAMRA and fluorescein, H1 is not valid.

The FLIM studies of G5-$NH_2$-$TAMRA_n$ resulted in a surprising set of lifetime images. In particular, the observation of both decreasing and increasing lifetimes for a given environmental condition as a function of n was not expected. In addition, the magnitudes of changes seen as a function of n for a given control environment was similar to the magnitude of change observed for constant n as a function of changing the environment. This indicates the interpretations of fluorescence lifetimes as resulting from changes in biological environment must be approached with great caution for stochastic dye-polymer conjugates, particularly if biological fractionation of the samples has taken place. In contrast to the initial hypothesis (H2), the components of a stochastic distribution of dye-polymer ratios do not have a similar collective trend in terms of environmental lifetime response. Furthermore, with respect to H3, variation in dye-polymer ratio is found to have a similar magnitude of impact on fluorescence lifetime as changes in the biological environment.

Upon testing the three hypotheses, it is clear that caution needs to be taken when using dye-polymer mixtures to determine cellular uptake and fluorescence lifetime. One good solution for achieving linear intensity profiles is the use of large Stokes shift dyes, as discussed by Mier et al.[16]

The strategy of using a stochastic mixture that contains very little of zero dye and one dye on the polymer, as delineated by Schroeder et al., can also provide a solution.[17] However, many scientifically and technologically important dyes (i.e. TAMRA, fluorescein, AlexaFluors, etc.) have small Stokes shifts, and dye substitution is not always a favorable option. Since dye-polymer ratio impacts biodistribution and function,[9-12, 15-17, 19-27] creation of a high mean stochastic ratio is not a general solution to the problem. In these cases, either direct synthesis of precise dye-polymer materials[36-38] or physical separation to obtain precise dye:polymer ratios[7, 8, 14, 29] is needed for quantitative uptake or lifetime studies.

### 4.4. Experimental Methods

Biomedical grade G5 PAMAM dendrimer was purchased from Dendritech Inc. and purified using rp-HPLC to give a molecular weight fraction free of trailing generations (G1-G4) as well as G5 dimers and higher oligomers.[28] Trifluoroacetic acid, HPLC grade water, GE PD-10 Sephadex columns, and HPLC grade acetonitrile were purchased from Fisher-Scientific and used as received. 5-carboxy tetramethylrhodamine succinimydyl ester (TAMRA) was purchased from Life Technologies. A 500 MHz Varian NMR instrument was used for all $^{1}H$ and $^{19}F$ NMR measurements. All MALDI-TOF MS measurements were performed on a Bruker Ultraflex III with sinapinic acid matrix (Sigma Aldrich) and sodium trifluoroacetate (Fischer Scientific) salt sample preparation. Serum-free DMEM (SFM) from life technologies was employed for cell culture of HEK293A cells, which were obtained from ATCC. Complete medium was made by adding 50 mL of fetal bovine serum (FBS) and 5 mL 100× of penicillin−streptomycin to 500 mL of SFM.

**4.4.1. Conjugation of TAMRA to G5 PAMAM Dendrimer.** TAMRA (0.0121 g, 0.023 mmol, 4.5 equiv) was dissolved in dimethyl sulfoxide (3.0 mL) and added dropwise to a stirred solution of G5 PAMAM dendrimer (0.1390 g, 0.0050 mmol, 1.0 equiv) dissolved in water (30.0 mL). The mixture was stirred at 20 °C overnight and purified using a GE PD-10 sephadex column. A pink solid was obtained after removal of solvent (75% yield). The product was characterized using $^{1}H$ NMR, UV-Vis absorption and fluorescence spectroscopy, analytical rp-UPLC, and MALDI-TOF MS.

**4.4.2. Isolation of Material Containing Precise TAMRA-Dendrimer Ratios.** Semi-preparative rp-HPLC isolation was carried out on a Waters Delta 600 HPLC. For analysis of the dendrimer and conjugates, a C18 silica-based rp-HPLC column (250 x 21.20 mm, 10μm particles) connected to a C18 guard column (50 x 21.20 mm) was used. The mobile phase for elution of the conjugates

was a linear gradient beginning with 95:5 (v/v) water/acetonitrile and ending with 65:35 (v/v) water/acetonitrile over 28 minutes at a flow rate of 12.00 mL/min. Trifluoroacetic acid (TFA) at 0.10 wt % concentration in both water and acetonitrile was used as a counter ion to make the dendrimer surfaces hydrophobic. Elution traces of the dendrimer-ligand conjugate were obtained at 210 nm. A concentration of 24 mg/mL per injection was used. 120 fractions of 6 seconds duration were collected starting at 9 minutes and 30 seconds. Selection of fractions for combination to yield the precise TAMRA:dendrimer ratios was based upon analysis of the chromatogram in Origin-Pro. Each isolated combination of fractions was reinjected onto an analytical UPLC to determine purity of the sample. $^{1}$H NMR spectra are provided in Figure S8.

**4.4.3. Analytical reverse phase Ultra Performance Liquid Chromatography (rp-UPLC).** Purity of G5-$NH_2$-$TAMRA_n$ materials was assessed at 210 nm (dendrimer absorption wavelength) using a Waters Acquity UPLC system controlled by Empower 2 software. A C18 silica-based column (Phenomenex) was employed with a mobile phase linear gradient beginning with 95:5 (v/v) water/acetonitrile and ending with 55:45 (v/v) water/acetonitrile over 17 minutes at a flow rate of 3.0 mL/min. Trifluoroacetic acid (TFA) at 0.14 wt % concentration in water and acetonitrile was used as a counter ion to make the dendrimer surfaces hydrophobic.

**4.4.4. Absorption and Emission Measurements.** Fluorescence (Fluoromax-4) and UV-Vis (Shimadzu UV-1601) measurements were taken at a concentration of 0.1 mg/mL. For all measurements, the concentration of the solutions were 0.1 mg/mL and within an error of ±0.02. For the fluorescence measurements an excitation of 530 nm and emission of 580 nm were used with a slit width of 2 nm.

**4.4.5. MALDI-TOF-MS Measurements.** Three solutions were prepared: 1) 10 mg/mL dendrimer in water 2) 20 mg/mL sinapinic acid in 1:1 (v/v) acetonitrile: water and 3) 20 mg/mL sodium trifluoroacetate in water. These were then combined in a ratio of 10:2:1 of matrix:dendrimer:salt solution. The plate was spotted with 1 µL volumes of solution and allowed to dry. At least 100 scans were averaged per measurement and a smoothing factor of 12 channels was employed.

**4.4.6. Cell Culture Materials.** DMEM high glucose with sodium pyruvate and glutamine (Life Technologies Inc) was the base media. Complete media was made by adding 50 mL of FBS, 5 mL of Non-essential Amino Acids (Thermo Scientific) and 5 mL of penicillin-streptomycin to 500 mL DMEM. PBS (1X) without $Ca^{2+}$ and $Mg^{2+}$ was obtained from Life Technologies. Cells were

maintained at 37 °C with 5% $CO_2$ in a humidified atmosphere and subcultured by trypsinization (Life Technologies).

**4.4.7. Measurement of G5-$NH_2$-$TAMRA_n$ Binding and Uptake in HEK293A cells using Flow Cytometry.** HEK 293 A cells were seeded in 12 well plates (Fisher Scientific, 3.8 $cm^2$) at a density of 150,000 cells per well in 1 mL of complete DMEM and incubated overnight at 37 °C with 5% $CO_2$. The complete media was removed prior to incubation with G5-$NH_2$-$TAMRA_n$. The cells were then rinsed with 1 mL of PBS, followed by addition of 0.8 mL of SFM. The cells were incubated for three hours at 37 °C with 0.5 μM G5-$NH_2$-$TAMRA_n$ (n = 0-4, 5+, $1.5_{avg}$) (~5.0 μL volume of 2 mg/mL solution added to each well). Each treatment was run in triplicate, and 4 independent biological repeats were performed. After incubation with G5-$NH_2$-$TAMRA_n$ material, the HEK293A cells were rinsed with PBS and harvested for flow cytometry by trypsinization. Trypsinization was performed by incubation with 200 μL of trypsin for 2 minutes at 37 ºC. After 2 minutes, 0.8 mL cold PBS was added to each well to inhibit the trypsin, and the suspensions were then centrifuged for 5 minutes at 2000 rpm. Cell pellets were resuspended in 400 μL of PBS. Cell fluorescence was measured using a BD C6 Accuri flow cytometer by collecting 10,000 events per sample. The cells were excited using a 488 nm laser and emission at the 585 ± 20 nm region was measured. Differences were determined according to a post hoc Games-Howell test using predictive analytics SPSS software. This statistical test was chosen because it does not assume equal variance, which we deemed most relevant for comparing multiple biological replicates of HEK 293A cells (* used in figures indicates a p value $< 0.05$).

**4.4.8. Cell Preparation for Confocal and Fluorescence Lifetime Microscopy.** HEK 293 A cells were seeded in 2 well confocal chambers (Nunc Labtek II, 4 $cm^2$) at a density of 50,000 cells per well in 1.5 mL of complete DMEM and incubated overnight at 37 °C with 5% $CO_2$. The complete media was removed prior to incubation with G5-$NH_2$-$TAMRA_n$. The cells were then rinsed with 1 mL of PBS, followed by addition of 0.5 mL serum free DMEM. Cells were incubated with 1 μM G5 TAMRA in serum free DMEM for 3 hours. The cells were then rinsed with PBS three times and fixed using 2% paraformaldehyde. The fixed cells were rinsed 3 times with PBS, two drops of prolong gold solution containing DAPI was added, and a 1.5 thickness coverslip was placed on each sample.

**4.4.9. Confocal Fluorescence Microscopy.** Confocal microscopy was performed using Leica SP5 inverted confocal microscope using a 40x oil immersion objective. The section thickness was set

at 1 μm. The excitation wavelength used was 555 nm, and the emission from 585 nm to 700 nm was measured.

**4.4.10. Time Domain Fluorescence Lifetime Imaging Microscopy (FLIM) of G5-$NH_2$-$TAMRA_n$ in HEK 293A Cells using a Multi Photon Laser.** Lifetime imaging for HEK293A cells was performed using a LEICA inverted SP5 confocal microscope in the multiphoton mode. The source was a Mai-Tai laser with a 20 MHz frequency. The excitation wavelength was 850 nm with 2.2 W power. A PMT detector and TCSPC counter were used to measure lifetime. Images shown were taken at approximately mid-cell height by first taking an image in the x-z plane and using the DAPI signal to estimate cell heights (about 8 μm for the HEK293A cells). The z position was then set to this value, and the x-y plane images shown in Figure 5 were obtained. Taking images too near the confocal chamber or coverslip surface induced low lifetime artifacts. Measurements were taken until a maximum of 1000 photons were measured for each pixel. The lifetime histograms and exponential fitting were performed using Symphotime software (Picoquant Inc). The FLIM images of cells presented here show the average lifetime per pixel calculated using the FastFLIM algorithm in Symphotime. For solution lifetimes, single exponential lifetimes were used. It has been reported that the lifetime of TAMRA changes with temperature.[39] In our experiments, the MP laser could heat samples and change lifetimes. To test for this, the lifetimes for free TAMRA and G5-$NH_2$-$TAMRA_1$ were measured using two sequential four minute scans (the average time to image a field of cells) to test if heating during image acquisition was affecting measured lifetime values. For free TAMRA, the sequentially measured lifetime values were 2.37 and 2.36 ns. For G5-$NH_2$-$TAMRA_1$ , the values were 2.46 and 2.40 ns. These results indicate that change in lifetime due to temperature is not a cause for concern in our study.

**4.4.11. Fluorescence Lifetime Imaging Microscopy (FLIM) Measurement of G5-$NH_2$-$TAMRA_n$ lifetime using Single Photon Laser Excitation.** Lifetime imaging in solution was performed using an Olympus IX-81 time resolved confocal microscope using avalanche photodiodes. The source was a SC-400-6-PP supercontinuum laser with 20 MHz frequency. The excitation wavelength was 530 nm with 6.0 W power. An APD detector and TCSPC counter were used to measure lifetime. The lifetime histograms and exponential fitting were performed using ALBA software. Single exponential fitting was performed to obtain solution lifetimes. The mean fluorescence intensity and fluorescence lifetime of each sample was measured. One-way ANOVA

followed by Games-Howell post hoc analysis was performed to test if the means were significantly different.

**4.4.12. Solution Conditions to Measure Control Fluorescence Lifetimes in FLIM.** Control measurements in water, 1X PBS, undiluted FBS (Thermo Fisher Scientific), NaCl (137mM), BSA (23 mg/mL), glucose (1.25 mg/mL), and ficoll (60 mg/mL) were performed using 200 μM G5-$NH_2$-$TAMRA_n$. Polyplex solutions were mixed at an N:P of 10:1 and 1:1 at a concentration of 500 nM G5-$NH_2$-$TAMRA_n$ based on published protocols.[40]

**4.4.13. Preparation of Cell Lysate.** HEK 293A cell lysate was prepared by washing a confluent plate of cells with 1X PBS. The cells were then treated with 2 mL trypsin for 2 min at 37° C. The trypsinization was stopped by adding 8 mL of complete DMEM. The cells were triturated and counted using a hemocytometer. The cells were centrifuged at 1400 g for 2 min and the supernatant was removed. The cells were then suspended in DI water such that there were 5 million cells per mL and sonicated in a bath sonicator for 15 min. The absence of intact cells was checked using a light microscope. For use in experiments, the lysate was diluted to 100,000 cells/mL. This protocol was used rather than typical cell lysate protocols in order to avoid detergents, which interfere with fluorescence lifetime solution measurements, and to include all cell lipid.

## 4.5. References


(1) Larson, N., and Ghandehari, H. (2012) Polymeric Conjugates for Drug Delivery. *Chem. Mater. 24*, 840-853.

(2) Lee, C. C., MacKay, J. A., Frechet, J. M. J., and Szoka, F. C. (2005) Designing dendrimers for biological applications. *Nature Biotech. 23*, 1517-1526.

(3) Haag, R., and Kratz, F. (2006) Polymer Therapeutics: Concepts and Applications. *Angew. Chem. Int. Ed. 2006*, 1198-1215.

(4) Mintzer, M. A., and Grinstaff, M. W. (2011) Biomedical applications of dendrimers: a tutorial. *Chem. Soc. Rev. 40*, 173-190.

(5) Mintzer, M. A., and Simanek, E. E. (2009) Nonviral Vectors for Gene Delivery. *Chem. Rev. 109*, 259-302.

(6) Chen, M. J., and Yin, M. Z. (2014) Design and development of fluorescent nanostructures for bioimaging. *Prog. Polym. Sci. 39*, 365-395.

(7) Mullen, D. G., Fang, M., Desai, A., Baker, J. R., Orr, B. G., and Holl, M. M. B. (2010) A Quantitative Assessment of Nanoparticle-Ligand Distributions: Implications for Targeted Drug and Imaging Delivery in Dendrimer Conjugates. *Acs Nano 4*, 657-670.

(8) Mullen, D. G., and Banaszak Holl, M. M. (2011) Heterogeneous ligand-nanoparticle distributions: a major obstacle to scientific understanding and commercial translation. *Acc. Chem. Res. 44*, 1135-1145.

(9) Alexis, F., Pridgen, E., Molnar, L. K., and Farokhzad, O. C. (2008) Factors affecting the clearance and biodistribution of polymeric nanoparticles. *Mol. Pharmaceutics 5*, 505-515.

(10) Duan, X. P., and Li, Y. P. (2013) Physicochemical Characteristics of Nanoparticles Affect Circulation, Biodistribution, Cellular Internalization, and Trafficking. *Small 9*, 1521-1532.
(11) Moyano, D. F., Goldsmith, M., Solfiell, D. J., Landesman-Milo, D., Miranda, O. R., Peer, D., and Rotello, V. M. (2012) Nanoparticle Hydrophobicity Dictates Immune Response. *J. Am. Chem. Soc. 134*, 3965-3967.
(12) van Dongen, M., Dougherty, C. A., and Banaszak Holl, M. M. (2014) Multivalent Polymers for Drug Delivery and Imaging: The Challenges of Conjugation. *Biomacromolecules 15*, 3215-3234.
(13) Duhamel, J. (2014) Global Analysis of Fluoresence Decays to Probe the Internal Dynamics of Fluorescently Labeled Macromolecules. *Langmuir 30*, 2307-2324.
(14) Dougherty, C. A., Furgal, J. C., van Dongen, M. A., Goodson, T., Holl, M. M. B., Manono, J., and DiMaggio, S. (2014) Isolation and Characterization of Precise Dye/Dendrimer Ratios. *Chem. Eur. J. 20*, 4638-4645.
(15) Pansare, V. J., Hejazi, S., Faenza, W. J., and Prud'homme, R. K. (2012) Review of Long-Wavelength Optical and NIR Imaging Materials: Contrast Agents, Fluorophores, and Multifunctional Nano Carriers. *Chem. Mater. 24*, 812-827.
(16) Wangler, C., Moldenhauer, G., Saffrich, R., Knapp, E. M., Beijer, B., Schnolzer, M., Wangler, B., Eisenhut, M., Haberkorn, U., and Mier, W. (2008) PAMAM Structure-Based Multifunctional Fluorescent Conjugates for Improved Fluorescent Labelling of Biomacromolecules. *Chem. Eur. J. 14*, 8116-8130.
(17) Kim, Y., Kim, S. H., Tanyeri, M., Katzenellenbogen, J. A., and Schroeder, C. M. (2013) Dendrimer Probes for Enhanced Photostability and Localization in Fluorescence Imaging. *Biophys. J. 104*, 1566-1575.
(18) Opitz, A. W., Czymmek, K. J., Wickstrom, E., and Wagner, N. J. (2013) Uptake, effux, and mass transfer coefficient of fluorescent PAMAM dendrimers into pancreatic cancer cells. *Biochem. Biophys. Acta 1828*, 294-301.
(19) He, C. B., Hu, Y. P., Yin, L. C., Tang, C., and Yin, C. H. (2010) Effects of particle size and surface charge on cellular uptake and biodistribution of polymeric nanoparticles. *Biomaterials 31*, 3657-3666.
(20) Santos, J. L., Oliveira, H., Pandita, D., Rodrigues, J., Pego, A. P., Granja, P. L., and Tomas, H. (2010) Functionalization of poly(amidoamine) dendrimers with hydrophobic chains for improved gene delivery in mesenchymal stem cells. *J. Controlled Release 144*, 55-64.
(21) Shakhbazau, A., Isayenka, I., Kartel, N., Goncharova, N., Seviaryn, I., Kosmacheva, S., Potapnev, M., Shcharbin, D., and Bryszewska, M. (2010) Transfection efficiencies of PAMAM dendrimers correlate inversely with their hydrophobicity. *Int. J. Pharm. 383*, 228-235.
(22) Vuorimaa, E., Urtti, A., Seppanen, R., Lemmetyinen, H., and Yliperttula, M. (2008) Time-resolved fluorescence spectroscopy reveals functional differences of cationic polymer-DNA complexes. *J. Am. Chem. Soc. 130*, 11695-11700.
(23) Ketola, T. M., Hanzlikova, M., Urtti, A., Lemmetyinen, H., Yliperttula, M., and Vuorimaa, E. (2011) Role of Polyplex Intermediate Species on Gene Transfer Efficiency: Polyethylenimine-DNA Complexes and Time-Resolved Fluorescence Spectroscopy. *J. Phys. Chem. B. 115*, 1895-1902.
(24) Yoo, H., and Juliano, R. L. (2000) Enhanced delivery of antisense oligonucleotides with fluorophore-conjugated PAMAM dendrimers. *Nucleic Acids Res. 28*, 4225-4231.

(25) Seib, F. P., Jones, A. T., and Duncan, R. (2006) Establishment of subcellular fractionation techniques to monitor the intracellular fate of polymer therapeutics I. Differential centrifugation fractionation B16F10 cells and use to study the intracellular fate of HPMA copolymer-doxorubicin. *J. Drug Target. 14*, 375-390.
(26) Yang, Y., Sunoqrot, S., Stowell, C., Ji, J. L., Lee, C. W., Kim, J. W., Khan, S. A., and Hong, S. (2012) Effect of Size, Surface Charge, and Hydrophobicity of Poly(amidoamine) Dendrimers on Their Skin Penetration. *Biomacromolecules 13*, 2154-2162.
(27) Perumal, O. P., Inapagolla, R., Kannan, S., and Kannan, R. M. (2008) The effect of surface functionality on cellular trafficking of dendrimers. *Biomaterials 29*, 3469-3476.
(28) van Dongen, M. A., Desai, A., Orr, B. G., Baker, J. R., and Holl, M. M. B. (2013) Quantitative analysis of generation and branch defects in G5 poly(amidoamine) dendrimer. *Polymer 54*, 4126-4133.
(29) Mullen, D. G., Borgmeier, E. L., Desai, A. M., van Dongen, M. A., Barash, M., Cheng, X. M., Baker, J. R., and Holl, M. M. B. (2010) Isolation and Characterization of Dendrimers with Precise Numbers of Functional Groups. *Chem. Eur. J. 16*, 10675-10678.
(30) Selwyn, J. E., and Steinfeld, J. I. (1972) Aggregation Equilibria of Xanthene Dyes. *J. Phys. Chem. 76*, 762-774.
(31) van Dongen, M., Orr, B. G., and Banaszak Holl, M. M. (2014) Diffusion NMR Study of Generation Five PAMAM Dendrimer Materials. *J. Phys. Chem. B. 118*, 7195-7202.
(32) Chen, L. C., Lloyd, W. R., Chang, C. W., Sud, D., and Mycek, M. A. (2013) Fluorescence Lifetime Imaging Microscopy for Quantitative Biological Imaging. *Methods Cell Biol. 114*, 457-488.
(33) Lin, H.-J., Herman, P., and Lakowicz, J. R. (2003) Fluorescence Lifetime-Resolved pH Imaging of Living Cells. *Cytometry Part A 52A*, 77-89.
(34) Unruh, J. R., Gokulrangan, G., Wilson, G. S., and Johnson, C. K. (2005) Fluoresence Properties of Fluorescein, Tetramethylrhodamine and Texas Red Linked to a DNA Aptamer. *Photochem. Photobiol. 81*, 682-690.
(35) Thomas, T. P., Majoros, I., Kotlyar, A., Mullen, D., Holl, M. M. B., and Baker, J. R. (2009) Cationic Poly(amidoamine) Dendrimer Induces Lysosomal Apoptotic Pathway at Therapeutically Relevant Concentrations. *Biomacromolecules 10*, 3207-3214.
(36) Xu, Z. J., He, B. C., Shen, J., Yang, W. T., and Yin, M. Z. (2013) Fluorescent water-soluble perylenediimide-cored cationic dendrimers: synthesis, optical properties, and cell uptake. *Chemical Communications 49*, 3646-3648.
(37) Ornelas, C., Lodescar, R., Durandin, A., Canary, J. W., Pennell, R., Liebes, L. F., and Weck, M. (2011) Combining Aminocyanine Dyes with Polyamide Dendrons: A Promising Strategy for Imaging in the Near-Infrared Region. *Chem. Eur. J. 17*, 3619-3629.
(38) Ornelas, C., Pennell, R., Liebes, L. F., and Weck, M. (2011) Construction of a Well-Defined Multifunctional Dendrimer for Theranostics. *Org. Lett. 13*, 976-979.
(39) Vámosi, G., Gohlke, C., and Clegg, R. M. (1996) Fluorescence Characteristics of 5-Carboxytetramethylrhodamine Linked Covalently to the 5' End of Oligonucelotides: Multiple Conformers of Single-Stranded and Double-Stranded Dye-DNA Oligomers. *Biophys. J. 71*, 972-994.
(40) Rattan, R., Vaidyanathan, S., Wu, G. S. H., Shakya, A., Orr, B. G., and Holl, M. M. B. (2013) Polyplex-Induced Cytosolic Nuclease Activation Leads to Differential Transgene Expression. *Mol. Pharmaceutics 10*, 3013-3022.

# Chapter 5.

# Controlling the Double Distribution on a G5 PAMAM Dendrimer

## 5.1. Introduction

A large interest in polymer theranostic materials has come about because of a multivalent polymer's ability to easily have multiple copies of small molecules such as drugs, imaging agents, and targeting ligands conjugated to it.[1-5] A theranostic is a material with the ability to both treat (therapeutic) and diagnose (diagnostic) a disease.[6-8] A multivalent polymer as a theranostic has the potential to provide a higher drug payload and achieve optimal imaging conditions[9-12] while specifically targeting the intended diseased cell/tissue. This targeting allows for healthy cells to be unharmed and reduces negative side effects.[13-15]

However, the conjugation of one small molecule to a multivalent polymer leads to a mixture of different ratios of small molecule to polymer.[16-18] The different ratios of small molecules to the polymer leads to differing toxicity, solubility, pharmacokinetics, and biodistribution for each ratio in biological applications.[17,19,20] The mixture of varying ratios of a small molecule to a polymer with many reactive sites is normally well approximated by a Poisson distribution.[16] Heterogeneity in the sample will also worsen with each small molecule conjugation, meaning more than one small molecule conjugation to the polymer will create a larger distribution.[17] For instance, in a general example of the synthesis of a polymer theranostic with 3 targeting ligands, 4 fluorescent dyes, and 5 therapeutic drugs, the resulting distribution is the multiplication of each individual Poisson distribution. In the case of attaching 3 targeting ligands, the ratio of 3 targeting ligands to the polymer represents 22.7 % of the entire sample from one conjugation. Conjugating an average of 4 fluorescent dyes results in only 4.5 % of the entire sample having the desired targeting ligand and fluorescent dye ratio. Once the third conjugation of an average of 5 therapeutic drugs is considered, only 0.8 % of the entire sample has the desired average of all three small molecules. This equates to about 1 out of every 250 particles is the desired theranostic material. Having such a large variety of ratios of targeting ligands, drugs, and dyes leads to a variety of different biological behaviors. Deciphering which ratios of materials are responsible for each biological behavior observed is impossible with such a large distribution of materials.

Several synthetic strategies have been attempted in order to decrease the heterogeneity of small molecules on the polymer in order to better understand the optimal ratio of small molecules to polymer to obtain desired biological behaviors of a theranostic.[21-30] These polymer platforms include using dendrons and convergent dendrimer synthesis,[21-23] fluorescent core dendrimers,[25-27] and using high averages to avoid the largest hydrophobicity differences in the sample.[30] Another strategy developed by the Banaszak Holl lab uses a divergent dendrimer platform and the isolation of precise ratios of a small molecule on the polymer by semi-preparative reverse-phase high performance liquid chromatography (rp-HPLC).[28,29] Isolating precise ratios of small molecules on a generation 5 poly(amidoamine) (G5 PAMAM) dendrimer has been demonstrated for both fully acetylated (neutral) and amine terminated (cationic) dendrimers.[28,29,31,32] The isolation of a precise ratio of fluorophores on an amine terminated dendrimer provides the opportunity for further conjugations of drugs or targeting ligands while still maintaining a precise ratio of fluorophores on a per particle level.

The conjugation of a monofluorinated cyclooctyne (MFCO) "click" ligand onto a G5-$NH_2$-$TAMRA_1$ and G5-$NH_2$-$TAMRA_2$ is reported. The material was fully acetylated to obtain G5-NHAc-$TAMRA_m$-$MFCO_n$ (m = 1, 2) and these materials were isolated by rp-HPLC. Obtaining precise ratios of MFCO was attempted for n = 1 - 4 and was characterized by $^1$H NMR, $^{19}$F NMR, MALDI-TOF-MS, and rp-UPLC. The MFCO linker provides a systematic ratio change on the dendrimer in order to conjugate on drugs or targeting ligands that are azide functionalized to a dendrimer with a precise ratio of fluorophores. The advantages and challenges of this particular double conjugation strategy are discussed. Other strategies to control the double distribution are also discussed as a potential way to control multiple ratios of small molecules on a polymer for theranostic applications.

**5.2. Results and Discussion**

A polymer with multiple reaction sites conjugated with a low average of small molecules under ideal reaction conditions (high stirring, dilute concentrations, and aiming for a low average of small molecules to polymer) will yield a Poisson distribution of small molecule-polymer ratios. The Poisson distribution can be resolved into individual ratios of small molecules to polymer using semi preparative rp-HPLC. The isolation has been proven to be successful using generation 5 poly(amidoamine) G5 PAMAM dendrimers and multiple small molecules, including "click" chemistry ligands and rhodamine dye (TAMRA) derivatives.[28,29,32] The resolved distribution is

isolated into each individual ratio as shown by the ultra-performance liquid chromatography (UPLC) trace indicating only one peak in each sample after isolation. The isolation of different ratios of TAMRA to G5 PAMAM dendrimer has been successful for both fully acetylated and amine terminated dendrimer materials.[29,31] The fully acetylated materials do not have an ability to be further functionalized, but the amine terminated precise ratio material can be used for second ligand conjugation. The second conjugation would result in another Poisson distribution.

Using amine terminated G5 PAMAM dendrimer conjugates with precise ratios of m=1 and m=2 of TAMRA dye, MFCO-N-hydroxysuccinimide ester (MFCO) was conjugated to the remaining primary amines by EDC/NHS coupling (Figure 5.1). Upon conjugation and full acetylation of the G5-$TAMRA_m$-$MFCO_n$ material, a distribution was observed by rp-HPLC (Figure 5.2). Since the starting material for both isolations was one single peak before conjugation, the presence of multiple resolved peaks indicates a successful conjugation of the MFCO linker to precise dye-dendrimer material. The ratio of MFCO to G5-NHAc-$TAMRA_m$ results in a retention

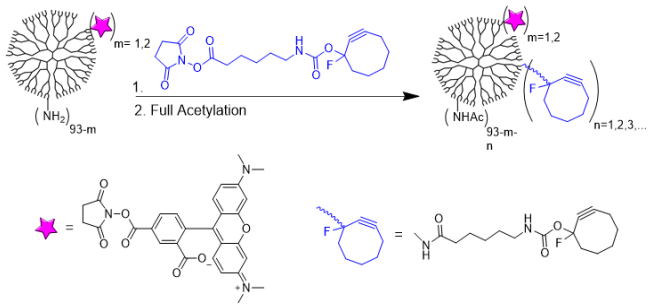


**Figure 5.1.** Conjugation of G5-$NH_2$-$TAMRA_m$ (m=1,2) with a monofluorinated cyclooctyne (MFCO) ligand and subsequent full acetylation.

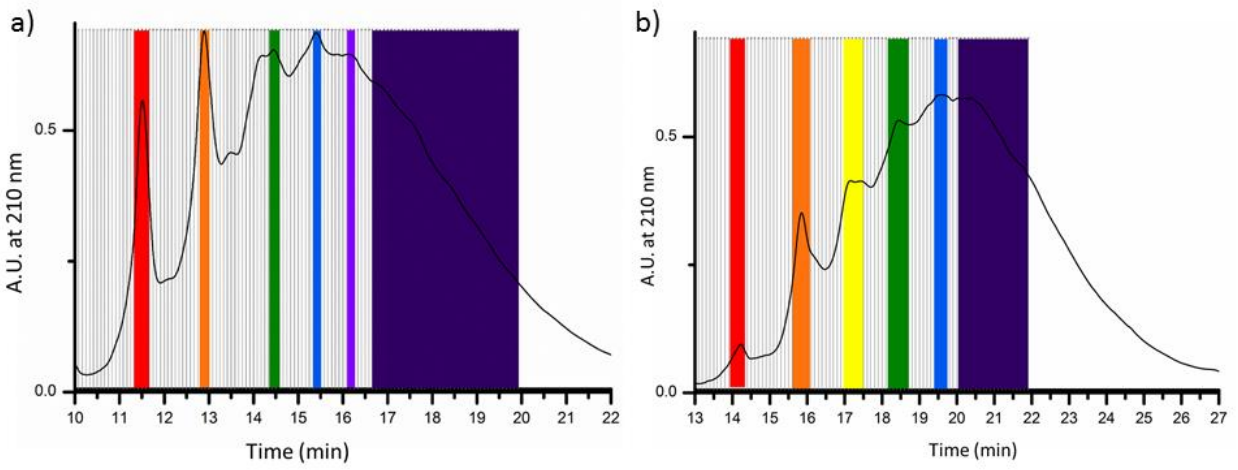


**Figure 5.2.** rp-HPLC isolation of a) G5-NHAc-$TAMRA_{m=1}$-$MFCO_n$ and b) G5-NHAc-$TAMRA_{m=2}$-$MFCO_n$. For m=1, n=0 (red), n=1 (orange), n=2 (green), n=3 (blue), n=4 (violet), and n=5+ (purple). For m=2, n=0 (orange), n=1 (yellow), n=2 (green), n=3 (blue), n=4+ (purple).

time shift in the HPLC chromatogram taken at 210 nm (absorption wavelength of the dendrimer). Individual fractions were collected and recombined as shown by the colored bars in Figure 5.2a and Figure 5.2b chromatograms. Figure 5.2a is the chromatogram of the G5-NHAc-TAMRA$_1$-MFCO$_n$ case, and Figure 5.2b is the chromatogram for the G5-NHAc-TAMRA$_2$-MFCO$_m$ material.

In order to ensure that there was still a precise ratio of TAMRA to dendrimer, fluorescence emission spectra were taken for the m=1 and n=1-3 materials G5-NHAc-TAMRA$_m$-MFCO$_n$ materials (Figure 5.3). At the same dendrimer concentration, all materials show the similar emission intensity, proving that the same ratio of TAMRA was present on all MFCO samples. However, this measurement does not help determine the ratio of MFCO linkers on the G5 PAMAM material, nor does it determine the homogeneity of MFCO-dendrimer ratio for each sample.

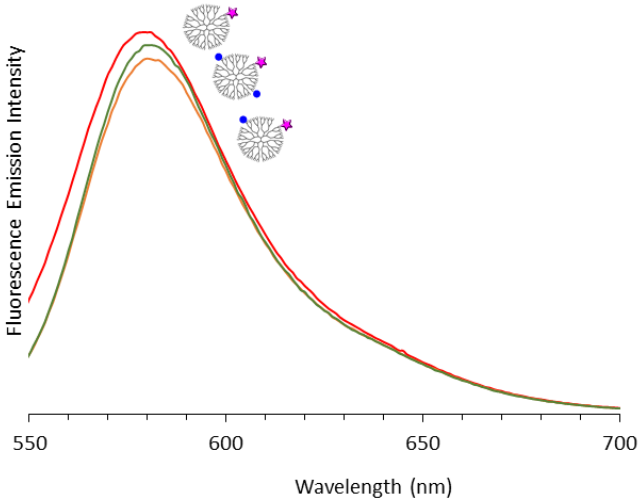


**Figure 5.3.** Fluorescence emission at 0.1mg/mL for G5-NHAc-TAMRA$_1$-MFCO$_n$ materials. All samples show similar fluorescence emission for m=1 and n=1, 2, and 3.

$^1$H NMR spectroscopy and $^{19}$F NMR spectroscopy were attempted for all the samples isolated to determine ratios of MFCO and TAMRA on the G5-NHAc-TAMRA$_m$-MFCO$_n$ material. While proton NMR suffers from signal to noise issues when attempting to determine ratios of small molecules to dendrimer, typically the integrated ratio is close to the desired ratio.[29,32] The G5-NHAc-TAMRA$_1$-MFCO$_n$ materials still retain approximately 1 TAMRA per dendrimer material after the second conjugation and isolation, 0.7-1.1 for all m by $^1$H NMR (Table 5.1). In order to determine the ratio of MFCO to G5, $^{19}$F NMR can be used. The MFCO small molecule proton peaks are in close proximity to the dendrimer peaks, and therefore, integration of these small molecules to determine ratio would be inaccurate. Using $^{19}$F NMR has been used previously to determine ratio of MFCO on a dendrimer.[29] In these samples, however, the fluorine signal was not large enough in order to measure the ratio of MFCO to G5 PAMAM. Only the n = 5+ sample

produces a fluorine signal. All other ratios did not have any fluorine signal in the m=1 samples, and therefore, a ratio of MFCO could be determined.

For the m = 2 material after the rp-HPLC isolation, the G5-NHAc-$TAMRA_2$-$MFCO_n$ material has TAMRA averages of 8.2, 3.6, 2.9, 12.5, and 2.4 for n = 0-3, 4+. The material should have had approximately 2 TAMRAs per dendrimer particle, so the number of TAMRAs per dendrimer particle cannot be defined as approximately the same for all n ratios isolated. The reason for the drastic difference in TAMRA ratio is unknown since the starting material had a precise ratio of 2 TAMRAs per dendrimer particle. The $^{19}F$ NMR spectra of m = 2 samples were concentrated enough to see a fluorine signal from the MFCO linker for all n ratios. The ratios determined by NMR, however, are not consistent with the predicted ratios as determined by UPLC retention time (Figure 5.4). For m = 0-3, 4+, the MFCO ratios are 0.0, 1.0, 2.1, 0.6, and 8.9 as determined by $^{19}F$ NMR peak areas.[29] While m = 0, 1, 2, and 4+ are consistent with the increased HPLC retention time, the m = 3 sample decreases in ratio as measured by $^{19}F$ NMR from unknown reasons. Because of the signal to noise issues between polymer and small molecules and inconsistencies in signal in both proton and fluorine NMR integrations for all samples, another analytical technique must be used in order to determine accurate ratios of MFCO to G5 PAMAM.

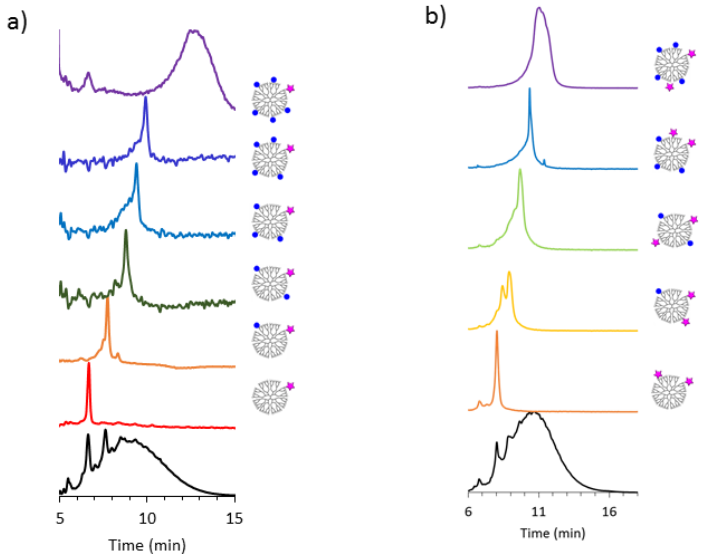


**Figure 5.4.** rp-UPLC reinjection of isolated materials to determine purity. a) m=1, n=0 (red), n=1 (orange), n=2 (green), n=3 (blue), n=4 (violet), and n=5+ (purple). b) m=2, n=0 (orange), n=1 (yellow), n=2 (green), n=3 (blue), n=4+ (purple).

Analytical UPLC chromatograms were obtained in order to determine peak shape and purity of both the m =1 and m = 2 rp-HPLC isolations (Figure 5.4). There is an increase in retention time with increasing ratio of MFCO. However, the peak shape does not resemble typical conjugations of a small molecule to a G5 PAMAM dendrimer. The observed peak purity has also decreased compared to typical isolated materials with one conjugation. All isolated materials

have at least 2 peaks at varying ratios in any one sample. This is due to the poor resolution and lack of baseline resolution between each ratio. Overlapping peaks result in multiple ratios of MFCO being isolated out together. Typical one conjugation isolations have the ability to isolate out with over 95% purity ratios of n=1-4 to the dendrimer. While the samples are not as pure as a single isolation, all MFCO ratio materials isolated show a difference in retention time, and have an ability to observe the purity and identify the ratio of MFCO linkers by this technique.

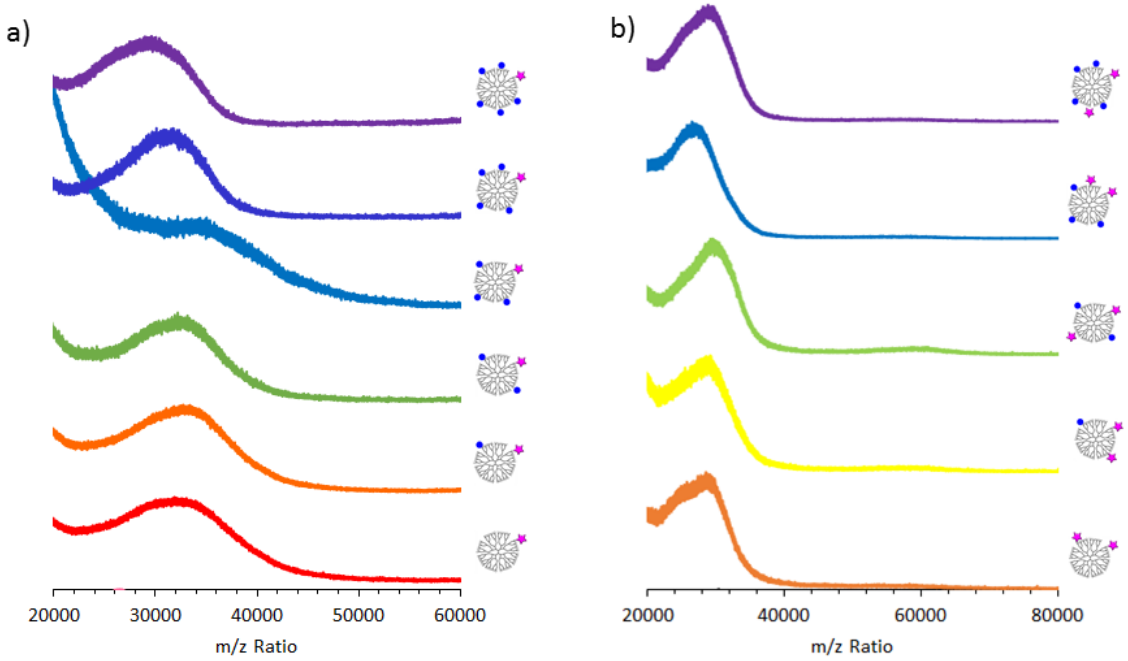


**Figure 5.5.** MALDI-TOF-MS spectra of precise ratio samples for G5-NHAc-TAMRA$_m$-MFCO$_n$ a) m=1 and b) m=2. For m=1, n=0 (red), n=1 (orange), n=2 (green), n=3 (blue), n=4 (violet), and n=5+ (purple). For m=2, n=0 (orange), n=1 (yellow), n=2 (green), n=3 (blue), n=4+ (purple).

MALDI-TOF-MS was taken for all samples (Figure 5.5). The width of the molecular weight distribution of the G5 PAMAM polymer ranges from ~21,000 to 28,000 g/mol. Therefore, the difference in molecular weight from the MFCO linker (286 g/mol) is smaller than the molecular weight distribution of the dendrimer material and cannot accurately determine the number of ligands present on each polymer particle. As shown in Figure 5.5 (and Table 5.1), the molecular weight obtained from MALDI-TOF-MS does not show an increase of 286 g/mol for each ratio. It does not even show a general increase in molecular weight. For example going from a theoretical ratio of n = 2 to n = 3 MFCO linkers on the G5-NHAc-TAMRA$_1$-MFCO$_n$ material, the m/z ratio decreases from 33,500 g/mol to 33,100 g/mol. The breadth of the molecular weight distribution of

the G5 PAMAM limits the accuracy for one isolation as shown in Chapters 2 and 4, and the accuracy only worsens with the second isolation. Rp-UPLC is the best analytical technique to determine purity and ratio of the samples compared to MALDI-TOF-MS, $^{1}$H NMR, and $^{19}$F NMR for the double conjugation materials.

| | ave # TAMRA | Fluorine Signal Ratio | m/z MALDI max |
|---|---|---|---|
| G5-NHAc-TAMRA$_1$-MFCO$_0$ | 1 | 0 | 33,000 |
| G5-NHAc-TAMRA$_1$-MFCO$_1$ | 0.8 | 0 | 33,500 |
| G5-NHAc-TAMRA$_1$-MFCO$_2$ | 1.1 | 0 | 33,100 |
| G5-NHAc-TAMRA$_1$-MFCO$_3$ | 1 | 0 | 35,000 |
| G5-NHAc-TAMRA$_1$-MFCO$_4$ | 0.9 | 0 | 31,600 |
| G5-NHAc-TAMRA$_1$-MFCO$_{5+}$ | 0.7 | 1375 (raw intensity) | 30,000 |
| G5-NHAc-TAMRA$_2$-MFCO$_0$ | 8.2 | 0 | 29,700 |
| G5-NHAc-TAMRA$_2$-MFCO$_1$ | 3.6 | 1.0 (set) | 29,700 |
| G5-NHAc-TAMRA$_2$-MFCO$_2$ | 2.9 | 2.1 | 30,400 |
| G5-NHAc-TAMRA$_2$-MFCO$_3$ | 12.5 | 0.6 | 27,800 |
| G5-NHAc-TAMRA$_2$-MFCO$_{4+}$ | 2.4 | 8.9 | 29,600 |

**Table 5.1.** Characterization summary for G5-NHAc-TAMRA$_n$-MFCO$_m$ material.

### 5.3. Conclusions

A double Poisson distribution of ligands is a major issue in developing polymer theranostic materials. A way to attempt to control both ratios of dyes and targeting agents/drugs on a polymer is to deconvolute the ratio of ligands from the molecular weight distribution of the polymer. This has been done using a G5 PAMAM dendrimer polymer platform. It has been shown that isolation of G5-NH$_2$-TAMRA$_m$ for m=1 and m=2 materials have the ability to be further functionalized with a second conjugation of the "click" ligand MFCO. However, due to lack of characterization and low yield, it was not definitively proven that precise ratios of TAMRA and MFCO were obtained on a G5 PAMAM dendrimer from rp-HPLC isolations. The HPLC isolation technique shows great

promise for the one conjugation materials,[29,31,32] but the lack of yield with the current system does not allow for significant amounts of materials to be obtained for the second conjugation isolation. New strategies must be attempted if the current rp-HPLC isolation methods are to be used. One way to obtain precise ratios of both dye and targeting agent/drug is to synthesize one small molecule that is both fluorescent and targeting/therapeutic. The fluorescence targeting/therapeutic molecule can be functionalized with an azide or alkyne in order to obtain precise ratios of fluorophore and targeting agent/drug on the dendrimer. This method is currently being explored for a fluorescent targeting molecules using a coumarin-azide dye conjugated to folic acid. The conjugation of the folic acid to the coumarin will allow for targeting of cancer tissue that overexpresses the folate receptor. The material also has an azide which can be clicked onto G5-NHAc-$MFCO_n$ material to provide fluorescence. The method of clicking onto G5-NHAc-$MFCO_n$ material has already proven to be a successful method to obtain precise ratios of a small molecule to a dendrimer.[28,29] The small molecule synthesis strategy is limited because it does not allow to keep one ratio of dye while systematically altering the targeting agent or drug ratio on the dendrimer. Since it is known that the fluorophore ratio has an impact on the dendrimer's biological and photophysical behavior,[31] it would be ideal to develop a strategy which allows for a single ratio of fluorophore while altering the targeting agent or drug ratio.

A second strategy in order to overcome the first strategy's major obstacle is to use click chemistry functionalized dendrons. A G3 bis MPA azide dendron can be purchased from Polymer Factory which has 4 hydroxy surface groups and an azide at the focal point. The 4 surface groups can be functionalized with one dye and 1.0, 2.0, or 3.0 equivalents of a targeting agent or drug. A distribution will not occur in the dendron case due to the low number of reactive sites. The dendron can then be clicked to G5-NHAc-$MFCO_m$ material. The dendron-dendrimer strategy provides an opportunity to determine how the ratio of increasing targeting agents and drugs alters the polymer's behavior without the typical convolution of changing fluorophore ratio as well.

**5.4. Experimental Methods**

Biomedical grade G5 PAMAM dendrimer was purchased from Dendritech Inc. and purified using rp-HPLC to give a molecular weight fraction free of trailing generations (G1-G4) as well as G5 dimers and higher oligomers.[33] Trifluoroacetic acid, HPLC grade water, GE PD-10 Sephadex columns, and HPLC grade acetonitrile were purchased from Fisher-Scientific and used as received. 5-carboxy tetramethylrhodamine succinimydyl ester (TAMRA) was purchased from Life

Technologies. A 700 MHz Varian NMR instrument was used for all $^{1}H$ NMR measurements and a 500MHz Varian NMR instrument was used for all $^{19}F$ NMR measurements. All MALDI-TOF MS measurements were performed on a Bruker Ultraflex III with sinapinic acid matrix (Sigma Aldrich) and sodium trifluoroacetate (Fischer Scientific) salt sample preparation. A Water Acuity system with a C18 silica-based UPLC column (Agilent) was employed for all rp-UPLC measurements. Conjugation and isolation of precise ratios of G5-$NH_2$-$TAMRA_n$ were prepared and obtained using previous published protocols.[31]

**5.4.1. Conjugation of MFCO to G5-$NH_2$-$TAMRA_m$.** In a 25 mL round bottom flask covered in aluminum foil, the G5-$NH_2$-$TAMRA_n$ (31.6mg, $1.1x10^{-3}$ mmol, 1.0 equiv) material was dissolved in 7.10 mL of water. In another vial, MFCO-N-hydroxysuccinimide (0.9 mg, $2.2x10^{-3}$ mmol, 2.0 equiv) was dissolved in 0.22 mL of acetonitrile. The MFCO solution was added dropwise to the dendrimer solution with the solution stirring rapidly. The solution stirred in the dark at 25 ˚C overnight. The solvent was removed, and the solid was redissolved in 3.0 mL of water. The solution was transferred to a 10,000 MW cutoff Slide-A-Lyzer dialysis cassette. The solution was dialyzed in the dark through 8 rounds of water for purification. The solvent was removed via lyophilization. A pink solid was obtained at 67% yield.

**5.4.2. Full Acetylation of G5-$NH_2$-$TAMRA_m$-$MFCO_n$.** In a 25mL round bottom flask covered in aluminum foil, the G5-$NH_2$-$TAMRA_n$-$MFCO_m$ was dissolved in 3.8 mL of methanol. 0.01 mL of acetic anhydride and 0.02 mL of trimethylamine was added to the round bottom flask, and the solution stirred for 4 hours 25 ˚C. The methanol was removed by a rotor evaporator, and the solid was redissolved in 3 mL of water. The solution was transferred to a 10,000 MW cutoff Slide-A-Lyzer dialysis cassette. The solution was dialyzed in the dark through 8 rounds of water for purification. The solvent was removed via lyophilization. A pink solid was obtained at 87% yield.

**5.4.3 Isolation of G5-NHAc-$TAMRA_m$-$MFCO_n$.** Semi-preparative rp-HPLC isolation was carried out on a Waters Delta 600 HPLC. For analysis of the dendrimer and conjugates, a C18 silica-based rp-HPLC column (250 x 21.20 mm, 10μm particles) connected to a C18 guard column (50 x 21.20 mm) was used. The mobile phase for elution of the conjugates was a linear gradient beginning with 95:5 (v/v) water/acetonitrile and ending with 65:35 (v/v) water/acetonitrile over 28 minutes at a flow rate of 12.00 mL/min. Trifluoroacetic acid (TFA) at 0.10 wt % concentration in both water and acetonitrile was used as a counter ion to make the dendrimer surfaces hydrophobic. Elution traces of the dendrimer-ligand conjugate were obtained at 210 nm. 120 fractions of 6

seconds duration were collected starting at 10 minutes. Selection of fractions for combination to yield the precise MFCO:TAMRA$_n$-dendrimer ratios was based upon analysis of the chromatogram in Origin-Pro. Each isolated combination of fractions was reinjected onto an analytical UPLC to determine purity of the sample.

**5.4.4. Analytical reverse-phase Ultra-high Performance Liquid Chromatography (rp-UPLC).** A linear gradient mobile phase beginning with 95:5 (v/v) water/acetonitrile and ending with 55:45 (v/v) water/acetonitrile over 22 minutes at a flow rate of 2.0mL/min was used. The water/acetonitrile mixture contained 0.10 wt % trifluoroacetic acid (TFA). Elution traces were measured at 210 nm (dendrimer). The instrument was also controlled by Empower 2 software.

**5.4.5. Emission Measurements.** Fluorescence (Fluoromax-4) measurements were taken at a concentration of 0.1 mg/mL. For all measurements, the concentration of the solutions were 0.1 mg/mL and within an error of ±0.02. For the fluorescence measurements an excitation of 530 nm and emission of 580 nm were used with a slit width of 2 nm.

**5.4.6. MALDI-TOF-MS Measurements.** Two solutions were prepared: 1) 1 mg/mL dendrimer in water and 2) 10 mg/mL DHB in 1:1 (v/v) acetonitrile: water. These were then combined in a ratio of 10:1 of matrix:dendrimer solution. The plate was spotted with 1 µL volumes of solution and allowed to dry. At least 100 scans were averaged per measurement.

**5.5. References**


(1) Duncan, R. The dawning era of polymer therapeutics. *Nat Rev Drug Discov* **2003**, *2*, 347-360.

(2) Lee, C. C.; MacKay, J. A.; Frechet, J. M. J.; Szoka, F. C. Designing dendrimers for biological applications. *Nat Biotechnol* **2005**, *23*, 1517-1526.

(3) Roglin, L.; Lempens, E. H. M.; Meijer, E. W. A Synthetic "Tour de Force": Well-Defined Multivalent and Multimodal Dendritic Structures for Biomedical Applications. *Angew Chem Int Edit* **2011**, *50*, 102-112.

(4) Stiriba, S. E.; Frey, H.; Haag, R. Dendritic polymers in biomedical applications: From potential to clinical use in diagnostics and therapy. *Angew Chem Int Edit* **2002**, *41*, 1329-1334.

(5) Sevenson, S.; Tomalia, D. A. Dendrimers in biomedical applications-reflections on the field. *Adv Drug Deliver Rev* **2012**, *64*, 102-115.

(6) Svenson, S. Theranostics: Are We There Yet? *Mol Pharm* **2013**, *10*, 848-856.

(7) Pasut, G.; Veronese, F. M. Polymer-drug conjugation, recent achievements and general strategies. *Prog Polym Sci* **2007**, *32*, 933-961.

(8) Kelkar, S. S.; Reineke, T. M. Theranostics: Combining Imaging and Therapy. *Bioconjugate Chem* **2011**, *22*, 1879-1903.

(9) Baker, J. R. Why I believe nanoparticles are crucial as a carrier for targeted drug delivery. *Wires Nanomed Nanobi* **2013**, *5*, 423-429.

(10) Duncan, R.; Gaspar, R. Nanomedicine(s) under the Microscope. *Mol Pharm* **2011**, *8*, 2101-2141.

(11) van der Meel, R.; Vehmeijer, L. J. C.; Kok, R. J.; Storm, G.; van Gaal, E. V. B. Ligand-targeted particulate nanomedicines undergoing clinical evaluation: Current status. *Adv Drug Deliver Rev* **2013**, *65*, 1284-1298.

(12) Boas, U.; Heegaard, P. M. H. Dendrimers in drug research. *Chem Soc Rev* **2004**, *33*, 43-63.

(13) Temming, K.; Schiffelers, R. M.; Molema, G.; Kok, R. J. RGD-based strategies for selective delivery of therapeutics and imaging agents to the tumour vasculature. *Drug Resist Update* **2005**, *8*, 381-402.

(14) Haag, R.; Kratz, F. Polymer therapeutics: Concepts and applications. *Angew Chem Int Edit* **2006**, *45*, 1198-1215.

(15) Ringsdorf, H. Structure and Properties of Pharmacologically Active Polymers. *J Polym Sci Pol Sym* **1975**, 135-153.

(16) Mullen, D. G.; Holl, M. M. B. Heterogeneous Ligand-Nanoparticle Distributions: A Major Obstacle to Scientific Understanding and Commercial Translation. *Accounts Chem Res* **2011**, *44*, 1135-1145.

(17) Mullen, D. G.; Fang, M.; Desai, A.; Baker, J. R.; Orr, B. G.; Holl, M. M. B. A Quantitative Assessment of Nanoparticle-Ligand Distributions: Implications for Targeted Drug and Imaging Delivery in Dendrimer Conjugates. *Acs Nano* **2010**, *4*, 657-670.

(18) van Dongen, M. A.; Dougherty, C. A.; Holl, M. M. B. Multivalent Polymers for Drug Delivery and Imaging: The Challenges of Conjugation. *Biomacromolecules* **2014**, *15*, 3215-3234.

(19) He, C. B.; Hu, Y. P.; Yin, L. C.; Tang, C.; Yin, C. H. Effects of particle size and surface charge on cellular uptake and biodistribution of polymeric nanoparticles. *Biomaterials* **2010**, *31*, 3657-3666.

(20) Alexis, F.; Pridgen, E.; Molnar, L. K.; Farokhzad, O. C. Factors affecting the clearance and biodistribution of polymeric nanoparticles. *Mol Pharm* **2008**, *5*, 505-515.

(21) Ornelas, C.; Lodescar, R.; Durandin, A.; Canary, J. W.; Pennell, R.; Liebes, L. F.; Weck, M. Combining Aminocyanine Dyes with Polyamide Dendrons: A Promising Strategy for Imaging in the Near-Infrared Region. *Chem-Eur J* **2011**, *17*, 3619-3629.

(22) Ornelas, C.; Pennell, R.; Liebes, L. F.; Weck, M. Construction of a Well-Defined Multifunctional Dendrimer for Theranostics. *Org Lett* **2011**, *13*, 976-979.

(23) Ornelas, C.; Broichhagen, J.; Weck, M. Strain-Promoted Alkyne Azide Cycloaddition for the Functionalization of Poly(amide)-Based Dendrons and Dendrimers. *J Am Chem Soc* **2010**, *132*, 3923-3931.

(24) Zhang, J. D.; Drugeon, G.; L'hermite, N. Synthesis of novel dendrimers incorporating a dye into the core. *Tetrahedron Lett* **2001**, *42*, 3599-3601.

(25) Xu, Z. J.; He, B. C.; Shen, J.; Yang, W. T.; Yin, M. Z. Fluorescent water-soluble perylenediimide-cored cationic dendrimers: synthesis, optical properties, and cell uptake. *Chem Commun* **2013**, *49*, 3646-3648.

(26) Yang, S. K.; Shi, X. H.; Park, S.; Doganay, S.; Ha, T.; Zimmerman, S. C. Monovalent, Clickable, Uncharged, Water-Soluble Perylenediimide-Cored Dendrimers for Target-Specific Fluorescent Biolabeling (vol 131, pg 9964, 2011). *J Am Chem Soc* **2011**, *133*, 13206-13206.

(27) Gilat, S. L.; Adronov, A.; Frechet, J. M. J. Light harvesting and energy transfer in novel convergently constructed dendrimers. *Angew Chem Int Edit* **1999**, *38*, 1422-1427.

(28) van Dongen, M. A.; Silpe, J. E.; Dougherty, C. A.; Kanduluru, A. K.; Choi, S. K.; Orr, B. G.; Low, P. S.; Holl, M. M. B. Avidity Mechanism of Dendrimer-Folic Acid Conjugates. *Mol Pharm* **2014**, *11*, 1696-1706.

(29) Dougherty, C. A.; Furgal, J. C.; van Dongen, M. A.; Goodson, T.; Holl, M. M. B.; Manono, J.; DiMaggio, S. Isolation and Characterization of Precise Dye/Dendrimer Ratios. *Chem-Eur J* **2014**, *20*, 4638-4645.

(30) Carberry, T. P.; Tarallo, R.; Falanga, A.; Finamore, E.; Galdiero, M.; Weck, M.; Galdiero, S. Dendrimer Functionalization with a Membrane-Interacting Domain of Herpes Simplex Virus Type 1: Towards Intracellular Delivery. *Chem-Eur J* **2012**, *18*, 13678-13685.

(31) Dougherty, C. A. V., S.; Orr, B.G.; Banaszak Holl, M.M. Fluorophore:Dendrimer Ratio Impacts Cellular Uptake and Intracellular Fluorescence Lifetime. *Bionjugate Chemistry* **2015**, *26*, 304-315.

(32) Mullen, D. G.; Borgmeier, E. L.; Desai, A. M.; van Dongen, M. A.; Barash, M.; Cheng, X. M.; Baker, J. R.; Holl, M. M. B. Isolation and Characterization of Dendrimers with Precise Numbers of Functional Groups. *Chem-Eur J* **2010**, *16*, 10675-10678.

(33) van Dongen, M. A.; Desai, A.; Orr, B. G.; Baker, J. R.; Holl, M. M. B. Quantitative analysis of generation and branch defects in G5 poly(amidoamine) dendrimer. *Polymer* **2013**, *54*, 4126-4133.

# Chapter 6.
# Conclusions and Future Outlook

## 6.1 Summary of Work and Future Directions

Multivalent polymers are materials of interest for many biological and biomedical applications, including the development of novel imaging agents and theranostics.[1,2] Imaging agents provide an ability to noninvasively explore disease pathways,[3] and theranostic materials have the capability to both detect and treat a disease. Multivalent polymers can have multiple copies of both an imaging agent and a therapeutic attached in order to achieve a high drug load for therapeutic capabilities and high sensitivity for imaging agents. With the ability to easily tune the number of small molecules attached, as well as the size, surface functionality, and structure of the polymer, these multivalent materials have the potential to create even more effective imaging agents and theranostics for the biomedical field.[4,5] Despite this promise, there are two major obstacles to obtaining an ideal polymer imaging agent or theranostic device: 1) the internal molecular weight distribution of the polymer and 2) the distribution of ratios of small molecules attached to the polymer.[6]

Overcoming the distribution of different ratios of small molecules, such as fluorophores, targeting agents, and drugs has been a major synthetic challenge in the development of multivalent polymers for the biomedical field.[7,8] The large distribution in the degree of hydrophobicity on a polymer can cause a variety of different biological behaviors.[6,9,10] The distribution of fluorophores on a polymer has the complication of a large difference in hydrophobicity and also a large difference in local fluorophore concentration. The difference in fluorophore concentration on a polymer can lead to a change in photophysical effects of the fluorophore.[11-13] While many efforts have been put forth to synthesize multivalent polymers with a controlled number of fluorophores,[14-18] no previous studies have shown the ability to synthesize, characterize, and determine the photophysical and biological properties of a multivalent polymer with a systematically varied fluorophore  polymer ratio.

Precise fluorophore-polymer ratios have been obtained for G3 and G5 PAMAM dendrimers by semi-preparative reverse phase high performance liquid chromatography (semi-prep rp-HPLC).[19,20] PAMAM dendrimers were chosen as the polymer platform due to their narrow molecular weight distribution as compared to other polymers of their size. A semi-prep rp-HPLC method has also been developed in order to separate out small and large molecular weight defects from the desired G3 and G5 PAMAM monomer material and achieves an even smaller molecular weight distribution of the starting polymer.[21] Two strategies were employed to obtain precise ratios, by either direct conjugation of the fluorophore to the dendrimer or by isolating precise ratios of click ligands and further functionalizing with a click functionalized fluorophore. Precise ratios of TAMRA dye were obtained on both fully acetylated G5 PAMAM and amine terminated G3 and G5 PAMAM dendrimers. All precise ratio materials have shown a difference in fluorescence emission intensity, proving that more fluorophores do not provide more fluorescence intensity.

Differences in biological behavior have been observed with the addition of fluorophores onto multivalent polymers at different ratios.[12,22-25] However, the materials used to observe biological behaviors in past studies have distributions in them, so the exact ratio, or ratios, responsible for the observed difference has been unknown. The amine terminated G5 PAMAM precise ratio TAMRA materials were used in HEK 293A cells to determine fluorophore ratio effects on cellular uptake and intracellular fluorescence lifetime. The cell uptake was shown to increase with increasing ratio of TAMRA. The increased cellular uptake conclusion was only obtained after "correcting" for the difference in fluorescence intensity of the ratios at the same concentration. The incorrect conclusion of less uptake with increasing TAMRA ratio would have been determined if the fluorescence correction was not taken into account. The fluorescence lifetime differences were consistent with environmental changes, indicating that the materials may be in different environmental conditions within a cell.

Since the precise ratio of fluorophore to polymer has shown to have photophysical and biological differences based on the ratio, this control must be taken into account when developing materials for diagnostics and therapeutics. An attempt to control both the fluorophore ratio and a targeting ligand/therapeutic has been shown in this thesis. However an inability to appropriately scale the reaction and isolation prevents adequate characterization of material with more than one precise ratio. Without the characterization, the material could not be further functionalized with a drug or targeting ligand. Since Chapter 5 was not able to successfully prove the isolation of precise ratios

for 2 different small molecules on a polymer, another strategy must be attempted in order to obtain precise ratios of both a fluorophore and a targeting agent or drug. One strategy with the ability to be scaled using the current methods of rp-HPLC isolation include synthesizing a fluorescent targeting ligand or fluorescent drug with an azide functionality to conjugate to precise ratios of a click ligand on a G5 PAMAM dendrimer. Another strategy includes conjugating an azide functionalized dendron with dyes and targeting ligands/drugs to precise ratios of a click ligand on a G5 PAMAM dendrimer.

The synthesis, photophysical characterization, and biological application of PAMAM dendrimers containing precise fluorophore-polymer ratios has been presented. The precise ratio materials have allowed for a better understanding of the dependence of photophysical properties on fluorophore-polymer ratio as well as the impact of the related changes in hydrophobicity on biological behavior. Using controlled ratios of TAMRA on a G5 PAMAM dendrimer, it was observed that more than 2 hydrophobic molecules on a hydrophilic polymer increases the amount of cellular uptake. The controlled ratios of TAMRA on a G5 PAMAM dendrimer also showed that the fluorescence lifetime of the fluorophore changes due to both ratio and environment. The change in lifetime based on ratio is roughly similar in magnitude to the environmental changes. Overall, using precise ratios of fluorophores on a polymer has provided a new understanding of fluorescence properties, such as fluorescence emission and lifetime, and cellular uptake based on hydrophobicity ratio, proving there is a need to control the number of hydrophobic small molecules on a polymer in polymer imaging agent and theranostic development.

### 6.2 References


(1) Wang, Z.; Niu, G.; Chen, X. Y. Polymeric Materials for Theranostic Applications. *Pharm Res-Dordr* **2014**, *31*, 1358-1376.

(2) Krasia-Christoforou, T.; Georgiou, T. K. Polymeric theranostics: using polymer-based systems for simultaneous imaging and therapy. *J Mater Chem B* **2013**, *1*, 3002-3025.

(3) Weissleder, R.; Pittet, M. J. Imaging in the era of molecular oncology. *Nature* **2008**, *452*, 580-589.

(4) Lee, C. C.; MacKay, J. A.; Frechet, J. M. J.; Szoka, F. C. Designing dendrimers for biological applications. *Nat Biotechnol* **2005**, *23*, 1517-1526.

(5) Duncan, R. The dawning era of polymer therapeutics. *Nat Rev Drug Discov* **2003**, *2*, 347-360.

(6) Mullen, D. G.; Fang, M.; Desai, A.; Baker, J. R.; Orr, B. G.; Holl, M. M. B. A Quantitative Assessment of Nanoparticle-Ligand Distributions: Implications for Targeted Drug and Imaging Delivery in Dendrimer Conjugates. *Acs Nano* **2010**, *4*, 657-670.

(7) Mullen, D. G.; Holl, M. M. B. Heterogeneous Ligand-Nanoparticle Distributions: A Major Obstacle to Scientific Understanding and Commercial Translation. *Accounts Chem Res* **2011**, *44*, 1135-1145.

(8) van Dongen, M. A.; Dougherty, C. A.; Holl, M. M. B. Multivalent Polymers for Drug Delivery and Imaging: The Challenges of Conjugation. *Biomacromolecules* **2014**, *15*, 3215-3234.

(9) Alexis, F.; Pridgen, E.; Molnar, L. K.; Farokhzad, O. C. Factors affecting the clearance and biodistribution of polymeric nanoparticles. *Mol Pharm* **2008**, *5*, 505-515.

(10) He, C. B.; Hu, Y. P.; Yin, L. C.; Tang, C.; Yin, C. H. Effects of particle size and surface charge on cellular uptake and biodistribution of polymeric nanoparticles. *Biomaterials* **2010**, *31*, 3657-3666.

(11) Pansare, V. J.; Hejazi, S.; Faenza, W. J.; Prud'homme, R. K. Review of Long-Wavelength Optical and NIR Imaging Materials: Contrast Agents, Fluorophores, and Multifunctional Nano Carriers. *Chem Mater* **2012**, *24*, 812-827.

(12) Kim, Y.; Kim, S. H.; Tanyeri, M.; Katzenellenbogen, J. A.; Schroeder, C. M. Dendrimer Probes for Enhanced Photostability and Localization in Fluorescence Imaging. *Biophys J* **2013**, *104*, 1566-1575.

(13) Selwyn, J. E.; Steinfel.Ji. Aggregation Equilibria of Xanthene Dyes. *J Phys Chem-Us* **1972**, *76*, 762-&.

(14) Ornelas, C.; Lodescar, R.; Durandin, A.; Canary, J. W.; Pennell, R.; Liebes, L. F.; Weck, M. Combining Aminocyanine Dyes with Polyamide Dendrons: A Promising Strategy for Imaging in the Near-Infrared Region. *Chem-Eur J* **2011**, *17*, 3619-3629.

(15) Ornelas, C.; Pennell, R.; Liebes, L. F.; Weck, M. Construction of a Well-Defined Multifunctional Dendrimer for Theranostics. *Org Lett* **2011**, *13*, 976-979.

(16) Xu, Z. J.; He, B. C.; Shen, J.; Yang, W. T.; Yin, M. Z. Fluorescent water-soluble perylenediimide-cored cationic dendrimers: synthesis, optical properties, and cell uptake. *Chem Commun* **2013**, *49*, 3646-3648.

(17) Yang, S. K.; Shi, X. H.; Park, S.; Doganay, S.; Ha, T.; Zimmerman, S. C. Monovalent, Clickable, Uncharged, Water-Soluble Perylenediimide-Cored Dendrimers for Target-Specific Fluorescent Biolabeling (vol 131, pg 9964, 2011). *J Am Chem Soc* **2011**, *133*, 13206-13206.

(18) Gilat, S. L.; Adronov, A.; Frechet, J. M. J. Light harvesting and energy transfer in novel convergently constructed dendrimers. *Angew Chem Int Edit* **1999**, *38*, 1422-1427.

(19) Dougherty, C. A.; Furgal, J. C.; van Dongen, M. A.; Goodson, T.; Holl, M. M. B.; Manono, J.; DiMaggio, S. Isolation and Characterization of Precise Dye/Dendrimer Ratios. *Chem-Eur J* **2014**, *20*, 4638-4645.

(20) Dougherty, C. A. V., S.; Orr, B.G.; Banaszak Holl, M.M. Fluorophore:Dendrimer Ratio Impacts Cellular Uptake and Intracellular Fluorescence Lifetime. *Bionjugate Chemistry* **2015**, *26*, 304-315.

(21) van Dongen, M. A.; Desai, A.; Orr, B. G.; Baker, J. R.; Holl, M. M. B. Quantitative analysis of generation and branch defects in G5 poly(amidoamine) dendrimer. *Polymer* **2013**, *54*, 4126-4133.

(22) Yoo, H.; Juliano, R. L. Enhanced delivery of antisense oligonucleotides with fluorophore-conjugated PAMAM dendrimers. *Nucleic Acids Res* **2000**, *28*, 4225-4231.

(23) Vuorimaa, E.; Urtti, A.; Seppanen, R.; Lemmetyinen, H.; Yliperttula, M. Time-resolved fluorescence spectroscopy reveals functional differences of cationic polymer-DNA complexes. *J Am Chem Soc* **2008**, *130*, 11695-11700.

(24) Seib, F. P.; Jones, A. T.; Duncan, R. Establishment of subcellular fractionation techniques to monitor the intracellular fate of polymer therapeutics I. Differential centrifugation fractionation B16F10 cells and use to study the intracellular fate of HPMA copolymer-doxorubicin. *J Drug Target* **2006**, *14*, 375-390.

(25) Shakhbazau, A.; Isayenka, I.; Kartel, N.; Goncharova, N.; Seviaryn, I.; Kosmacheva, S.; Potapnev, M.; Shcharbin, D.; Bryszewska, M. Transfection efficiencies of PAMAM dendrimers correlate inversely with their hydrophobicity. *Int J Pharmaceut* **2010**, *383*, 228-235.

# Appendix A.

## Isolation and Characterization of Precise Dye-Dendrimer Ratios

## Supplemental Information

**Table A.1.** Characterization of precisely defined G5-Ac-TAMRA$_n$ (n = 1 – 3, 3+).

| # TAMRA dyes per G5 | Yield (mg) | % Yield (determined by theoretical Poisson Distribution) | % Separation Yield (by mass of material placed on column) | % Yield (total mass from starting materials) | UPLC Average | $^1$H NMR Ratio | MALDI-TOF-MS (g/mol) |
|---|---|---|---|---|---|---|---|
| **1** | 11.7 | 40 | 15 | 7 | 1 | 0.7 | 28800 |
| **2** | 6.9 | 43 | 9 | 4 | 2 | 1.6 | 29600 |
| **3** | 2.1 | 36 | 3 | 1 | 3 | 3.1 | 31000 |
| **3+** | 2.5 | >95 | 3 | 2 | 5.1 | 4.4 | 32300 |

**Table A.2.** Characterization of precisely defined G5-Ac-FC$_n$ (n = 1 – 4).

| # Fluorescein Dyes per G5 | % Yield | $^1$H NMR Average | UPLC Average | $^{19}$F NMR Ratio | MALDI-TOF-MS (g/mol) |
|---|---|---|---|---|---|
| **1** | 55 | 1.2 | 0.9 | 0.8 | 28,300 |
| **2** | 57 | 1.8 | 1.5 | 1.6 | 29,900 |
| **3** | 48 | 3.3 | 2.7 | 2.9 | 30,600 |
| **4** | 51 | 3.0 | 3.5 | 4 (Set) | 30,800 |

**Table A.3.** Optical properties of precisely defined G5-Ac-FC$_n$ (n = 1 – 4). Extinction coefficients and quantum yield values calculated on per particle basis. Quantum Yield by Joseph C. Furgal.

| # Fluorescein Dyes per G5 | ε ($M^{-1}cm^{-1)}$ | Fluorescence Ratio | Quantum Yield |
|---|---|---|---|
| **1** | 5.40E+05 | 1.0 (Set) | 0.21 |
| **2** | 1.00E+06 | 1.5 | 0.20 |
| **3** | 1.20E+06 | 1.5 | 0.13 |
| **4** | 7.00E+06 | 1.3 | 0.14 |

**Table A.4.** Optical Properties of precisely defined G5-Ac-TAMRA$_n$ (n = 1 – 3, 3+). Quantum Yield by Joseph C. Furgal.

| # TAMRA Dyes per G5 | Fluorescence Ratio | Quantum Yield |
|---|---|---|
| 1 | 1.0 (Set) | 0.14 |
| 2 | 0.7 | 0.06 |
| 3 | 0.6 | 0.04 |
| 3+ | 0.5 | 0.04 |

**Figure A.1.** $^{19}$F NMR spectra (DMSO-d$_6$) of pre and post-click materials for the small molecule MFCO and MFCO-Fluorescein.

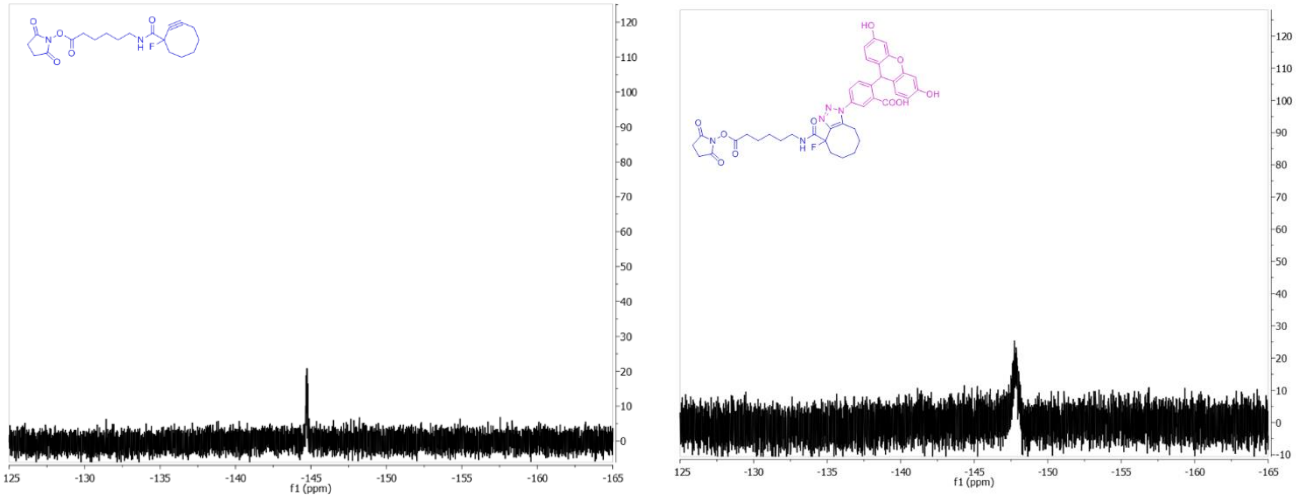


**Figure A.2.** $^{19}$F NMR (1:1 DMSO-d$_6$:D$_2$O) spectra of the addition of G5 PAMAM dendrimer to the post clicked small molecule material.

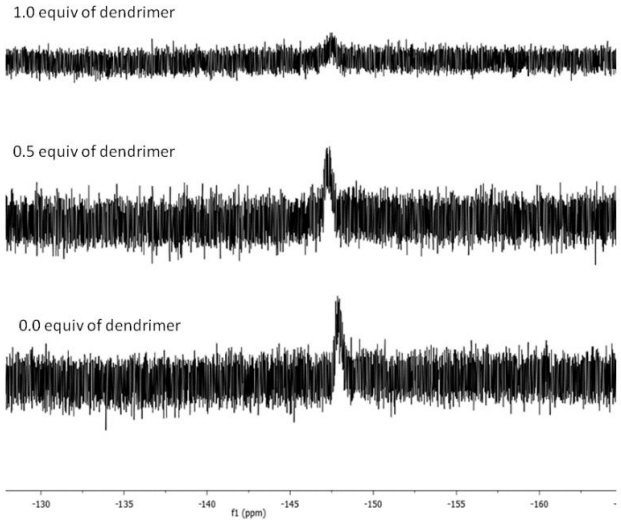

**Figure A.3.** MALDI-TOF-MS spectra for a) G5-Ac-$FC_n$ (n = 1 – 4) and b) G5-Ac-$TAMRA_n$ (n = 1-3, 3+).

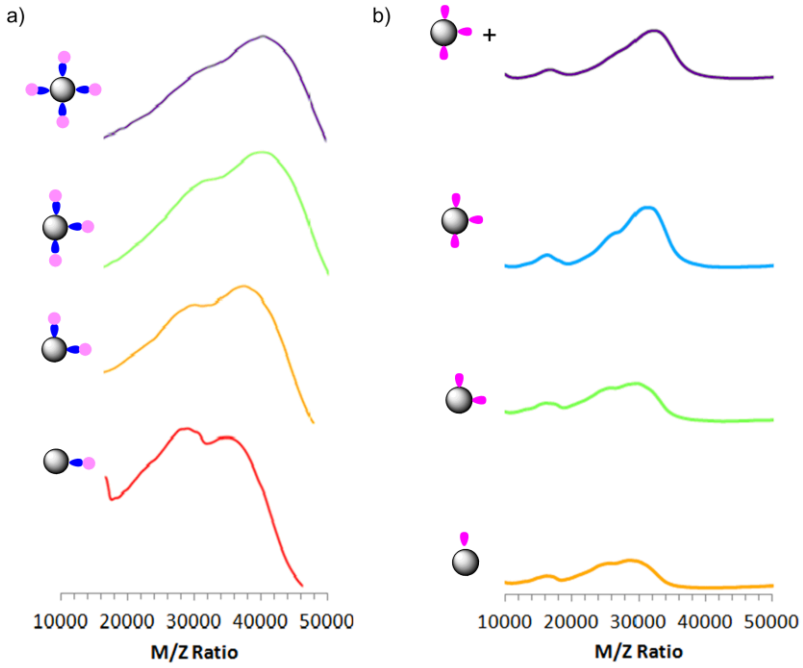


**Figure A.4.** MALDI-TOF-MS spectra for G5-$NH_2$ PAMAM Dendrimer.

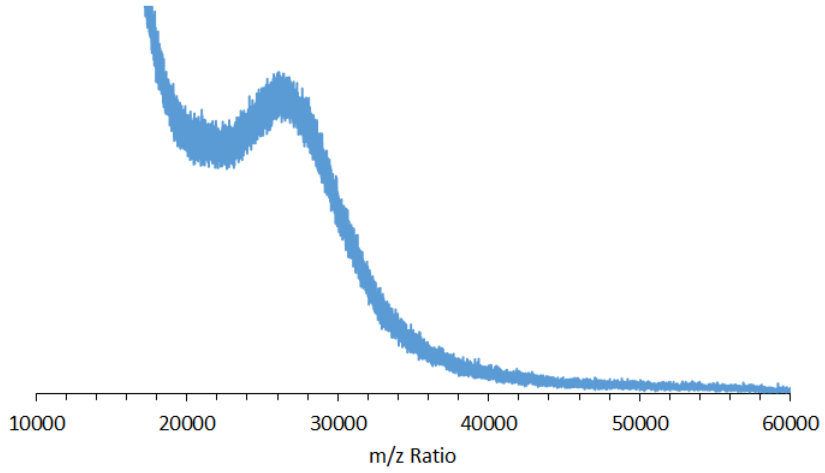

# Appendix B.

## Generation 3 PAMAM Dendrimer TAMRA Conjugates Containing Precise Dye-Dendrimer Ratios Supplemental Information

**Table B.1.** MALDI-TOF-MS summary of G3-$NH_2$ samples from Scheme 3.1a.

| **G3-$NH_2$ Sample** | **Average MW m/z Ratio** |
|---|---|
| **Trailing Generation G2 (Purple)** | 3550 |
| **G3 Monomer (Red)** | 6850 |
| **G3-G3 Dimer (Blue)** | 13100 |

**Table B.2.** Summary of G3m-$TAMRA_n$ samples from Scheme 3.2d.

| | **Yield (mg)** | **Average MW from m/z Ratio** | **Fluorescence Ratio** | **Avg Number of Dyes** |
|---|---|---|---|---|
| | | | | **Proton NMR** |
| **G3m-$(TAMRA)_{3.8(AVG)}$-$NH_2$** | - | - | 0.07 | 3.8 |
| **G3m-$(TAMRA)_1$-$NH_2$** | 2.61 | 7190 | 1.00 (defined) | 0.8 |
| **G3m-$(TAMRA)_{2a}$-$NH_2$** | 2.93 | 7620 | 0.26 | 1.9 |
| **G3m-$(TAMRA)_{2b}$-$NH_2$** | 0.94 | 7650 | 0.17 | 2.0 |
| **G3m-$(TAMRA)_3$-$NH_2$** | 6.70 | 7980 | 0.07 | 2.9 |
| **G3m-$(TAMRA)_{4+}$-$NH_2$** | 8.15 | - | 0.01 | 6.0 |

**Table B.3.** Summary of G3d-$TAMRA_n$ samples from Scheme 3.2b.

| | **Yield (mg)** | **MW from m/z Ratio** | **Fluorescence Ratio** | **Avg Number of Dyes** |
|---|---|---|---|---|
| | | | | **Proton NMR** |
| **G3d-$(TAMRA)_{2.2(AVG)}$-$NH_2$** | - | - | 0.63 | 2.2 |
| **G3d-$(TAMRA)_1$-$NH_2$** | 1.69 | 7180 | 1.00 (defined) | 0.8 |
| **G3d-$(TAMRA)_2$-$NH_2$** | 0.59 | 7610 | 0.21 | 2.4 |
| **G3d-$(TAMRA)_3$-$NH_2$** | 1.72 | 8050 | 0.12 | 3.4 |
| **G3d-$(TAMRA)_{4+}$-$NH_2$** | 0.42 | - | 0.07 | 4.6 |

**Figure B.1.** A stacked plot of MALDI-TOF-MS spectra for G3d-$NH_2$-$TAMRA_{2.2(avg)}$ (black) and G3d-$NH_2$-$TAMRA_n$ (n = 1, 2, 3, 4+) conjugates from Scheme 3.2b.

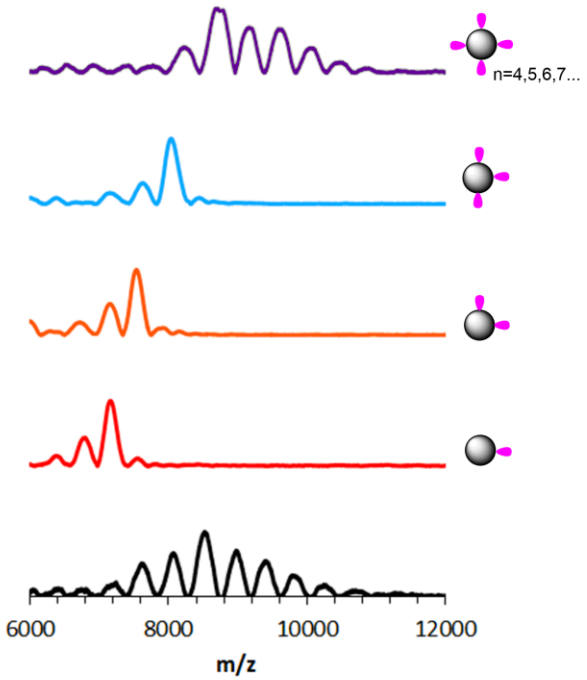


**Figure B.2.** a) Absorption and b) emission spectra of G3d-$TAMRA_n$-$NH_2$ (n = 1, 2, 3, 4+) conjugates from Scheme 3.2b at 1 x $10^{-5}$ M; 1 TAMRA (red), 2 (orange), 3 (blue), 4+ (purple), and average (dashed black). c) Absorbance of TAMRA n=1, 2, and 3 at a concentration of 3 x $10^{-5}$ M, and the absorbance traces of d) n=3 (blue) and an equimolar mixture of n=1 and n=2 (black).

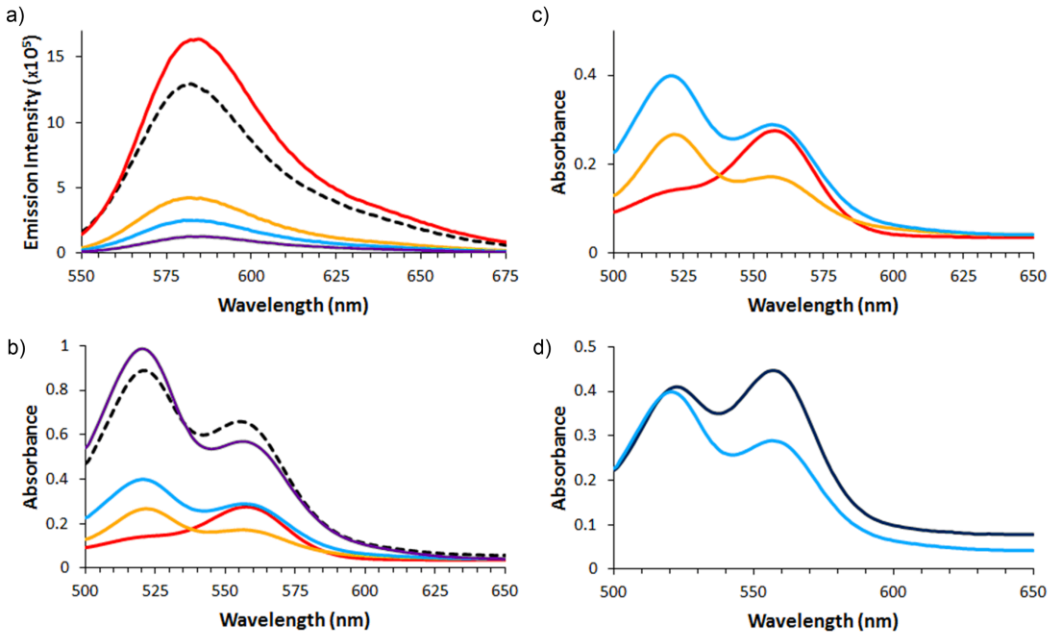

**Figure B.3.** Theoretical Fluorescence of Stochastic Samples of G3 PAMAM Dendrimer TAMRA Conjugates Based on Precise Ratio Sample Fluorescence Measurements at 0.1mg/mL.

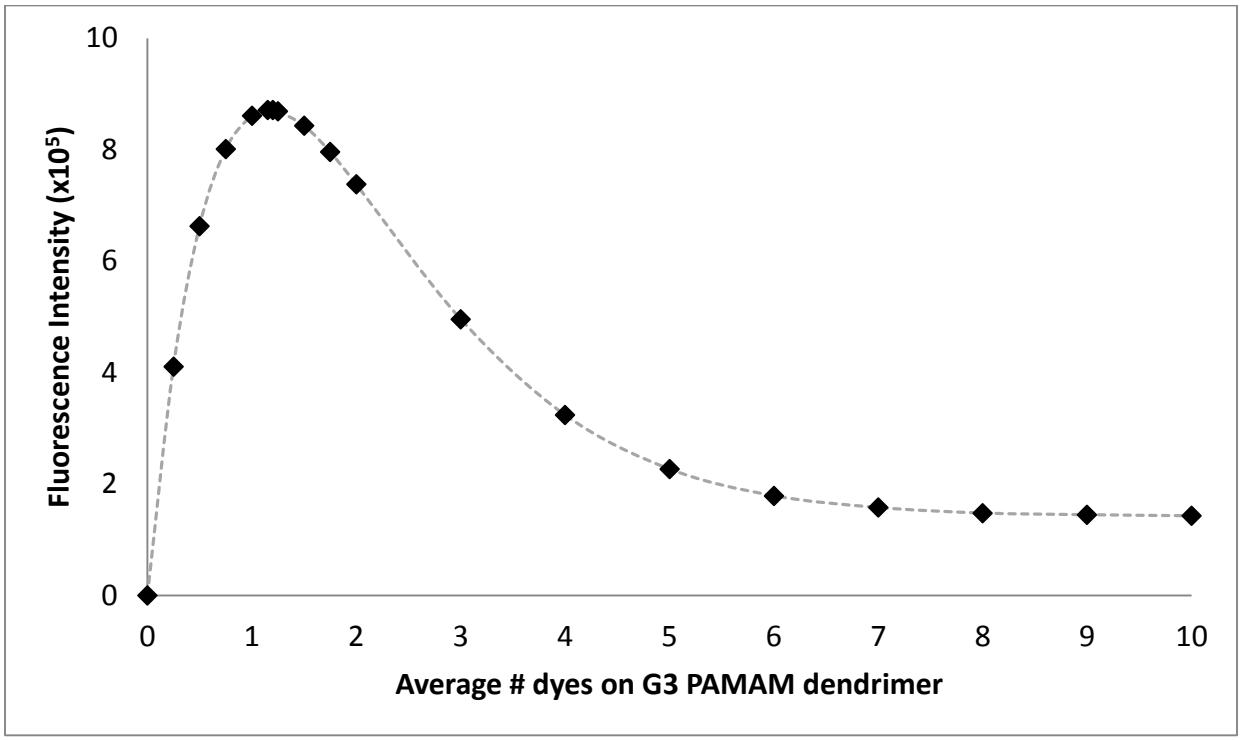

# Appendix C.

# Fluorophore-Dendrimer Ratio Impacts Cellular Uptake and Intracellular Fluorescence Lifetime Supplemental Information

**Table C.1.** Characterization summary for G5-$NH_2$-$TAMRA_n$ material.

| | Yield (mg) | MALDI-TOF-MS m/z ratio | % Yield | Equivalents of TFA | Average Number of Dyes | |
|---|---|---|---|---|---|---|
| | | | | | UPLC | Proton NMR |
| G5-$(TAMRA)_{1.5(AVG)}$-$NH_2$ | 121.0 | 27500 | 86 | 0.32 | 1.5 | 5.9 |
| G5-$NH_2$-$(TAMRA)_0$ | 1.0 | 24600 | 27* | 0.79 | 0.0 | 0.0 |
| G5-$NH_2$-$(TAMRA)_1$ | 5.2 | 24300 | 21* | 0.05 | 1.0 | 0.9 |
| G5-$NH_2$-$(TAMRA)_2$ | 2.5 | 25900 | 28* | 0.20 | 2.0 | 1.8 |
| G5-$NH_2$-$(TAMRA)_3$ | 3.5 | 26400 | 23* | 5.24 | 3.0 | 3.3 |
| G5-$NH_2$-$(TAMRA)_4$ | 4.6 | 26800 | 23* | 5.90 | 4.0 | 4.5 |
| G5-$NH_2$-$(TAMRA)_{5+}$ | 15.3 | 28900 | 23* | 1.35 | 6.8 | 6.9 |
| * % Yield calculated based on fractional amount of each species present in G5-$NH_2$-$(TAMRA)_{1.5AVG}$ as determined by peak fitting the rp-UPLC trace. | | | | | | |

**Table C.2.** Fluorescence lifetime for solutions that mimic cell conditions. All values are in ns with standard deviations obtained from at least three independent measurements given in parentheses. The data corresponds to Figures 4.1 and 4.6. Data taken with Sriram Vaidyanathan.

| | water | FBS | PBS | NaCl | ficoll | BSA | glucose | DCS |
|---|---|---|---|---|---|---|---|---|
| Cy3 | 0.61 (0.04) | - | - | - | - | - | - | - |
| TAMRA | 2.46 (0.04) | - | - | - | - | - | - | - |
| $G5T_{1.5avg}$ | 1.92 (0.12) | 2.5 (0.08) | 2.24 (0.04) | 2.35 (0.03) | 2.32 (0.01) | 2.21 (0.08) | 1.87 (0.04) | 2.51 (0.03) |
| $G5T_1$ | 2.32 (0.15) | 1.71 (0.08) | 2.18 (0.05) | 2.22 (0.02) | 2.12 (0.04) | 1.92 (0.08) | 1.81 (0.06) | 1.86 (0.04) |
| $G5T_2$ | 1.78 (0.11) | 1.77 (0.05) | 1.66 (0.01) | 1.66 (0.07) | 1.59 (0.07) | 1.82 (0.11) | 1.62 (0.03) | 1.88 (0.11) |
| $G5T_3$ | 1.51 (0.03) | 1.56 (0.11) | 1.6 (0.03) | 1.58 (0.06) | 1.56 (0.05) | 1.5 (0.03) | 1.42 (0.06) | 1.82 (0.13) |
| $G5T_4$ | 1.70 (0.05) | 1.72 (0.14) | 1.48 (0.04) | 1.43 (0.04) | 1.4 (0.02) | 1.45 (0.16) | 1.31 (0.06) | 1.38 (0.05) |
| $G5T_{5+}$ | 1.23 (0.11) | 1.77 (0.05) | 1.63 (0.03) | 1.6 (0.02) | 1.48 (0.03) | 1.48 (0.11) | 1.1 (0.01) | 2.51 (0.03) |

**Figure C.1.** MALDI-TOF-MS spectra of G5-$NH_2$-$TAMRA_n$ materials. Numbers for m/z ratios for each sample are reported in Table C.1.

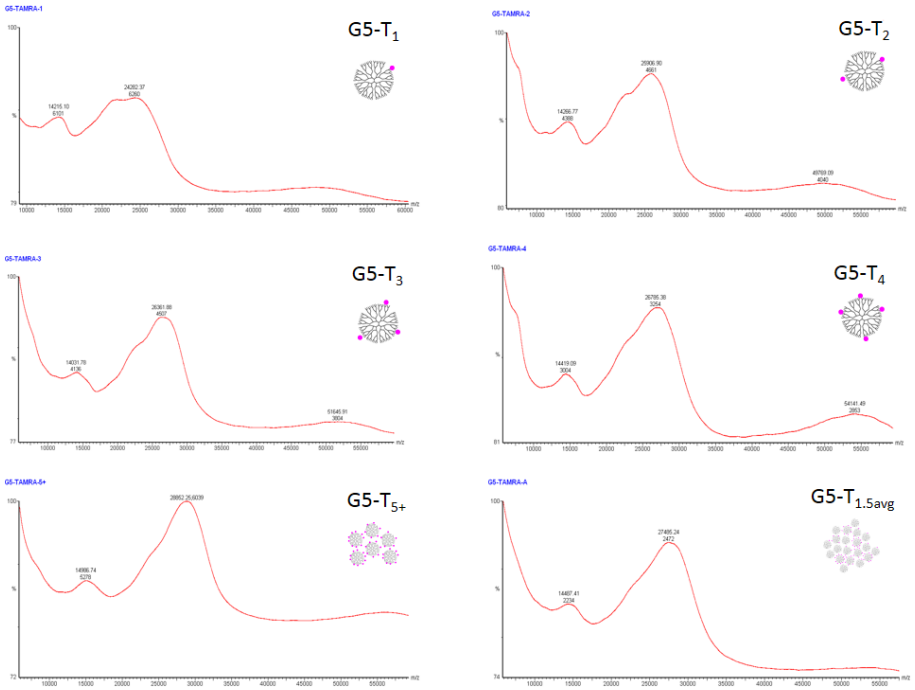

**Figure C.2.** Fluorescence emission intensities of 0.1 mg/mL samples of G5-$NH_2$-$TAMRA_n$ (n=1, 2, 3, 4, 5+, and $1.5_{avg}$) for the various control solutions.

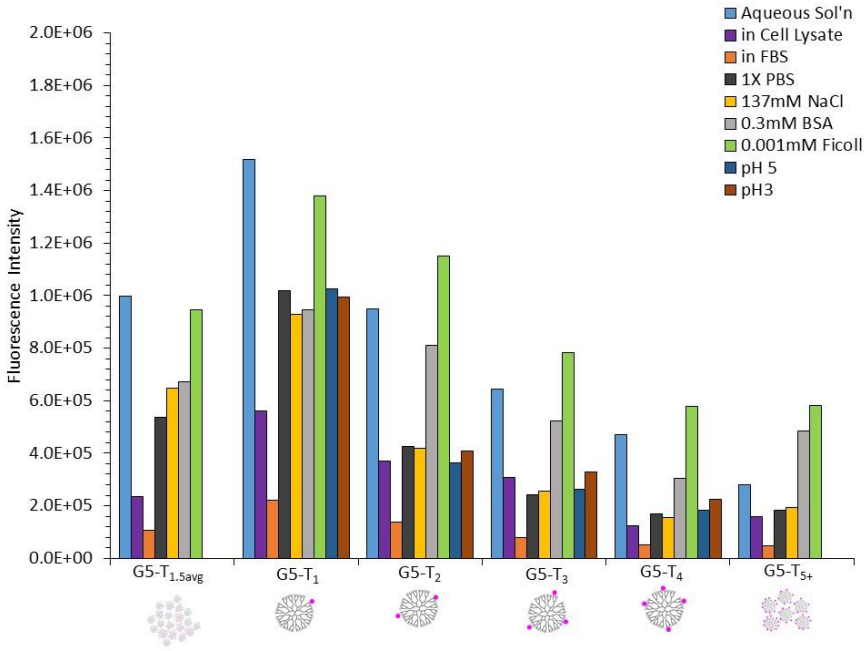


**Figure C.3.** Fluorescence emission spectra of G5-$NH_2$-$TAMRA_n$ in solution with various controls in comparison to materials in aqueous solution. PBS, FBS, NaCl, DNA, BSA, and ficoll show similar fluorescence intensity ratios to those obtained in water (Figure 4.1c). n=1 (orange), n=2 (yellow), n=3 (green), n=4 (blue), n=5+ (purple), and $n=1.5_{avg}$ (black).

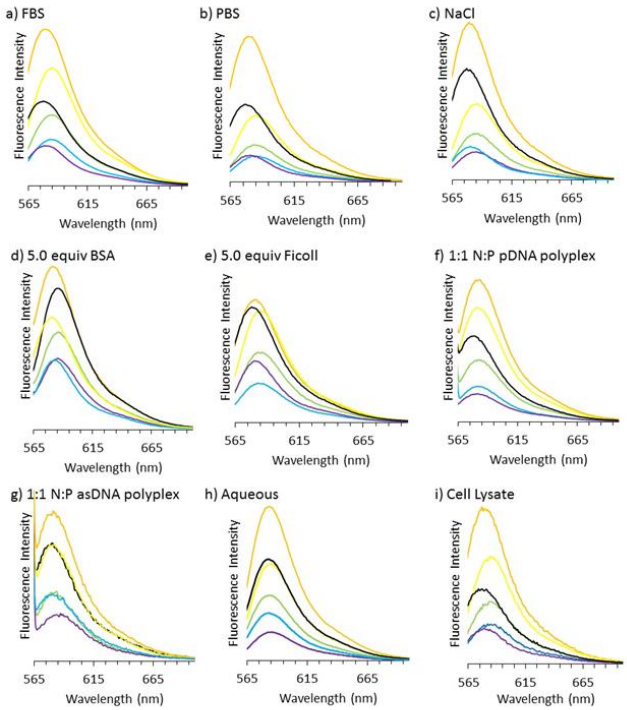

**Figure C.4.** FLIM images of HEK293A cells from Figure 4.5 with a) G5-$NH_2$-$TAMRA_1$ b) G5-$NH_2$-$TAMRA_2$ c) G5-$NH_2$-$TAMRA_3$ d) G5-$NH_2$-$TAMRA_4$ e) G5-$NH_2$-$TAMRA_{5+}$ f) G5-$NH_2$-$TAMRA_{1.5(avg)}$ after an incubation of 3 hours (40x objective, 6.5 zoom). The images are lifetime color coded with high to low lifetimes going from red (2.0 ns) to blue (0.5 ns). All samples show more intense fluorescence in punctate spots. Scale bar is 20 μm. Data taken by Sriram Vaidyanathan.

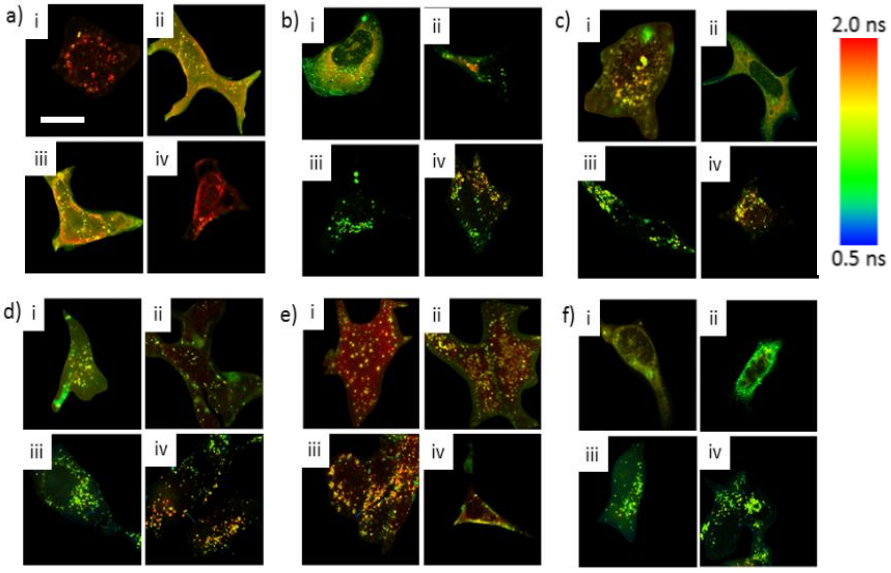


**Figure C.5.** Solution fluorescence lifetime controls for cell data comparing aqueous fluorescence lifetimes to lifetimes of materials in buffers at a pH = 3 and pH = 5. Data taken with Sriram Vaidyanathan.

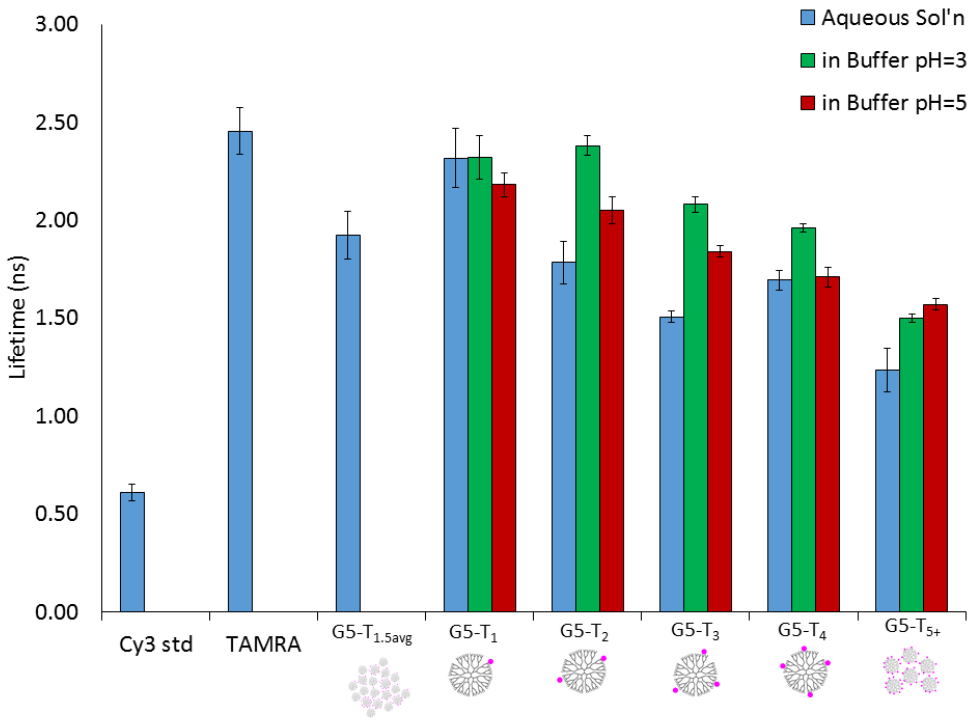

**Figure C.6.** Fluorescence lifetime of G5-$NH_2$-$TAMRA_n$:DNA polyplexes in aqueous solution. Data taken with Sriram Vaidyanathan.